

## ORT DOCUMENTATION PAGE

DUE FILE COPY

1a. <b>AD-A228 067</b>		1b. RESTRICTIVE MARKINGS	
2a.		3. DISTRIBUTION/AVAILABILITY OF REPORT Approved for public release; distribution unlimited.	
2b. DECLASSIFICATION/DOWNGRADING SCHEDULE		5. MONITORING ORGANIZATION REPORT NUMBER ARO 23802.1-MS-F	
4. PERFORMING ORGANIZATION REPORT NUMBER(S)		7a. NAME OF MONITORING ORGANIZATION U. S. Army Research Office	
6a. NAME OF PERFORMING ORGANIZATION The Univ. of Michigan College of Engineering	6b. OFFICE SYMBOL (if applicable)	7b. ADDRESS (City, State, and ZIP Code) P. O. Box 12211 Research Triangle Park, NC 27709-2211	
6c. ADDRESS (City, State, and ZIP Code) Dept. of Nuclear Engineering 2355 Boni. eel Blvd. Ann Arbor, MI 48109	9. PROCUREMENT INSTRUMENT IDENTIFICATION NUMBER DAAL03-86-G-0052		
8a. NAME OF FUNDING/SPONSORING ORGANIZATION U. S. Army Research Office	8b. OFFICE SYMBOL (if applicable)	10. SOURCE OF FUNDING NUMBERS	
8c. ADDRESS (City, State, and ZIP Code) P. O. Box 12211 Research Triangle Park, NC 27709-2211		PROGRAM ELEMENT NO.	PROJECT NO.
		TASK NO.	WORK UNIT ACCESSION NO.
11. TITLE (Include Security Classification) Ion Beam Modification of Surface for Improved High Temperature Performance of Materials			
12. PERSONAL AUTHOR(S) Was, Gary S. and Cavasin, Daniel			
13a. TYPE OF REPORT Final	13b. TIME COVERED FROM 9/1/86 TO 4/31/90	14. DATE OF REPORT (Year, Month, Day) July 27, 1990	15. PAGE COUNT 104
16. SUPPLEMENTARY NOTATION The view, opinions and/or findings contained in this report are those of the author(s) and should not be construed as an official Department of the Army position, policy, or decision, unless so designated by other documentation.			
17. COSATI CODES		18. SUBJECT TERMS (Continue on reverse if necessary and identify by block number)	
FIELD	GROUP	SUB-GROUP	
		metastable materials	
		phase transformation	
		calorimetry	
19. ABSTRACT (Continue on reverse if necessary and identify by block number)			
<p>A novel experimental technique, "Thin Film Calorimetry" (TFC), has been developed to determine the enthalpy of transformation from metastable to stable equilibrium structures in thin films. This technique has been applied to investigate metastable-stable transformations occurring in thin films of nominal composition NiAl<sub>3</sub>. Elemental Ni and Al are codeposited directly onto the surface of a pure Al calorimeter sample pan to form a 0.75 - 0.90 <math>\mu</math>m thick, extended solid solution of NiAl<sub>3</sub>. The as-deposited microstructure in this case is a metastable configuration, and the reaction heat accompanying its transformation to the stable, equilibrium <math>\epsilon</math>-NiAl<sub>3</sub> phase is measured directly in the calorimeter. The mean change in enthalpy, <math>\Delta H</math>, for a series of such measurements, is -4.16 kcal/mole. A second approach involves annealing the as-deposited film to form the <math>\epsilon</math> phase, then irradiating the as-annealed film, using 1.5 MeV Ni<sup>++</sup> ions, to doses of <math>\geq 5 \times 10^{15}</math> ions/cm<sup>2</sup>, to form an amorphous structure. The enthalpy associated with the transformation of this structure to the equilibrium <math>\epsilon</math> is then measured in the DSC. The mean <math>\Delta H</math> found for this reaction is -5.02 kcal/mole. The measured values in both cases compare favorably with recent calculations performed using the embedded atom computer simulation program.</p>			
20. DISTRIBUTION/AVAILABILITY OF ABSTRACT <input type="checkbox"/> UNCLASSIFIED/UNLIMITED <input type="checkbox"/> SAME AS RPT. <input type="checkbox"/> DTIC USERS		21. ABSTRACT SECURITY CLASSIFICATION Unclassified	
22a. NAME OF RESPONSIBLE INDIVIDUAL G. Was		22b. TELEPHONE (Include Area Code) (313) 763-4675	22c. OFFICE SYMBOL

~~METASTABLE PHASE TRANSFORMATIONS IN ION~~  
IRRADIATED  $\text{NiAl}_3$  THIN FILMS

FINAL REPORT

GARY S. WAS AND D. CAVASIN

AUGUST, 1990

U. S. ARMY RESEARCH OFFICE

GRANT #DAAL03-86-G-0052

Accession For	
NTIS GRA&I	<input checked="" type="checkbox"/>
DTIC TAB	<input checked="" type="checkbox"/>
Unannounced	<input type="checkbox"/>
Justification	
By _____	
Distribution/	
Availability Codes	
Dist	Avail and/or Special
A-1	

THE UNIVERSITY OF MICHIGAN  
DEPARTMENT OF NUCLEAR ENGINEERING

APPROVED FOR PUBLIC RELEASE;  
DISTRIBUTION UNLIMITED



Use title and date on Report Documentation  
Page per telecon Sylvia Hall. Army Re-  
search Office. P. O. Box 12211. Re-  
search Triangle Park, NC 27709-2211.

VHG

11/07/90

## ACKNOWLEDGEMENTS

Many individuals contributed significantly to the progress of this research endeavor and I would like to thank them all for their contributions: My advisor, Professor Gary Was, for providing me a most challenging and interesting research assignment with which to expand my knowledge of materials science; Professor David Van Aken, for the use of his thermal analysis equipment, and expertise in a field which I had previously been uninitiated; Dr. John F. Mansfield, for his help and guidance in efficient use of the Electron Microprobe Analysis Laboratory equipment; Professor Michael Atzmon, for providing valuable insight into thermal analysis, as well as use of his Ar flow annealing furnace; Dr. James Eridon, for providing assistance in understanding and effectively utilizing the embedded atom simulations which he performed as part of his doctoral thesis at the U.-M.; Dr. Richard W. Smith, who developed the embedded atom computer simulation code; Dr. Victor Rotberg, for his valuable assistance in day to day operation of the Michigan Ion Beam Laboratory equipment used to perform a large portion of this work; Mr. Ali Mashayekhi, for being of inestimable assistance in virtually every aspect of laboratory operations, as well as a valuable resource for technical matters; Ms. Pam Derry, Department of Nuclear Engineering, for being the one person whom I could always count on to straighten out my frequent paperwork fiascos; and last, but certainly not least, my soulmate and confidant, Ms. Lisa Palmer, whose patience and understanding during the completion of this project deserves my deepest, heartfelt appreciation.

In addition to those mentioned above, I would like to thank my fellow graduate students at the Michigan Ion Beam Laboratory, along with those in the Nuclear Data Laboratory, for their advice, assistance, and camaraderie during my stay at the U.-M.

Funding for this project was provided by the Army Research Office, grant DAAL03-86-0052.

## TABLE OF CONTENTS

ACKNOWLEDGEMENTS.....	ii
LIST OF FIGURES.....	v
LIST OF TABLES.....	vi
ABSTRACT.....	vii
CHAPTER	
1. INTRODUCTION .....	1
1.1 Motivation for Study .....	1
1.2 Objective.....	2
2. BACKGROUND.....	2
2.1 Metastable Equilibrium.....	2
2.2 Metastable Phase Formation.....	5
2.2.1 Vapor Deposition.....	5
2.2.2 Ion Beam Irradiation .....	6
2.2.3 Thermodynamic Modeling .....	9
2.2.4 Thermal Analysis of Metastable Phase Materials.....	10
3 EXPERIMENTAL.....	11
3.1 Design of Experiment .....	11
3.2 Sample Preparation .....	13
3.2.1 Coevaporation .....	13
3.2.2 Thermal Processing.....	14
3.2.3 Ion Irradiation.....	16
3.3 Sample Analysis .....	17
3.3.1 Chemical Analysis.....	17
3.3.2 Microstructural Analysis.....	20
3.3.3 Thermal Analysis.....	22
4 RESULTS AND DISCUSSION .....	23
4.1 Amorphous-->ordered-orthorhombic transformation enthalpy measurements.....	23
4.1.1 Potential Sources of Measurement Error. ....	33
4.1.2 Effect of Sample Holder Geometry on Sample Group A1. ....	35
4.1.3 Effect of Sample Pan Distortion on Thermal Analysis.....	36

4.1.4 Embedded Atom Simulation of Amorphous Transformation	
Energies. ....	40
4.2 F.C.C. Solid Solution-->Ordered Orthorhombic Transformation	
Enthalpy Measurements. ....	44
5. CONCLUSIONS.....	53
6. FUTURE WORK.....	54
7. REFERENCES.....	55
APPENDICES.....	58

## LIST OF FIGURES

1)	Metastable Equilibrium: Free Energy vs. Atomic Configuration	4
2)	Coevaporation Schematic	15
3)	5 MeV TRIM Simulations, 1 $\mu\text{m}$ Film	18
4)	1.5 MeV TRIM Simulations, 1 $\mu\text{m}$ Film	19
5)	RBS Spectrum/Chemical Composition Profile	21
6)	5 MeV TRIM Simulation, 0.1 $\mu\text{m}$ Film	25
7)	TEM Sample Holder Schematic	26
8)	TEM SADP and Micrograph for as-Annealed Film	27
9)	TEM SADP and Micrograph for as-Irradiated Film	29
10)	DSC Thermogram for $a \rightarrow \epsilon$ Transformation	31
11)	TEM SADP and Micrograph for as-Transformed ( $a \rightarrow \epsilon$ ) Sample	32
12)	DSC Pan Processing Holders	34
13)	DSC Sample/Reference Cell Configuration	37
14)	Comparative DSC Thermograms-High/Low Quality	38
15)	Pair Distribution Functions, Crystalline and Amorphous	41
16)	Low Ion Dose DSC Thermograms	43
17)	TEM SADP and Micrograph, as-Deposited Films	45
18)	DSC Thermogram, $f.c.c. \rightarrow \epsilon$ Transformation	46
19)	TEM SADP and Micrograph of $f.c.c. \rightarrow \epsilon$ Transformation	47
20)	DSC Thermogram of as-Manufactured DSC Sample Pan	50

## LIST OF TABLES

I)	Enthalpy Data for the $\alpha \rightarrow \epsilon$ Transformation Measurements	30
II)	Enthalpy Data for the f.c.c. $\rightarrow \epsilon$ Transformation Measurements	48
III)	Simulated vs. Experimental Enthalpy Data	53

## ABSTRACT

Although metastable phase materials are of importance in a wide variety of engineering applications, much of the basic information governing the apparent "stability" of these materials and, in particular, the thermodynamic quantities associated with their formation and transformation, is poorly understood. A novel experimental technique, entitled "Thin Film Calorimetry" (TFC), has been developed, to determine the enthalpy of transformation from metastable to stable equilibrium structures in thin films. This technique has been applied to investigate metastable-->stable transformations occurring in thin films of nominal composition  $\text{NiAl}_3$ .

Elemental Ni and Al are codeposited directly onto the surface of a pure Al calorimeter sample pan to form a 0.75 - 0.90  $\mu\text{m}$  thick, extended solid solution of  $\text{NiAl}_3$ . The as-deposited microstructure in this case is a metastable configuration, and the reaction heat accompanying its transformation to the stable, equilibrium  $\epsilon$   $\text{NiAl}_3$  phase is measured directly in the calorimeter. The mean change in enthalpy,  $\Delta H$ , for a series of such measurements, is - 4.157 kcal/mole.

A second approach involves annealing the as-deposited film to form the  $\epsilon$  phase, then irradiating the as-annealed film, using 1.5 MeV  $\text{Ni}^{++}$  ions, to doses of  $\geq 5 \times 10^{15}$  ions/ $\text{cm}^2$ , to form an amorphous structure. The enthalpy associated with the transformation of this structure to the equilibrium  $\epsilon$  is then measured in the DSC. The mean  $\Delta H$  found for this reaction is - 5.023 kcal/mole. The measured values in both cases compare favorably with recent calculations performed using the embedded atom computer simulation program.

## 1. INTRODUCTION

### 1.1 Motivation for Study

Metastable materials are of vast importance in modern engineering applications. Progress in the development of high technology materials is generally incidental to the development and study of metastable phases, and in fact, few commercially important materials exist in a state of true stable equilibrium. Common examples include martensite, a metastable byproduct of diffusionless transformations observed in a variety of metallic compounds, and utilized extensively for hardening in ferrous alloys; artificially doped semiconductors; certain high  $T_c$  superconductors; and amorphous metallic compounds, which have been widely exploited for their superior magnetic and physical properties.

A host of novel metastable materials have been produced using ion irradiation. Many of these materials exhibit highly desirable properties for commercial application, while others are valuable as scientific curiosities. Due to the fact that ion beam modification is a near-surface treatment, sample thicknesses in most cases are limited to several thousand angstrom units, with 2-3 microns representing the practical limit. On this scale, characterization of mechanical and chemical properties is difficult, but techniques have been developed, and continue to evolve, which allow virtually all of the standard material properties of interest (i.e., hardness, tensile strength, fracture toughness, elastic modulus, residual stress, etc.), to be determined quite accurately. On the other hand, measurement of thermodynamic quantities associated with metastable-->stable reactions in ion beam processed materials has not been extensively pursued, due to the low heat evolution or absorption characteristics of these types of reactions, and the limit of usable sensitivity available in the majority of thermal analysis devices. Without knowledge of these thermodynamic properties, it becomes very difficult to predict the conditions necessary for

such materials to remain in a state of metastable equilibrium, and it is thus very difficult to determine their usefulness in different engineering applications.

## 1.2 Objective

The purpose of this project was to experimentally determine the enthalpies of two well-documented metastable-->stable phase transitions observed in ion-irradiated NiAl<sub>3</sub>: the amorphous-->ordered orthorhombic (€), and the f.c.c. solid solution-->€ transformation. Although this particular compound has little technological importance, it is easily amorphized using ion beam irradiation, and has been extensively studied by many researchers. Additionally, it is one of the few compounds for which atomistic simulation data is available for the reactions of interest, thereby allowing for direct comparison of experimentally measured quantities with those predicted based on theory. It thus represented a highly desirable system with which to develop and refine the experimental technique necessary to accomplish thermal analysis of thin films, a process hereafter referred to as "thin film calorimetry" (TFC).

## 2. BACKGROUND

### 2.1 Metastable Equilibrium

The classical laws of thermodynamics state that for any material of a given chemical composition, at a specified temperature and pressure, the atomic configuration with the lowest Gibbs free energy,  $G$ , will exist in a state of stable equilibrium. The Gibbs free energy of a system is characterized by the equation

$$G = H - TS,$$

1.1

where  $H$  is the enthalpy,  $T$  the absolute temperature, and  $S$  the entropy of the system. Enthalpy is the measure of the heat contained within the system, and is a function of its energy,  $E$ , pressure,  $P$ , and volume,  $V$ . It can be represented by the following equation:

$$H = E + PV. \quad 1.2$$

For condensed phases (i.e.: solids and liquids), the second term,  $PV$ , is usually quite small relative to the first, and the enthalpy may be approximated by the internal energy of the system:

$$H \approx E. \quad 1.3$$

The internal energy consists of two components, the potential and kinetic energies. In solids, kinetic energy is associated with atomic vibrations, and potential energy is a function of the atomic bonding within the system. Heat which is absorbed or evolved during a reaction will be dependent upon the associated change in internal energy.

In accordance with equation 1.1, a system will obtain its most stable state when the free energy is at a minimum, a condition which can be described as:

$$dG = 0. \quad 1.4$$

However, for any given system, it may be possible to satisfy the above condition for stability without having truly reached the absolute minimum in free energy possible for that system. This is illustrated schematically in figure 1. For this hypothetical system, two different atomic configurations are presented as a function of their respective free energies. Although the configuration with the lowest free energy,  $A$ , represents the stable state for the system, there also exists another configuration,  $B$ , whose local minimum on the free

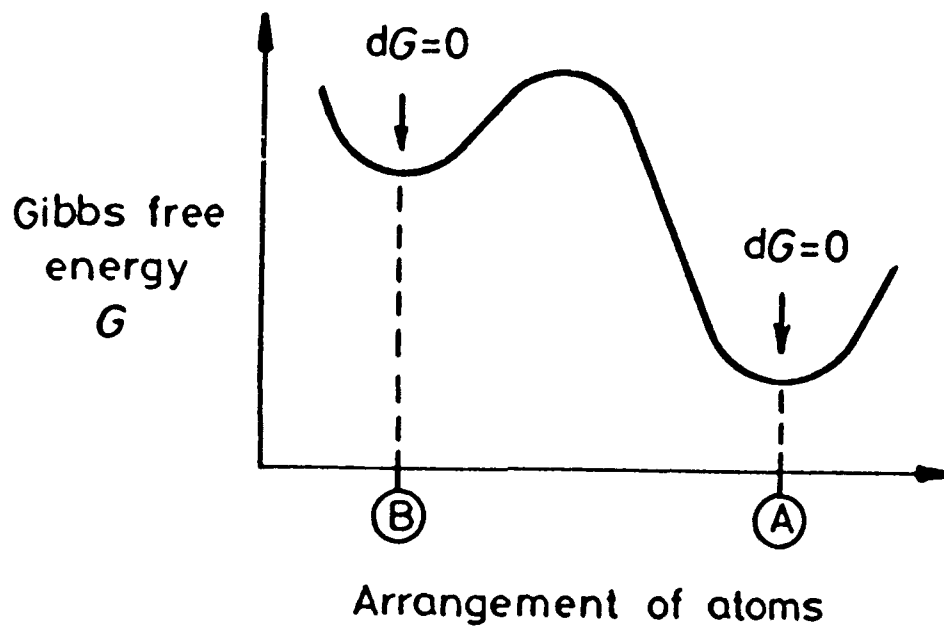


**FIGURE 1**

Gibbs free energy as a function of atomic configuration. Configuration B, while occupying a local minimum on the free energy curve, is at a higher free energy than configuration A, and is thus metastable with respect to the stable equilibrium state, A. From [1].

energy curve satisfies equation 1.4 as well. Configuration B is therefore described as a *metastable* state of this system [1]. A perfect example of this phenomenon is seen in the case of elemental carbon. At atmospheric pressure and temperature, the configuration for which the Gibbs free energy is lowest is the hexagonal, A9 crystal structure, commonly known as graphite. However, it also can exist under the same conditions in the cubic, A4 configuration, diamond, the allotropic form at high temperature and pressure.

## 2.2 Metastable Phase Formation

Metastable phases may be formed by a variety of techniques. In the work presented herein, vapor codeposition and ion beam irradiation were the methods utilized to produce the structures investigated. A discussion of the mechanisms involved in these processes, as well as the application of molecular dynamics simulations and thermal analysis to this area of materials research, follows.

### 2.2.1 Vapor Deposition

Film growth via vapor phase deposition is a commonly used technique [2]. Chemical vapor deposition (CVD), electron gun evaporation, and r.f. sputtering are popular examples. Using these methods, films consisting of a wide variety of atomic species may be deposited with a high level of consistency to various thicknesses on heated or cooled substrates. The use of high vacuums and rapid deposition rates minimize the probability of sample contamination by foreign elements.

The crystallography and structural ordering of the deposited film will depend to a large extent on the mobility of the atoms being deposited. Hence, substrate temperature can play an important role in the morphology of the resulting film. Low substrate temperature may limit atomic mobility to the extent that an atom comes to rest at or near its point of

impingement, resulting in many cases in the formation of non-equilibrium configurations, including amorphous, supersaturated solid solution, and disordered phases [3]. Similarly, high substrate temperatures may favor the formation of equilibrium structures.

Atomic species which are normally immiscible under equilibrium conditions have been formed as intimate mixtures using vapor deposition [4]. Similarly, alloys known to have limited solid solubility can be produced with solute concentrations far in excess of the equilibrium solubility limit. For instance, the equilibrium solubility of Al in Ni is  $\approx 10$  at.% at temperatures below  $620^{\circ}\text{C}$ . However, Al/Ni films which were electron gun codeposited onto substrates held at  $90^{\circ}\text{C}$  retained the f.c.c. Ni lattice structure at compositions in excess of 30 at.% Al, a solute composition which would normally be characterized by the presence of both the  $\gamma'$  (ordered f.c.c.), and  $\beta'$  (ordered b.c.c.), phases [5]. Other studies of the same system, using films sputter deposited on  $\text{LN}_2$  cooled substrates, have shown that at this low temperature, formation of all of the equilibrium intermetallic compounds ( $\gamma'$ ,  $\beta'$ ,  $\delta$  and  $\epsilon$ ), is suppressed, with only the disordered f.c.c. and b.c.c. structures observed [6]. In a similar vein, the equilibrium solubility of Ni in Al at temperatures below  $620^{\circ}\text{C}$  is limited to 0.02 at.%. Studies involving techniques identical to those listed above have shown retention of the f.c.c. Al lattice at Ni concentrations ranging from 0 to 40 at.% [7]. Thus, for many alloy systems, quenching from the vapor state allows for solubility limits well extended over those observed for liquid quenching, and greatly extended beyond those documented for equilibrium conditions.

### 2.2.2 Ion Beam Irradiation

In comparison to all other techniques of metastable phase production, ion irradiation offers the unique capability of introducing virtually any atomic specie into any host lattice, under athermal conditions. Indeed, many new, previously inaccessible alloys, both equilibrium and non-equilibrium, have been prepared and studied using this method [8,9].

Two dominant mechanisms govern the nature and extent of ion-induced changes observed in irradiated materials: physical microstructural alteration, and chemical compositional alteration. Since the scope of this research relies primarily on the former process, this discussion will be limited to the nature of the physical ion/solid interactions.

Ion species accelerated in the keV energy range impinge on the target substrate with energies generally approaching four to five orders of magnitude greater than the binding energy of the host atoms. As the ion traverses the substrate, this energy is dissipated through ballistic interactions with the lattice atoms, resulting in a localized "collision cascade"[10]. The collision events which occur during this process result in the introduction of point defects, such as vacancies and self-interstitials, and the penetrating ion is completely thermalized within  $10^{-11}$  to  $10^{-13}$  seconds [11,12]. If the substrate temperature is sufficient to activate defect recombination processes, the affected region will move toward a state of thermodynamic equilibrium. In situations where there is insufficient activation energy for defect annihilation, the radiation damage is in effect "frozen in" to the host material. It follows that, with sufficient accumulation of such defects, the free energy of the system may be elevated to levels where, consistent with figure 1, it becomes energetically favorable for the host atoms to rearrange into alternate configurations, thus entering states of metastable equilibrium. The formation of polymorphic, quasi-crystalline, disordered, and amorphous phases resulting from this process is typically observed.

Ion-induced transformation of intermetallic compounds has attracted the attention of many researchers [13,14,15]. Several binary metallic systems, in which a number of intermetallic equilibrium phases may be observed, have been investigated. Certain intermetallics have been demonstrated to completely amorphize under proper irradiation conditions, while others simply transform into alternate crystal structures, irregardless of dose, temperature, or irradiating specie or energy. Knowledge of the parameters governing the amorphization process has been aggressively pursued, with the result being the

establishment of a set of empirical rules, contributed to by several different individuals, which, although not entirely accurate in their predictive quality, offer a basis by which such compounds may be evaluated with respect to their ease of amorphization via ion irradiation [16,17,18]. A complete review of these rules would be impossible in the context of this work; one may be found in the article by D.M. Follstaedt [19]. However, two of the criteria for ion beam induced amorphization have been more widely verified, and are thus of interest here. The first states that easily amorphized compounds exist over a chemical composition range of less than a few atomic percent [20]. This makes intuitive sense from a thermodynamic perspective, since, when atomic disorder is introduced in such a compound (for instance, a line compound), local perturbations in solute concentration will arise, significantly increasing the free energy of the system. The second suggests that compounds with complex equilibrium crystal structures will be more readily transformed [21]. The rationale in this case is that additional time is required for the more complex crystalline structures to nucleate subsequent to a disordering event. During the extremely rapid quench of the affected zone following the collision cascade, if atomic mobility is insufficient to achieve the equilibrium configuration, formation of the crystalline phase will be inhibited.

The underlying concept which governs the susceptibility of a particular system to achieve metastability under ion bombardment is the rise in system free energy corresponding to the increase in defect density introduced during irradiation. It follows that any such change in atomic configuration can be correlated to a specific change in free energy of the system. Since, for transformations in the crystalline state, the change in configurational entropy,  $S$ , is relatively small, the dominant component of equation 1.1 is  $H$ , the enthalpy of the system [22]. Thus,  $\Delta G$  will be directly proportional to  $\Delta H$ , which, as mentioned previously, depends primarily upon the atomic bonding energies of the stable and metastable phases [23]. The effective "stability" of the metastable phase, in turn, will be dictated by the amount of energy necessary to transform it back to the equilibrium form,

a quantity which will be exactly equivalent to and opposite that necessary for its initial formation from the same starting structure.

### 2.2.3 Thermodynamic Modeling

Information regarding formation heats of a wide variety of compounds is available in standard thermochemical reference texts [24,25]. However, only limited information exists concerning metastable phase materials, and virtually none can be found with respect to the several newly discovered phases exclusive to ion beam processing. This general lack of such thermodynamic information has led to the development of computer models, by which detailed calculations involving interatomic potentials may be performed, resulting in prediction of the desired thermodynamic information [26,27,28]. The usefulness of the computed values from these simulations depends to a large extent on the validity of the interatomic potentials utilized. Great advances have been made in the last decade in improving the accuracy of the derived values for these potentials in metallic systems, and very sophisticated programs have evolved concomitant to the increase in computing speed available in modern computers [29]. Traditional methods, involving the use of pair potentials to simulate interatomic forces in metals, have been proven deficient in many aspects. A more recently developed approach relies on the use of pairwise potentials plus an additional term, which provides for consideration of the local electron density sensed by each lattice atom, or the "embedding energy". This model has been named the "Embedded Atom" (EA), model [30].

The EA model treats each atom in the crystal as an 'impurity', whose energy is described by the following equation:

$$E_{\text{tot}} = \sum F_i(\rho_i) + 1/2 \sum \phi_{ij}(r_{ij}) \quad 2.2.3.1$$

where:

- $F_i$  = energy of 'impurity' atom  $i$  as a function of electron density at site  $i$ , otherwise referred to as the 'embedding energy',
- $\rho_i$  = host lattice electron density at site  $i$ ,
- $\phi_{ij}$  = repulsive potential between atoms  $i$  and  $j$ ,
- $r_{ij}$  = distance between atoms  $i$  and  $j$ .

The first term in the equation considers the electronic interaction of the 'impurity' atom with the surrounding lattice, or 'host' atoms, and as such is generally negative. The second term deals with the core-core electrostatic interaction (repulsion) between the atoms. Based on this relationship, the total energy of any crystal of a given composition and structure may be computed. Therefore, energies of both stable and metastable configurations of the same atomic composition may be determined, their difference being equal to the enthalpy of transformation.

Using the EA model, simulations of the formation energies of the intermetallic compounds found in the Ni-Al system have been performed [31,32]. Also, it has been applied by at least one group to the calculation of formation enthalpies for the ion beam-induced metastable phases currently known to exist in this system [33]. These latter computed values are used herein for comparison to the experimental data obtained for NiAl<sub>3</sub>.

#### 2.2.4 Thermal Analysis of Metastable Phase Materials.

Differential Scanning Calorimetry (DSC), is a widely used technique for obtaining quantitative thermodynamic data for various reactions in many different material systems. Due to its high sensitivity, accuracy, and precision, compared to other calorimetric measurement devices, the DSC is the instrument of choice for materials research where constraints are imposed due to small sample masses or reaction heats. Since both

constraints are typically encountered for materials prepared using rapid solidification processes (RSP), the technique has been widely applied in this area.

Metastable materials prepared by rapid quenching, melt spinning, r.f. sputtering, triode sputtering, solid state reaction, and mechanical alloying have been characterized using DSC [34-38]. Sample masses typically examined in these cases were  $\geq 10\text{mg}$ , although in the case of the solid state reaction studies, masses of  $\geq 0.2\text{mg}$  were successfully utilized. In general application, masses of 10-1000+mg are the norm.

Limited work using DSC has been performed on elemental Si samples which were amorphized using ion beam irradiation [39,40]. Here, sample masses of  $\approx 0.5\text{mg}$  were studied, and the enthalpy of transformation from the amorphous to crystalline state was measured. Similar work involving ion beam modified materials is rare, due to the difficulty involved in gathering sufficient sample masses to allow reasonably reliable measurements to be performed. The above referenced work involving studies on amorphous Si (a-Si), is somewhat anomalous in this context, due to the fact that the amorphous samples studied were prepared by directly bombarding the surface of relatively thick Si discs, using  $\text{Si}^+$  ions. This processing scheme alleviates the problem of having to separate the processed film layer from the processing substrate, one of the major obstacles encountered in previous attempts at preparing DSC samples of ion beam processed materials [41,42]. However, it also introduces an additional heat transfer barrier to be overcome prior to registration of the heat signal by the calorimeter. Additionally, amorphization of a pure element via ion irradiation is an extremely rare phenomenon, observed to date only in the elements Si and Ge.

### 3 EXPERIMENTAL

#### 3.1 Design of Experiment

A great deal of work has been performed to document the experimental conditions necessary for metastable phase formation in the Ni-Al system, using ion beam irradiation [43,44]. However, literature regarding calorimetry of binary metallic, ion beam modified thin films is non-existent. As such, few precedents were available with which to guide development of a workable experimental technique. Additionally, there was concern that the presence of a substrate, as in the previous a-Si studies, might result in an unacceptable contribution to the background noise level, and should therefore be avoided. The requirements which served as *initial* guidelines for the experimental design were thus as follows: 1) To generate sample masses of  $\geq 1\text{mg}$ , in order to obtain a useful instrumental sensitivity for the reactions of interest; 2) To examine transformations whose predicted enthalpies were relatively large, to further enhance usable instrument sensitivity; 3) To generate self supporting (i.e., "free standing"), sample films, to avoid substrate noise contributions to the DSC signal; and 4) To regulate irradiation conditions such that the irradiating ions would completely traverse the target film, in an effort to prevent any alteration of sample stoichiometry.

$\text{NiAl}_3$  was selected for this study, due to the fact that it is the most easily amorphized intermetallic in the Ni-Al system, and has no intermediate transformation products. To satisfy condition #1, calculations based on the density of  $\text{NiAl}_3$ , and film thickness limitations to allow for complete through-penetration of the irradiating ion, resulted in required sample dimensions of  $1\text{ cm}^2$  area by  $1\mu\text{m}$  thickness. In order to satisfy condition #3, it was necessary to select a substrate for vapor deposition from which the deposited film could be easily removed, subsequent to processing. Consequently, single crystal NaCl was selected as a substrate material, due to its common availability in  $1\text{ cm}^3$  size, and ease of aqueous dissolution.  $\text{Ni}^{++}$  was chosen as the irradiating ion, since it could be easily accelerated to energies necessary to satisfy condition #4, based on the available energy capabilities of the General Ionex 1.7 MeV Tandem accelerator used in this work. An added advantage of using this ion was its chemical compatibility with the film species.

Using this approach, sample films of the desired composition were prepared by coevaporation onto cleaved 1-2mm thick NaCl substrates, to thicknesses of  $\approx 1\mu\text{m}$ . The films were then irradiated using 5MeV  $\text{Ni}^{++}$  ions, to doses ranging from 0.001 to  $5 \times 10^{17}$  ions/ $\text{cm}^2$ , to form the desired amorphous phase. Attempts to retrieve the sample film, intact, both before and after this step, via dissolution of the NaCl substrate in water, proved impossible. In every case, as the film began to separate from the dissolving substrate, it immediately dispersed into a myriad number of very fine granules, which proved impossible to collect from the surface of the solvent media. This effect is due to the retention of a high degree of residual stress within the sample films, a well-documented artifact of the vapor deposition process [45,46]. Even when collection of a small number of granules, through extremely tedious straining methods, was possible, the further requirement of subjecting the collected granules to a number of rinsing cycles (decontamination), sufficient to remove the remaining brine residue, effectively prevented any further pursuit of this technique. It was then determined that deposition of the sample films directly onto the DSC sample pan surface would provide a means by which the above problems could be avoided, and also obtain the most desirable sample film/pan heat transfer interface for thermal analysis.

### 3.2 Sample Preparation

#### 3.2.1 Coevaporation

Sample films of nominal atomic composition  $^{23}\text{Ni}$ -77Al were deposited using a multiple hearth, dual electron gun source, in a cryo-pumped chamber holding a base vacuum of  $0.5 - 5 \times 10^{-7}$  Torr. The presence of a small amount of residual Al (2-3 atomic % for all samples produced), was desirable, as previous studies [47,48] have demonstrated that, under conditions where insufficient Al was available for complete reaction with Ni to

form  $\text{NiAl}_3$ , intermediate phases, such as  $\text{Ni}_2\text{Al}_3$ , were also formed. The presence of such intermediates, which have been found to undergo ion-induced transformations of their own [29], is much less desirable than the small Al residue, which does not polymorphically transform under these conditions. Both species were simultaneously deposited (coevaporated), at independently controlled evaporation rates of 1.0 Å/sec (Ni), and 4.3 Å/sec (Al), to thickness equivalents of  $\approx 1.6$  and 6.9 kÅ, respectively, resulting in total film thicknesses of  $\approx 0.80$ -0.90  $\mu\text{m}$ . Monitoring of the individual evaporation rates and corresponding thicknesses was accomplished using water-cooled, quartz crystal thickness monitors, which were isolated by means of a simple shield arrangement, to "see" only the evaporation source of interest. This arrangement is schematically represented in figure 2. Evaporation rate control was achieved via a feedback loop which varied e-gun power input, based on the independently monitored evaporation rate of the respective elements. Using this method, the Ni evaporation rate was observed to vary  $\pm 10\%$  of the programmed value, with the Al rate being considerably more erratic, commonly  $\pm 20$ -25% of the desired value. Variation in electron gun evaporation rates of this order is not uncommon for materials like Al, which have low densities and high thermal conductivities. Bulk film composition was, however, not significantly affected by this seemingly high rate of fluctuation, as the individually programmed thickness limits were obtained in all cases, and are more precise indicators of overall film composition. Deposition substrates consisted of as-manufactured, pure Al, Perkin-Elmer DSC sample pans and lids. No attempt was made to control substrate temperature during the deposition process.

### 3.2.2 Thermal Processing

Subsequent to film deposition, samples intended for use in the investigation of the amorphous-->ordered ( $\epsilon$ ) transformation were annealed at 500°C for two hours. This

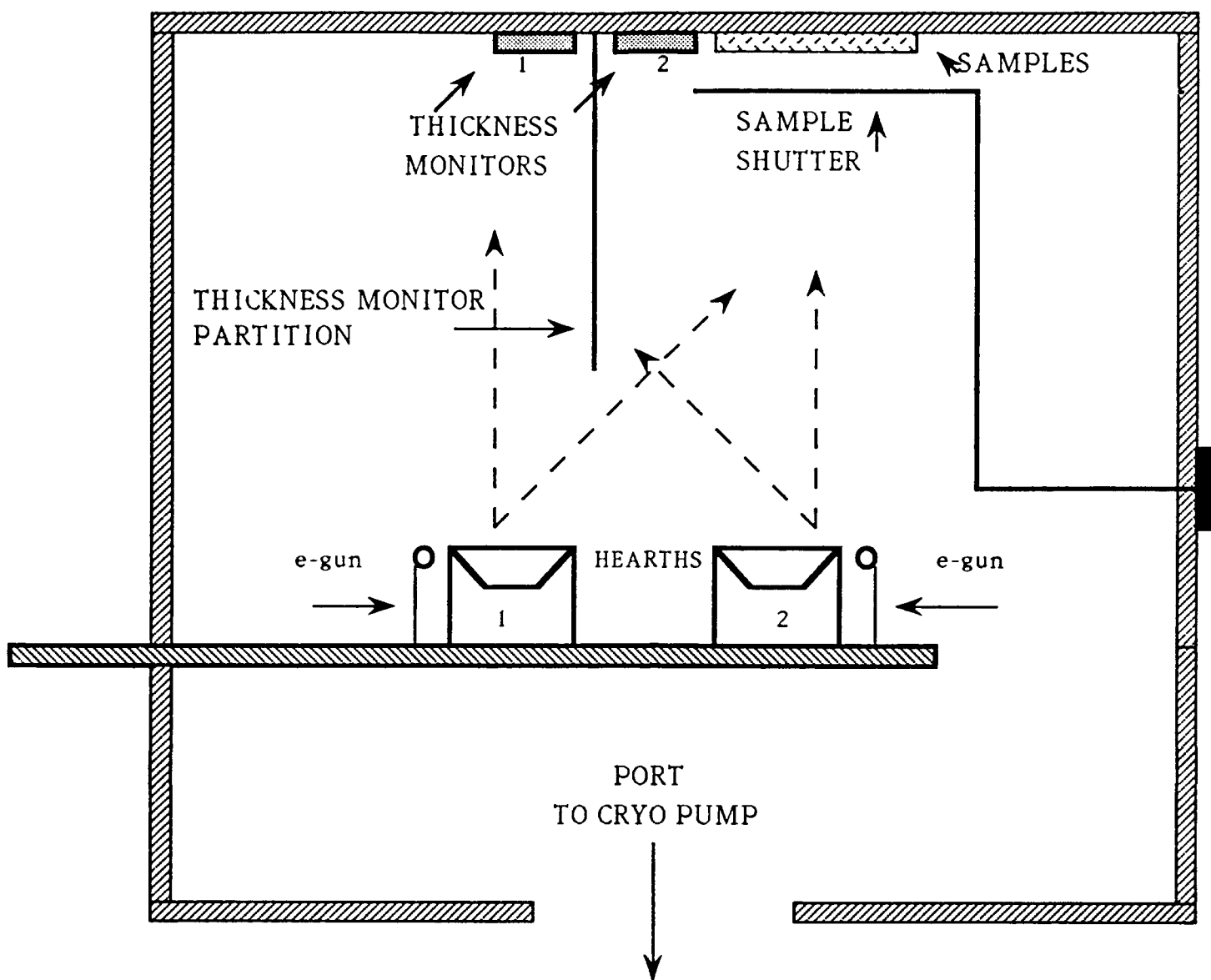


**FIGURE 2**

Schematic of coevaporation chamber arrangement. Thickness monitors are isolated to register evaporation rates of the individual hearths, while samples are situated such that both elements are simultaneously deposited.

treatment was sufficient to form the stable intermetallic compound,  $\text{NiAl}_3$ . Annealing was performed in a Ti-gettered, high purity Ar flow tube furnace, to minimize the possibility of contamination. In order to avoid unnecessary thermal shock, the samples were introduced into the furnace at room temperature, and slowly ramped to the anneal temperature. At the completion of the heat treatment, the samples were allowed to furnace cool. The slow heating and cooling cycles were performed as a precautionary measure, to avoid possible delamination of the sample films due to thermal mismatch with the substrate.

### 3.2.3 Ion Irradiation

Sample films were irradiated with  $\text{Ni}^{++}$  ions under two different sets of irradiation conditions: 1) 5 MeV accelerating energy; 1.0-1.4  $\mu\text{A}$  current on target; 0.1, 0.5, 1, 5, 10, 50, and  $100 \times 10^{15}$  ions/ $\text{cm}^2$ ; 2) 1.5 MeV energy; 200-400 nA current on target; 5, 6, 8, 10, and  $20 \times 10^{15}$  ions/ $\text{cm}^2$ . For the first set of conditions, simulations performed using TRIM (The Stopping and Range of Ions in Matter) software [55], showed complete film penetration by the irradiating ions. Mean ion range was computed to be 2.15  $\mu\text{m}$ , placing the concentration profile well into the substrate material. Ion-induced damage at the film surface was found to be  $\approx 0.2$  target displacements/ion/ $\text{\AA}$ , and increased fairly uniformly to a value of  $\approx 0.4$  at the maximum deposited film depth. Preliminary investigations using 1000 $\text{\AA}$  thick films deposited on Cu grids, and irradiated under duplicate conditions, showed complete amorphization of the target film, as verified with electron diffraction information. It was therefore assumed that the entire film thickness, in the case of the 8-9k $\text{\AA}$  samples, would amorphize under similar conditions, as even the depths with the lowest ion-induced damage values (i.e., the surface), had been observed to transform in the preliminary work.

Simulations performed for the second set of conditions showed an ion concentration peak at  $\approx 7400\text{\AA}$  in the film. Ion-induced damage, as measured in total target

displacements/ion/Å, was computed to be  $\approx 0.6$  at both the film surface (depth = 0Å), and the film/substrate interface (depth=7800-9000Å), with a peak value of  $>1.0$  found at a depth of  $\approx 6000$ Å. These data for both sets of conditions are graphically represented in figures 3 and 4. The reason for the variation in irradiating conditions will be addressed in the results and discussion section.

Target chamber pressure in all cases was between  $1-5 \times 10^{-8}$  Torr, and all irradiations were performed at room temperature ( $\approx 300$ K). The DSC pans which comprised the sample film substrates were retained in individual recesses in a solid Al holder which was used for both the vapor deposition process and the irradiations. The holder used for the irradiation studies was configured so as to prevent the deposition of material, due to shadowing of the evaporation source by the sample retaining plate, on the sides of the sample pan, which would then lie unexposed to the irradiating beam, and prevent complete amorphization of the deposited film. This modification was not necessary for the case of the samples prepared for as-evaporated transformation studies.

### 3.3 Sample Analysis

#### 3.3.1 Chemical Analysis

Rutherford Backscattering Spectroscopy (RBS) was utilized to verify chemical composition of the sample films. Spectra were obtained using 2 MeV  $\text{He}^+$  ions, beam direction normal to the sample surface, with a detector-to-beam angle of  $25^\circ$ . Multi-Channel Analyzer (MCA) calibration was performed prior to each analysis, using backscattered energies from pure Au, Ni, and Al target foils. A representative RBS spectrum is shown in figure 5a. Spectrum-fitting simulation performed using RUMP simulation software [56], allowed positive composition determination to an accuracy of within  $\pm 1\%$ , and is seen in the figure as the dashed line. The sample composition profile

**TRIM-89**

Command: SB, E, P, V, L, N, F2

Version: 5.7

Ion-Ni 58 5 MeV

1- NiAl<sub>3</sub>

-4.25 g/cm<sup>3</sup>

Target 2- Al substrate

Layers 3- -2.7 g/cm<sup>3</sup>

3-

Ion Number : 1057

Ion Energy : 1.93 MeV

Cascade E : 0 eV

Backscatter: 0

Transmit. : 243

AVERAGES

Mean Range : 2.15  $\mu$ m

Straggling : 3068  $\text{\AA}$

Vac./ Ion : 10131

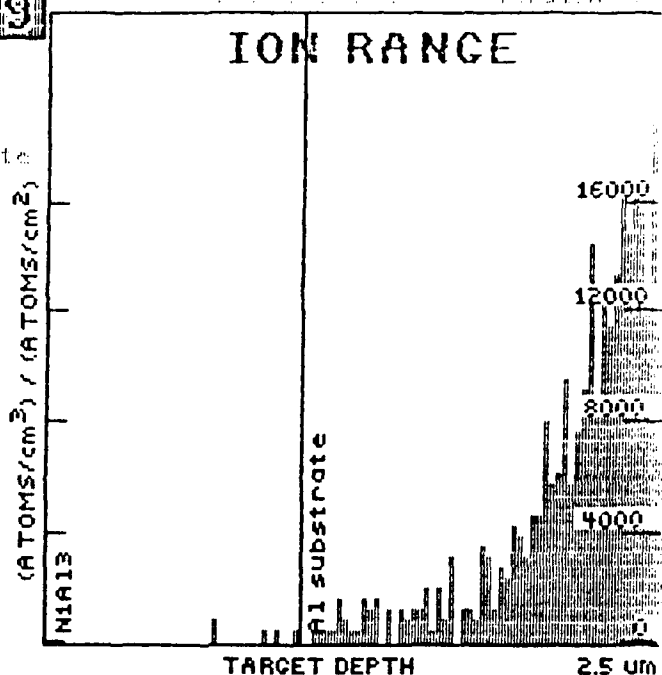
ENERGY LOSS (%)

IONS RECOILS

Ioniz.: 77.9 9.8

Vac. : 3 4.8

Phon. : 2 7.1 0



**A**

**TRIM-89**

Command: SB, E, P, V, L, N, F2

Version: 5.7

Ion-Ni 58 5 MeV

1- NiAl<sub>3</sub>

-4.25 g/cm<sup>3</sup>

Target 2- Al substrate

Layers 3- -2.7 g/cm<sup>3</sup>

3-

Ion Number : 1057

Ion Energy : 1.93 MeV

Cascade E : 0 eV

Backscatter: 0

Transmit. : 243

AVERAGES

Mean Range : 2.15  $\mu$ m

Straggling : 3068  $\text{\AA}$

Vac./ Ion : 10131

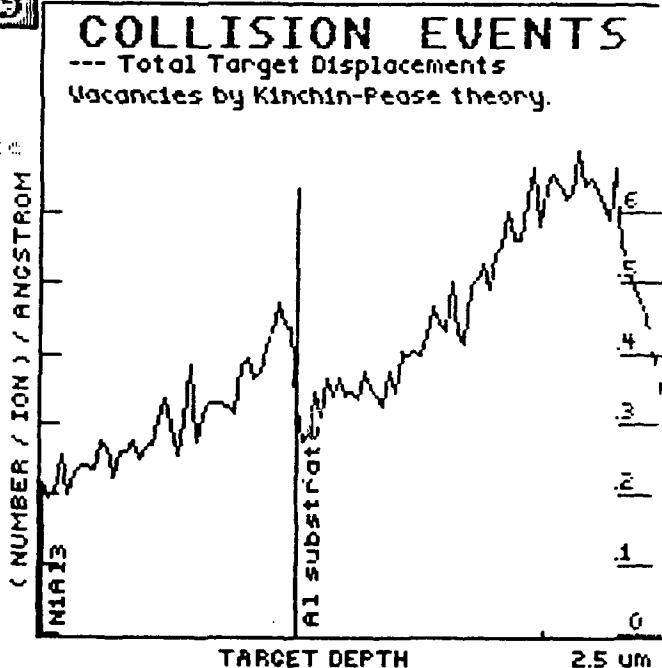
ENERGY LOSS (%)

IONS RECOILS

Ioniz.: 77.9 9.8

Vac. : 3 4.8

Phon. : 2 7.1 0



**B**

**FIGURE 3**

TRIM simulation for 5 MeV Ni ion irradiation of 1  $\mu$ m layer of NiAl<sub>3</sub> on surface of Al DSC pan. A) Mean ion range simulation. B) Target displacements (damage profile) simulation.

**TRIM-8.9**

Command: SB, E, R, V, E, N, F2

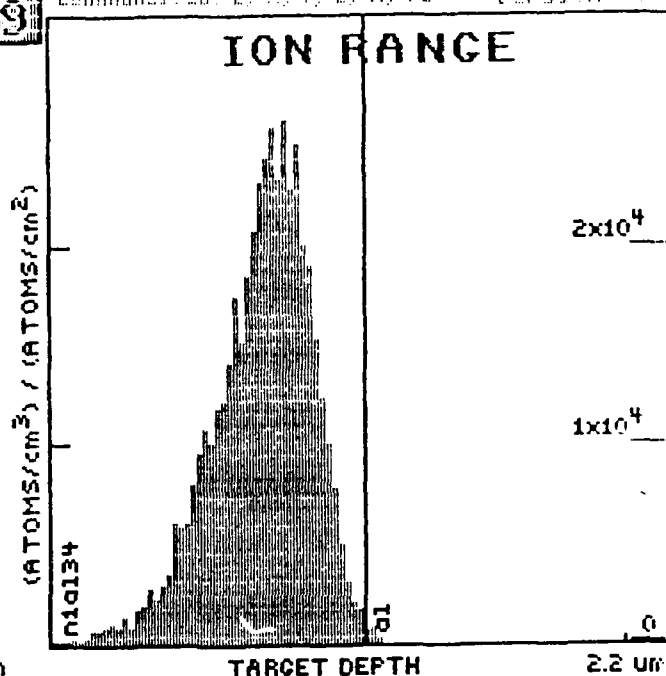
Version: 1.0

Ion-Ni 58 1.5 MeV  
1-ni0134  
-4.25 g/cm3  
Target 2-al  
Layers 3-  
-2.7 g/cm3  
3-

Ion Number : 5090  
Ion Energy : 294. keV

Cascade E : 0 eV  
Backscatter: 0  
Transmit. : 0

AVERAGES  
Mean Range : 7404 Å  
Straggling : 1741 Å  
Vac./ Ion : 7516  
ENERGY LOSS (%)  
IONS RECOILS  
Ioniz.: 50.2 19.4  
Vac. : .6 11.9  
Phon. : .3 17.8

**A****TRIM-8.9**

Command: SB, E, R, V, E, N, F2

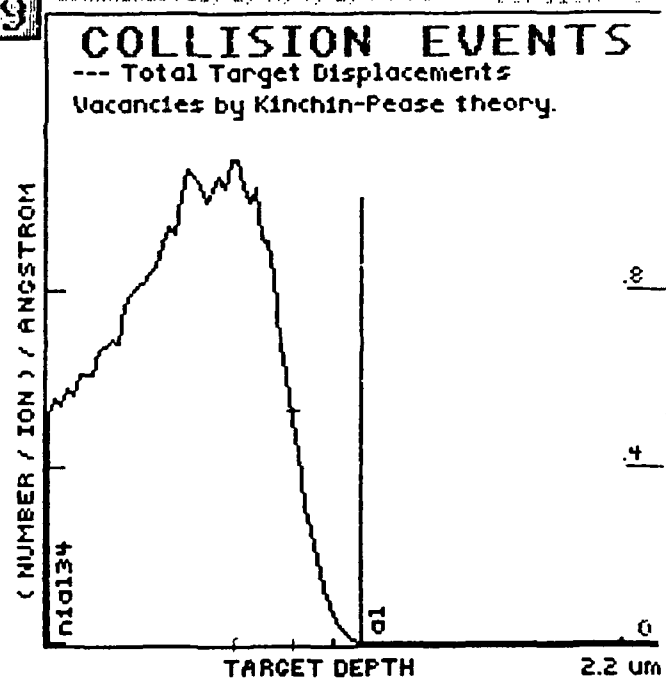
Version: 1.0

Ion-Ni 58 1.5 MeV  
1-ni0134  
-4.25 g/cm3  
Target 2-al  
Layers 3-  
-2.7 g/cm3  
3-

Ion Number : 5090  
Ion Energy : 294. keV

Cascade E : 0 eV  
Backscatter: 0  
Transmit. : 0

AVERAGES  
Mean Range : 7404 Å  
Straggling : 1741 Å  
Vac./ Ion : 7516  
ENERGY LOSS (%)  
IONS RECOILS  
Ioniz.: 50.2 19.4  
Vac. : .6 11.9  
Phon. : .3 17.8

**B****FIGURE 4**

TRIM simulation for 1.5 MeV Ni ion irradiation of 1 uM layer of NiAl<sub>3</sub> on surface of Al DSC pan. A) Mean ionic range simulation. B) Target displacements (damage profile) simulation.

on which the simulation is based is shown in figure 5b. No Al enrichment was observed in post-anneal spectra for any of the sample groups. This was of concern, since the anneal temperatures are very significant relative to  $T_m(\text{Al})$ . However, as documented by previous research, the native oxide layer present on the surface of pure Al ( $\approx 30\text{-}40\text{\AA}$ ), is an extremely effective barrier to diffusion, even at these elevated temperatures [49].

### 3.3.2 Microstructural Analysis

Transmission Electron Microscopy (TEM), was relied upon for phase verification after each step of the processing sequence. A JEOL 2000FX analytical electron microscope, operating at 200 kV, was utilized, both in bright field imaging mode, for determination of grain size and morphology, and electron diffraction mode, for determination of crystallographic structure. Samples for TEM analysis were prepared as follows:

- 1) 3 mm diameter discs were core drilled from the as-deposited, as-annealed, as-irradiated, and as-transformed films on the DSC pans.
- 2) Stop-off lacquer was applied to the film surfaces, and the discs were electrochemically jet-thinned from the substrate side, using a solution consisting of 6%  $\text{HClO}_4$ , 35% butyl cellosolve, and 59% methanol, by volume. Solution temperature was held between 0 and 9°C.
- 3) After perforation, the stop-off lacquer was removed from the film surface by dissolution in acetone. Samples were then rinsed in methanol and allowed to air dry.

Samples thus prepared were then examined as described above, in order to provide an exact correlation between processing history and microstructural evolution. The rationale for reliance upon the electron diffraction information gathered from the nearest-surface regions of the film (the regions made electron transparent through the back-thinning

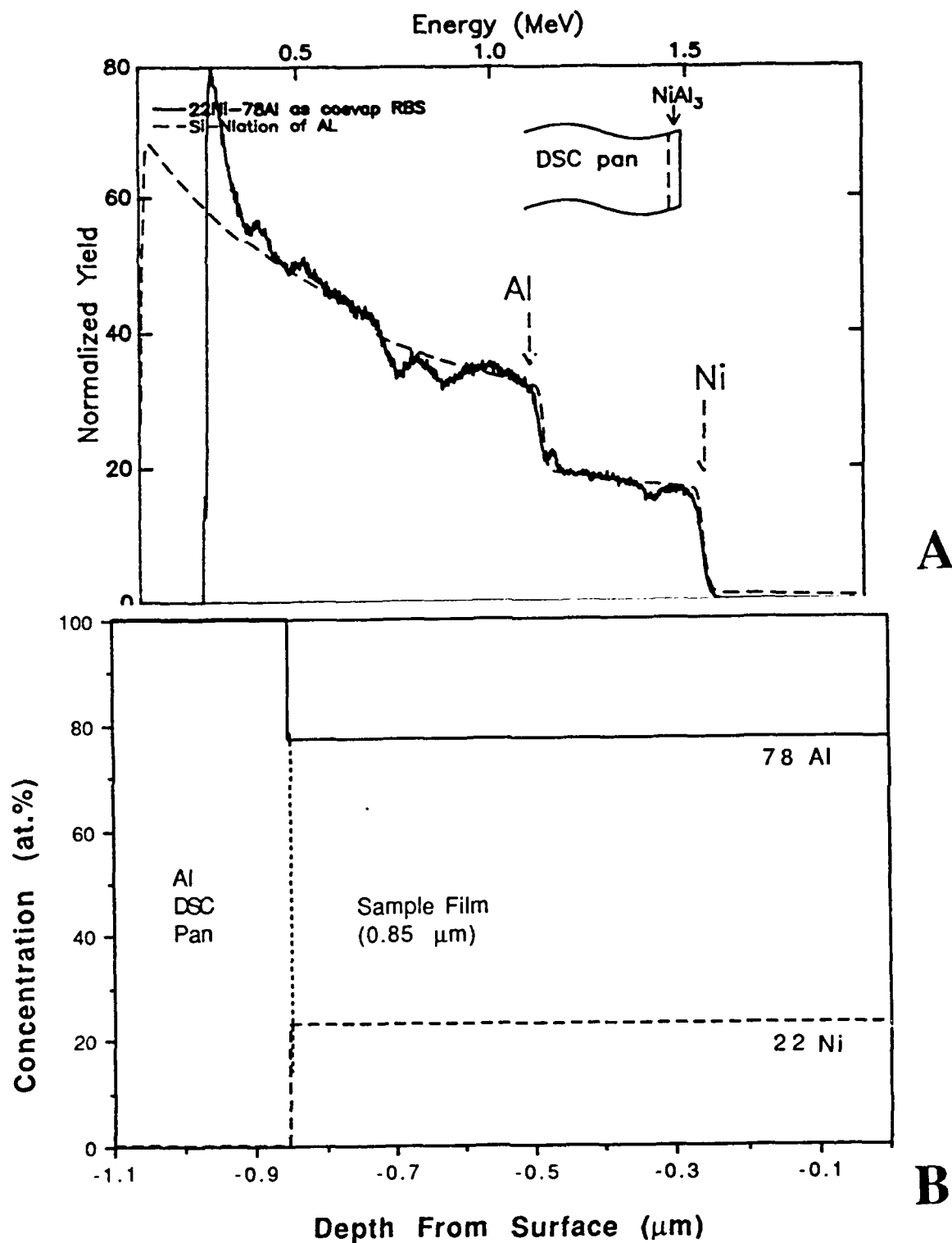


**FIGURE 5**

A) As-deposited RBS spectrum for composition 22Ni-78Al. Dashed line is RUMP simulation. Discontinuities in raw spectrum due to variation in elemental evaporation rates. B) Average chemical composition profile used to generate RUMP simulation fit.

process), as characteristic of the microstructure of the entire film thickness, has been discussed in the previous section.

### 3.3.3 Thermal Analysis

Enthalpies associated with the metastable-->stable transformations of interest were measured using a Perkin-Elmer DSC-7 Differential Scanning Calorimeter, with quantitative analysis provided by TASC-7 software. Sample cells were flushed at all times with dry nitrogen. Sample pans were weighed before and after film deposition, to obtain net sample weight, using a Perkin-Elmer AD- 4 Microbalance. After limited experimentation with different heating rates of 5, 10, 15, and 20°C/min, a rate of 10°C/min was chosen for the bulk of the DSC work. Similarly, after verification of the approximate transition temperatures for the reactions of interest, a temperature scanning range of 50-275°C was selected.

The DSC output represents the net energy (heat), released as a result of the phase transformation which occurs in the sample holder. The temperature of both the sample and an inert reference material is increased, using independently controlled heating units, at a constant rate,  $dT/dt$ , programmed by the operator. Temperatures of both cells are monitored independently, and power input to the cells is constantly varied to maintain a zero temperature differential. When a temperature difference arises between the sample and reference, due to an exo- or endothermic reaction in the sample, the power is adjusted to instantaneously compensate for this difference. A signal proportional to the heat input difference,  $dH/dt$ , between the sample and reference, is recorded. Thus, the DSC output consists of this signal,  $dH/dt$ , represented as heat flow, versus temperature (or time). The area of any peak which results from a reaction in the sample cell may be integrated, the resulting value representing the change in enthalpy,  $\Delta H$ , of the corresponding transformation.

In order to exactly duplicate all conditions between the reference and sample cells, except for the metastability of the sample itself, the reference cell was loaded with samples of thermally equilibrated  $\text{NiAl}_3$  ( $\epsilon$ ), in masses equivalent to those used in the sample cell. Generation of a baseline curve, a common method employed in DSC work with reversible transformations, was not necessary in this case. Due to the irreversibility of the amorphous-->ordered and disordered-->ordered transformations in the samples of interest, a second scan (post-transformation), was run on every sample, then subtracted from the first scan, to give the net heat release measured during the reaction.

## 4 RESULTS AND DISCUSSION

### 4.1 Amorphous-->ordered-orthorhombic transformation enthalpy measurements.

As described in section 3.2.3, two sets of irradiation conditions were employed for preparation of the amorphous films. The first set of conditions (5 MeV, 1-1.4  $\mu\text{A}$  on target), failed to amorphize the DSC samples, in contradiction to the findings of preliminary experiments (section 2.2), performed for the purpose of verifying the appropriateness of these processing parameters.

The preliminary studies were performed using a processing scheme developed in order to satisfy the initial guidelines for this research, outlined in section 3.1. Hence, 5 MeV ions were required to insure complete translation of the film thickness,  $\approx 1 \mu\text{M}$ , and a target current of  $\geq 1 \mu\text{A}$  was necessary to complete the irradiations in a reasonable time frame. These studies were performed using 1000 $\text{\AA}$  thick films, deposited on Cu TEM grids, to allow for straightforward TEM examination subsequent to irradiation. This served the purpose of allowing direct examination of the sample region exposed to the *least* amount of radiation damage, as determined using TRIM simulations, Figure 6, by ions of this energy.

Hence, amorphization of this thickness would correspond to amorphization of the entire thickness for the 1  $\mu\text{m}$  samples.

The TEM grid holder used for these initial studies is shown in figure 7. In this configuration, the ions completely traversed the sample film, terminating in the Cu backing disc. The Cu TEM support grid was in loose contact with, and the sample film was located (in relative terms), quite far from, the backing disc. Thus, heat buildup within the sample film was minimal, and the amorphous configuration was easily formed. However, in the case of the  $\approx 1\mu\text{m}$  thick films, direct-deposited onto the DSC pan surface, heat transfer between the pan and film was optimal, and thus the films were self-annealed during the course of the irradiation, preventing the formation of the amorphous structure. The selected area diffraction pattern (SADP) for this self-annealed, equilibrium orthorhombic structure is shown in figure 8, along with the corresponding TEM micrograph, indicating average post-anneal grain sizes of 500-800nm. Hence, regardless of ion dose, no change in the as-annealed film structure was observed for these samples.

As a result, the decision was made to change the requirement for complete ion penetration of the sample film, as the actual compositional variation which would result from the incorporation of Ni at the targeted doses amounts to  $\leq 1$  at.%, well within the limits of accommodation based on the amount of residual Al available in the sample films. By allowing for Ni termination within the thickness limits of the sample film itself, a substantial reduction in beam energy, along with a significant increase in ion-induced damage (refer figure 5), would be achieved.

Through use of TRIM simulations and actual experimentation, optimal processing conditions, corresponding to those outlined in the second set of irradiation conditions in section 3.1.3, were established. As such, maximum power input to the target samples was held in most irradiations to  $\leq 0.3$  W (200 nA on-target). TEM examination of samples processed under these conditions indicated the presence of the desired amorphous phase in all films irradiated to a dose of  $\geq 5 \times 10^{15}$  ion/cm<sup>2</sup>. Selected area diffraction patterns



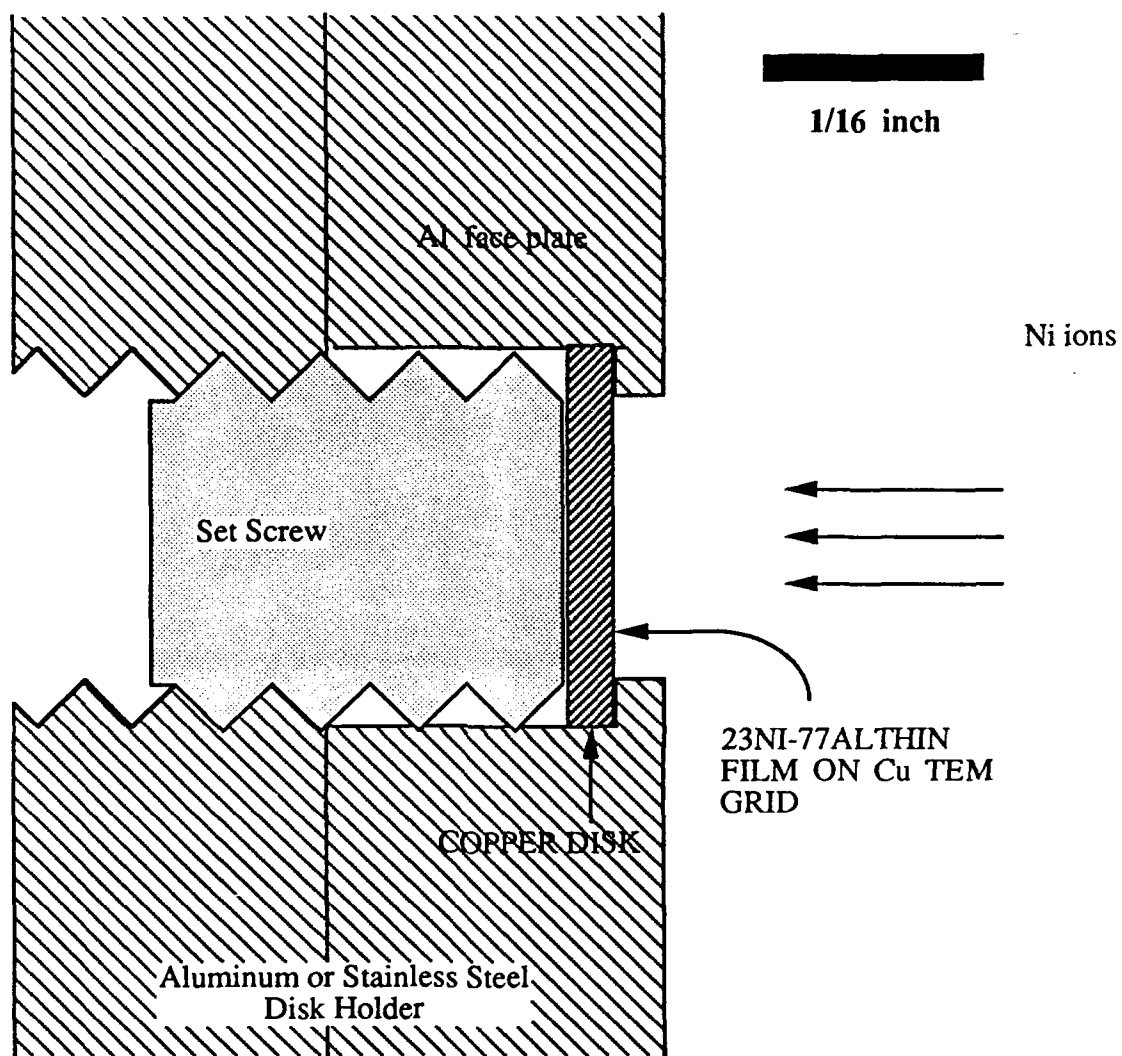


**FIGURE 7**

Sample holder schematic for preliminary TEM studies performed on 1000Å films supported on Cu grids.

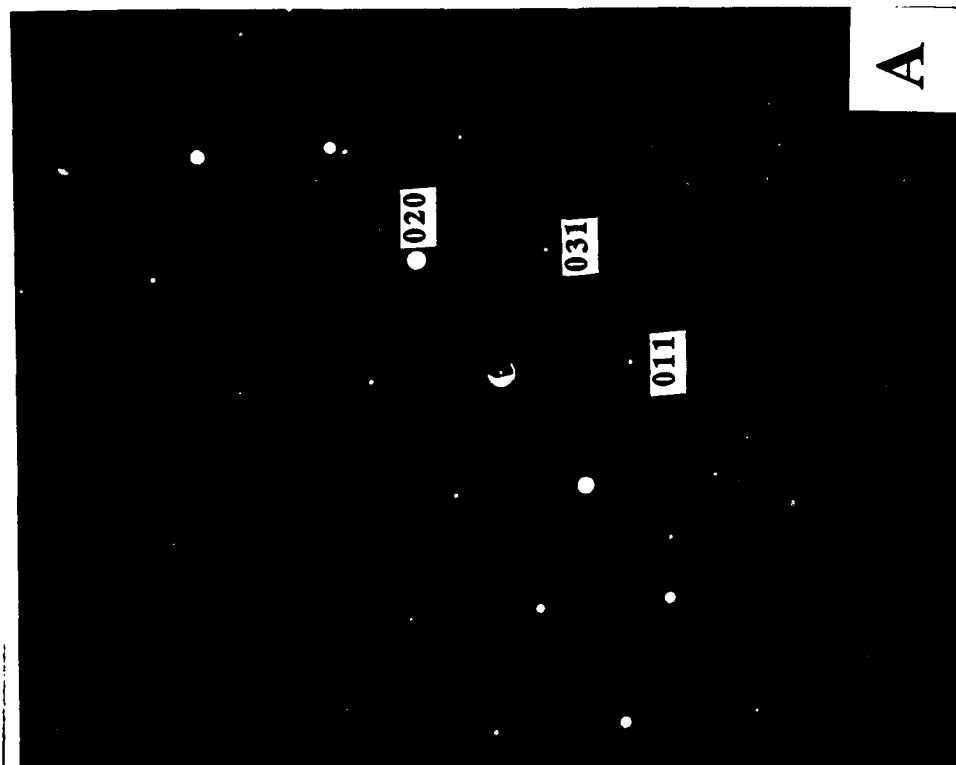


**FIGURE 8**

A) SADP OF AS-ANNEALED (500°C, 2 HRS.), 23Ni-77Al SAMPLE FILM. STRUCTURE IS THAT OF ORTHORHOMBIC, EQUILIBRIUM  $\epsilon$  PHASE. B) GRAIN MORPHOLOGY OF SAME SAMPLE.

(SADP's), and surface micrographs for these samples are presented in figure 9. Sample amorphicity is confirmed by the presence of broad, diffuse halos in the SADP, and the complete lack of contrast in the surface micrograph is typical of such a structure.

Enthalpies for the  $a \rightarrow \epsilon$  transformation, as a function of ion dose, are presented in Table I. Group designations (A1, A2, etc.), in column 1 of the table correspond to sample batches processed to a given ion dose, shown in column 2. The number of measurements recorded per group, represented as  $x$ , are given in column 3, with the average sample mass of each group following in column 4. Column 5 gives the temperature associated with the transformation exotherm peak, an example of which can be found in figure 10. The  $\Delta H$  value given in column 6 of the table represents the arithmetic mean of the measurements within each corresponding sample group. Errors associated with the measurements, for uncertainties in mass and chemical composition, are presented in columns 7 and 8, and their combined contribution to predicted measurement error is given in column 9. These error contributions will be discussed more thoroughly in the following section.

Figure 10 represents a DSC trace typical for the studied reactions, and a complete compilation of the DSC data obtained in the course of this work can be found in Appendix A. TEM verification of the as-transformed ( $a \rightarrow \epsilon$ ) phase is presented in figure 11, in which both SADP's and micrographs are utilized to verify the transition of the amorphous structure back to the equilibrium crystalline form. The arithmetic mean of the eleven measurements made for sample groups A2-A6 is -5.023 kcal/mole. Group A1 measurements were not included in calculation of this value, for reasons addressed in section 4.1.2.



**FIGURE 9**  
 A) DIFFRACTION PATTERN OF AS-IRRADIATED AMORPHOUS STRUCTURE. B) SURFACE OF (A).

TABLE I

Pertinent data accumulated from thermal analyses of the amorphous-->ordered  $\epsilon$  phase transformation.

SAMPLE GROUP NUMBER	DOSE $\text{ion/cm}^2$ $\times 10^{15}$	# DATA POINTS (x)	AVG. SAMPLE MASS (mg)	PEAK TEMP. (°C) (MEAN)	MEAN $\Delta H$ $\text{kcal/mole}$	MASS SENSITIVITY ERROR ( $\pm 5 \mu\text{g}$ ) ( $\text{kcal/mole}$ )	ERROR DUE TO RESIDUAL AI of 2 at. % ( $\text{kcal/mole}$ )	TOTAL ERROR DUE TO MASS AND COMPOSITION ERRORS ( $\text{kcal/mole}$ )
A 1	5	3	0.096	236	-3.980	$\pm 0.279$	-0.119	+0.279, -0.398
A 2	6	2	0.070	230	-4.849	$\pm 0.339$	-0.145	+0.339, -0.484
A 3	7	2	0.068	214	-5.201	$\pm 0.364$	-0.156	+0.364, -0.520
A 4	8	2	0.072	229	-5.134	$\pm 0.359$	-0.154	+0.359, -0.513
A 5	10	2	0.072	245	-5.330	$\pm 0.373$	-0.160	+0.373, -0.533
A 6	20	3	0.069	204	-4.741	$\pm 0.332$	-0.142	+0.332, -0.474

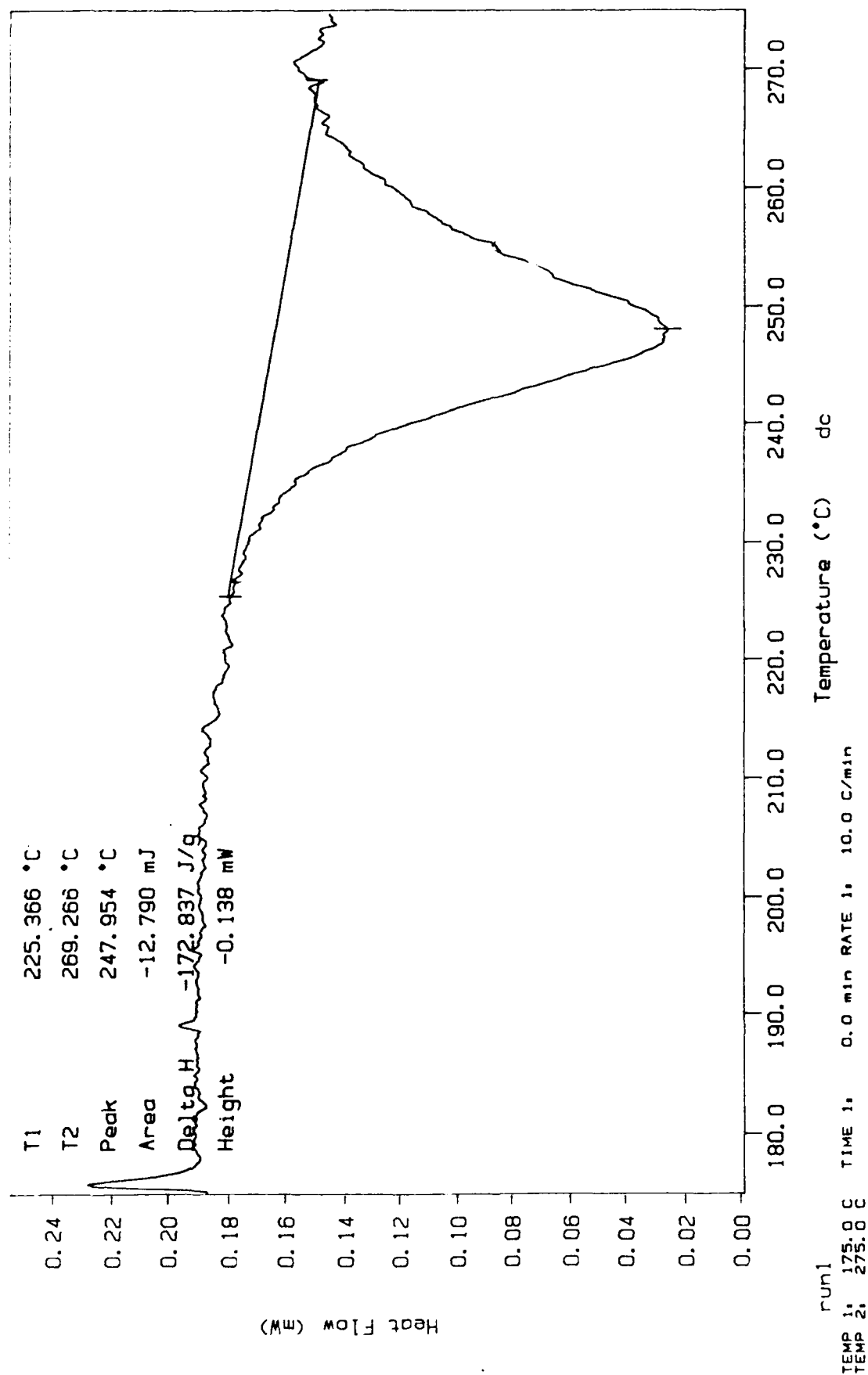


**FIGURE 10**

Representative DSC thermogram for the amorphous-->ordered orthorhombic ( $\epsilon$ ) transformation. Note well-defined exotherm, onset and peak temperatures. Ion dose= $8 \times 10^{15}$  ion/cm<sup>2</sup>.

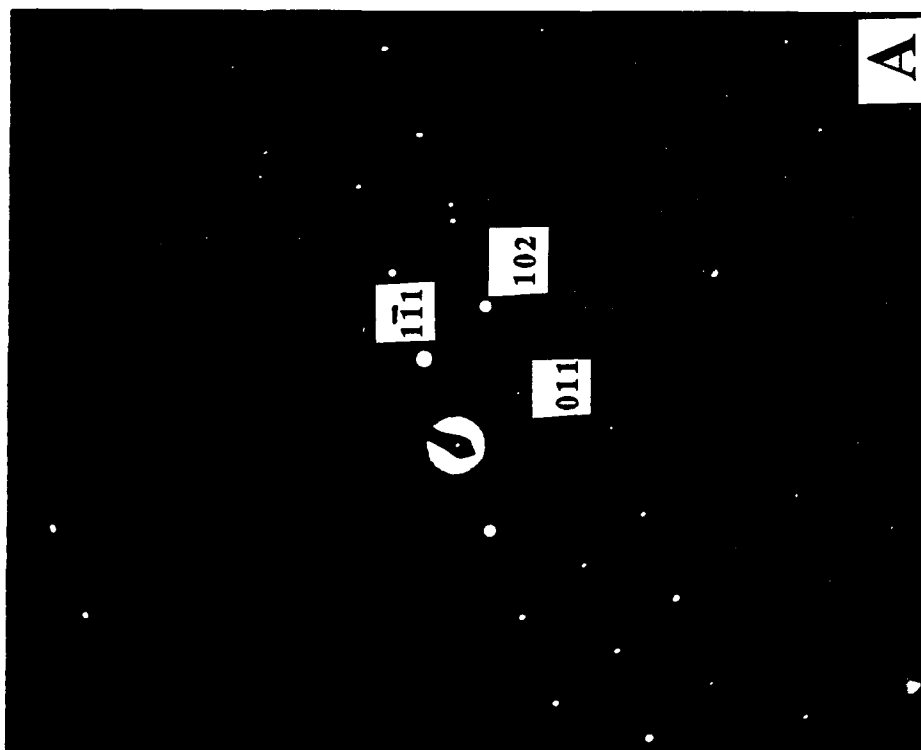


**FIGURE 11**

A) SADP OF DSC-TRANSFORMED STRUCTURE, INDICATING TRANSFORMATION TO STABLE ORTHORHOMBIC PHASE. B) GRAIN MORPHOLOGY OF (A).

#### 4.1.1 Potential Sources of Measurement Error.

Several sources of potential error exist in enthalpy measurements performed under these experimental conditions. Those to which approximate values may be assigned have been included in table I, and consist of: 1) Error associated with incomplete transformation of the entire sample mass, due to sample-nonstoichiometry (i.e., residual Al), and 2) Error associated with sensitivity limitations of the microbalance used to obtain net sample mass. Because the majority of samples prepared contained a fairly consistent amount of residual Al, as evidenced by the RBS analysis data, the contribution from this error source was calculated based on the presence of 2 at.% residual Al, or an average sample stoichiometry of 77Al-23Ni. The error contribution in this case amounts to  $\approx 3\%$  (negative), of the projected enthalpy for a perfectly stoichiometric sample. For the second case, microbalance sensitivity is specified by the manufacturer as  $\pm 5 \mu\text{g}$  (.005 mg). The error associated with this source, as presented in table I, was calculated based on an average sample mass measurement of .070 mg, and, has a maximum value of  $\pm 7\%$  of the mean enthalpy measured.

Other sources of error, much more difficult to quantify, also have an effect on the measured enthalpy values. These include distortion of the sample pan/sample cell contact surface, which introduces a heat transfer problem which will be addressed in detail in the following section; inexact duplication of sample pan position within the measurement cell between sample runs, along with inexact duplication of cell cover position, both of which affect temperature sensing in the DSC control loop; and error associated with exact definition of the onset and termination of the exothermic peak, via cursor positioning (refer figure 10), as input parameters for which peak area computations (reaction enthalpies) are performed with the thermal analysis software.

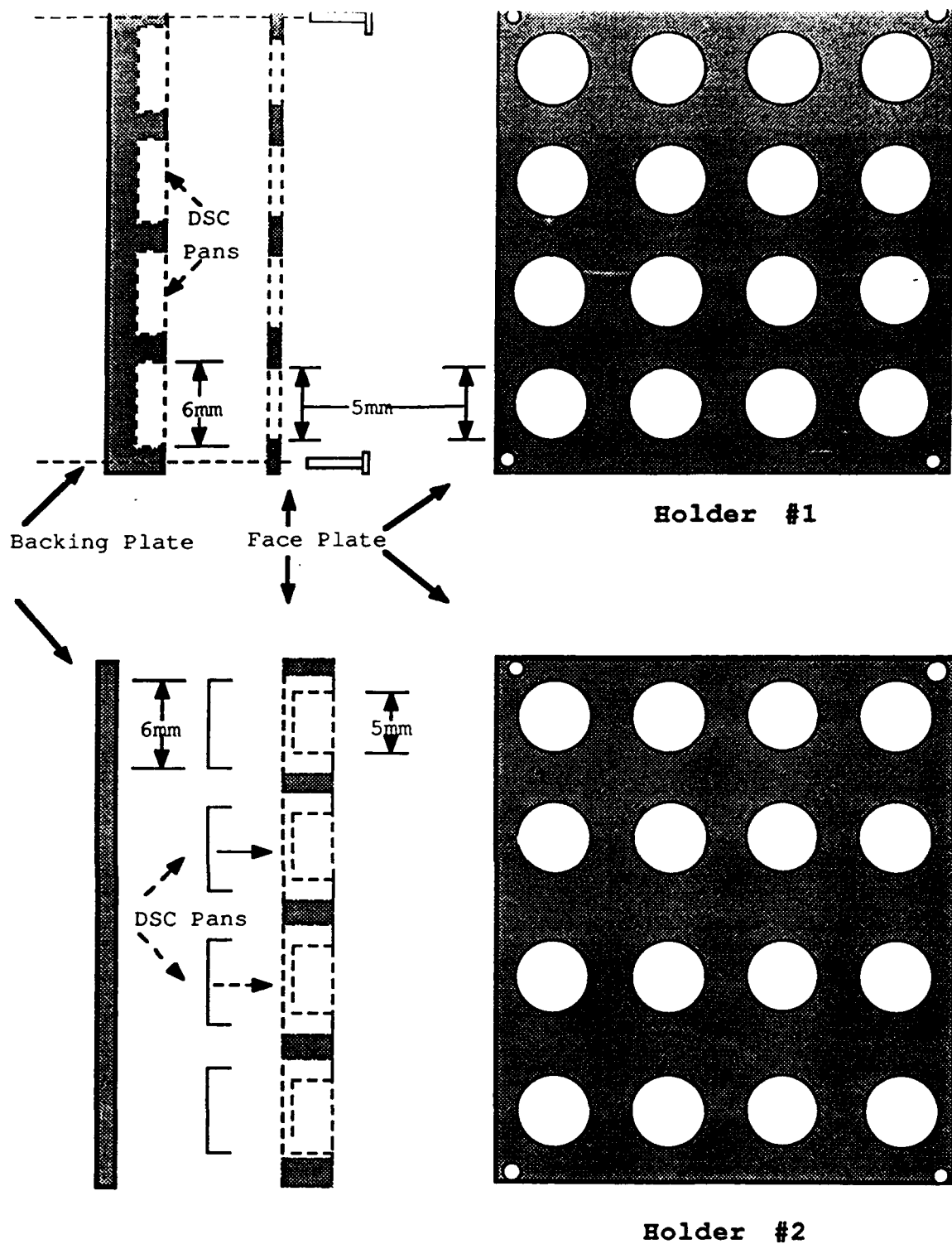


**FIGURE 12**

Sample holders for DSC pan processing. Holder #1 proved unsuitable for irradiation processing, as evaporant was allowed to collect on inner walls of sample pan, out of the ion beam line-of-sight. Holder #2 shields pan sides from evaporant.

#### 4.1.2 Effect of Sample Holder Geometry on Sample Group A1.

At first glance, the data in table I seem to indicate an increase in transformation enthalpy for the  $a \rightarrow \epsilon$  reaction corresponding to the increase in dose between 5 and  $6 \times 10^{15}$  ions/cm<sup>2</sup>. This increase, however, is attributed to a change in the *sample retention methods* utilized during processing of the first successfully analyzed batch of samples (group A1), and all the sample groups processed subsequent to this (A2-A6). A brief discussion of this observed variation is warranted.

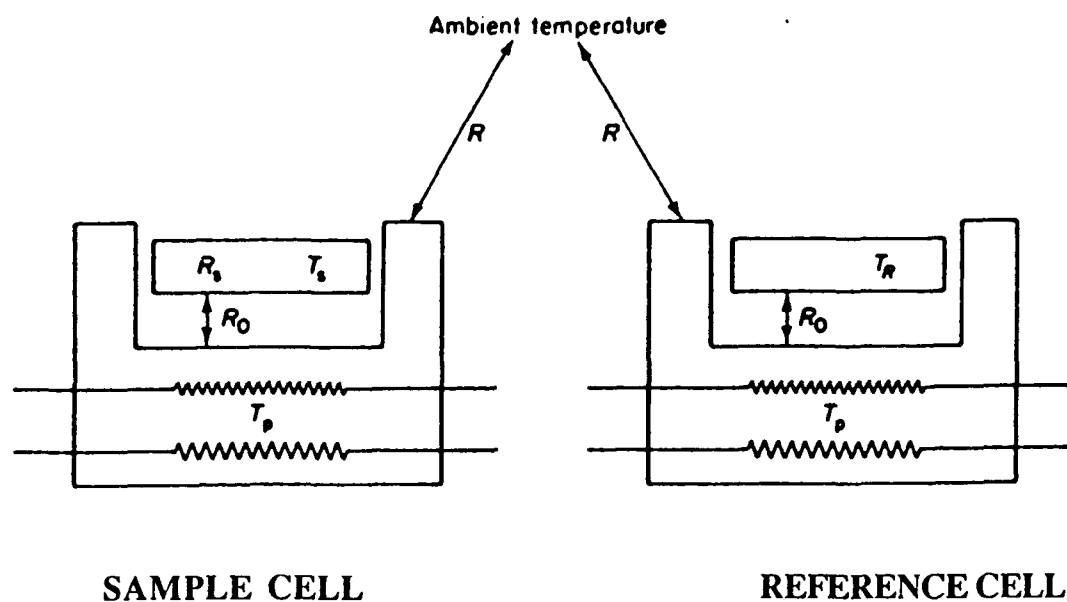
Reference to table I shows average sample masses for the A1 group  $\approx$  30% greater than those for the remaining groups. Since total film thickness variations between the groups were minor ( $\leq 500 \text{ \AA}$ ), it remains that the only other factor which would contribute to such a substantial increase in sample mass for this first group would be the square area covered on the sample pan during the coevaporation process. This was in fact the case, and is attributable to the difference in sample holder geometry, specifically, pan retention methods, used in processing this sample group. The respective sample holder configurations are illustrated in figure 12. During the vapor deposition sequence, the sample retainer for group A1 allowed for a substantial amount of film to be deposited on the inner walls of the sample pans, since they are in the line-of-deposition sight of the hearths, as the sample holder itself is offset from the position of the hearths. During subsequent irradiation, this area of film was "shadowed" from the ion beam because the retainer plate opening was, by necessity, a slightly smaller diameter than that of the sample pan. Thus, only the portion of film directly exposed to the ion beam was transformed to the amorphous phase, while the shadowed portion remained in the as-annealed ( $\epsilon$ ) state. The calculated values for the DSC recorded  $a \rightarrow \epsilon$  transformation enthalpies, being a function of sample mass, were consequently in error by as much as 20%, depending on pan position in the holder, and consequent extent of beam shadowing. Another sample holder, for use in irradiation processing, was then designed, shown in figure 12 as holder

#2, to avoid any film deposition on non-line-of-beam-sight areas. The enthalpy data from group A1 were tabulated and included in this report for illustrative purposes, but, as mentioned previously, were not included in determination of the mean transformation enthalpy value for this reaction, -5.023 kcal/mole.

#### 4.1.3 Effect of Sample Pan Distortion on Thermal Analysis.

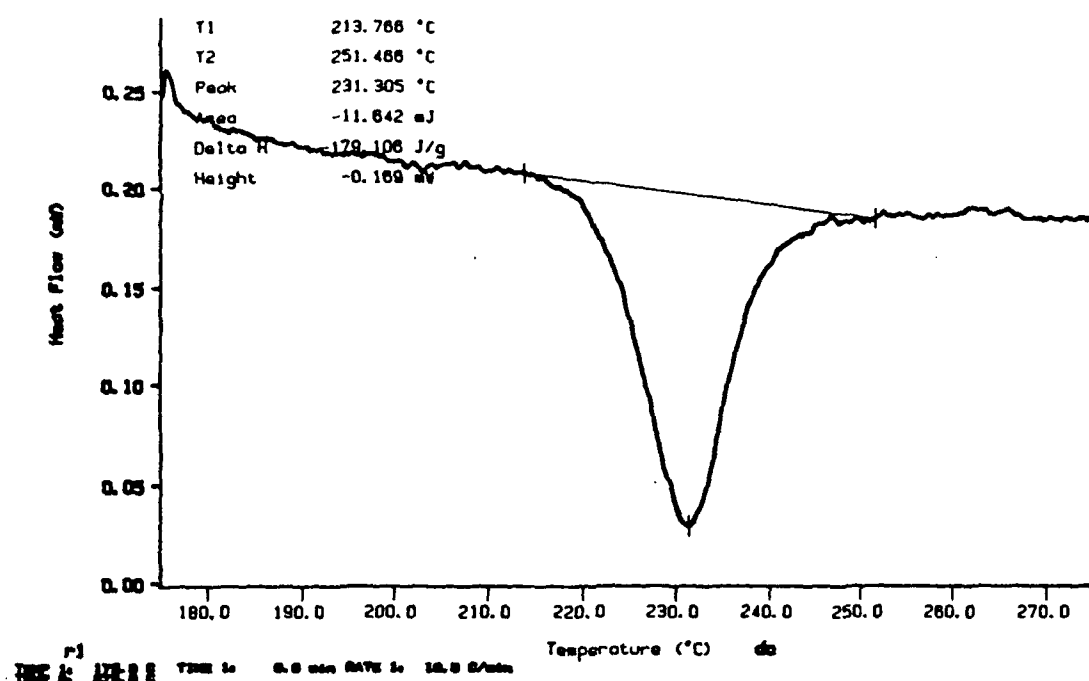
Appendix A contains all 25 separate DSC analyses of ion-irradiated thin films. Of these, only 14 provided suitably distinct exothermic traces to be objectively analyzed, and, for reasons just mentioned, only 11 of the 14 comprised the statistically analyzed group. The original group consisted of 32 irradiated samples, but for various reasons, 7 of the 32 proved unacceptable for inclusion in the calorimetry work. Heat transfer problems, arising from the handling methods used to process this group of samples, which tended to distort the sample pan/sample cell contact surface, were found to be the reason for this low ( $\approx 45\%$ ), measurement success rate.

Figure 13 is a schematic illustrating the arrangement of the DSC sample and reference cells and pans, and indicating the important heat transfer variables to be considered. The case of a thin film in intimate contact with the sample pan (i.e., vapor deposited), represents what is perhaps the best heat transfer interface attainable in the standard sample/pan configuration, thus minimizing  $R_s$  (thermal resistance between sample and pan), with respect to  $R_o$  (thermal resistance between pan and holder). Additionally, it has been proven that the slope of the leading edge of a melting endotherm will be given by  $(1/R_o)(dH/dt)$ , where  $dH/dt$  is the programmed scanning rate. With scanning rate held constant then, variation in the value of  $R_o$  will directly affect the shape of the endo- or exothermic peak [51]. This change in peak shape as a function of  $R_o$  is readily apparent in the DSC curves compared in figure 14. Even though the peak area in principle remains unchanged, in this sensitivity regime it becomes impossible to determine the exact onset

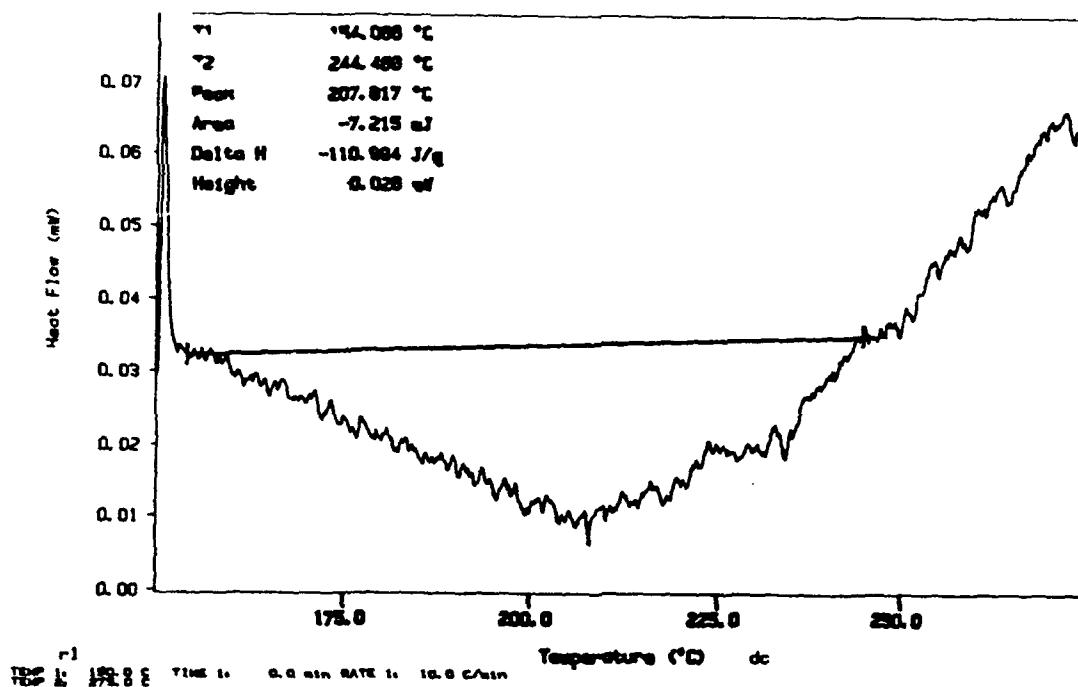


**FIGURE 13**

Schematic of DSC sample and reference cell arrangement. The sample pan rests within the Pt cell, its thermal resistance in contact with the cell being  $R_0$ . The sample's temperature and thermal resistance with the sample pan is represented by  $T_s$  and  $R_s$ , respectively. The cell temperature is given as  $T_p$ . Distortion of the sample pan/sample cell contact surface results in substantially increased  $R_0$ .



A



B

**FIGURE 14**

Comparison between high and poor quality thermograms collected for a->ε transformation. A) High quality thermogram, with easily established onset and peak temperatures, and well-defined peak area. B) Poor quality thermogram, with virtually impossible to define peak temperatures and area.

and termination of the recorded exotherm for samples where  $R_0$  was relatively large, and the peak shape was consequently distorted beyond sensible interpretation. In the cases where peak shape prevented accurate interpretation, the measurement was omitted from the group of analyzed data. The reasons for this apparently large degree of variation in  $R_0$  will now be addressed.

The pure Al sample pans most commonly used in DSC work are manufactured via a simple drawing operation, to a net pan thickness of  $\approx 0.11$  mm (110  $\mu$ m) [52]. The pans are not subject to heat treatment. In the as-manufactured condition, the pans exhibit a fair degree of work hardening-enough to allow for careful handling, under normal conditions, without substantial geometric distortion. However, as detailed in section 3.1.2, the deposited films utilized in the amorphous phase studies require thermal annealing at  $\geq 400^\circ\text{C}$  for  $\geq 2$  hrs., in order to achieve formation of the equilibrium  $\epsilon$  structure, necessary for successful ion-induced amorphization. This is a *very* significant temperature and time schedule for the pan material, well beyond even the most conservative estimates for complete recovery from the as-manufactured state. Hence, handling of the pans subsequent to this thermal cycling becomes a very tedious operation at best, due to their extremely delicate (i.e., soft, thin), condition. Extensive handling is, however, necessary, as the pans must be first removed individually from the anneal furnace (the tube diameter would not accommodate the entire sample holder, so the pans were annealed separately), replaced in the sample holder, irradiated, removed again, weighed, and finally placed in the DSC sample cell for thermal analysis. It is virtually impossible, during this handling sequence, to avoid imparting some amount of distortion to the pan geometry, such that the pan/sample cell contact surface (the pan bottom), does not remain fixed between samples. Since  $R_0$  is determined by this contact surface, it is easy to deduce the source of the peak-shape reproducibility problem. That the source of the problem is the thermal treatment of the samples is further demonstrated by the fact that the sample group analyzed for the f.c.c-

->E transition , which required no heat treatment, exhibited a 100% (23/23), measurement success rate.

#### 4.1.4 Embedded Atom Simulation of Amorphous Transformation Energies.

Effective modeling of an amorphous solid, for use in molecular dynamics simulations, is a difficult task, and has elicited much debate amongst those involved in this area. The approach used to create the amorphous structures used by Eridon [29] in the EA simulations performed for the metastable phase transformations of interest in this work is described as follows: To create the amorphous structure, each atom in the host lattice was 'moved' off its equilibrium lattice position in a random direction, by a small amount, given as  $\delta$ .  $\delta$  was allowed to vary between zero and a maximum displacement, given as  $\Delta$ , described as the "amorphization parameter". The value of  $\Delta$  was chosen to correspond to the half-width at half-maximum of the Gaussian radius distribution observed in the crystalline pair distribution function peaks (PDF's) of the material,  $\text{NiAl}_3$ , of interest. The effectiveness of this "computer amorphization" process was then verified by computing the PDF resulting from a given value of  $\Delta$ , and comparing it to the PDF for a truly amorphous substance. The use of the PDF to characterize a liquid or an amorphous solid is well established, and it is thus a logical approach to computer modelling of these structures. Schematic PDF's for both crystalline and amorphous solids are shown in figure 15.

Calculations performed by Eridon using the EA model, for the amorphous-->E transformation, resulted in a range of enthalpy values between -1.38 and -5.83 kcal/mole. As the amorphization parameter is increased (i.e., each lattice atom is increasingly displaced from its equilibrium lattice position ), the value of the PDF as a function of distance (radius), from the displaced atom converges toward unity. This is characteristic of the change from the long range atomic order (LRO) of the crystalline solid, to the short range order (SRO) of the amorphous material. Liquids and amorphous solids display PDF's in

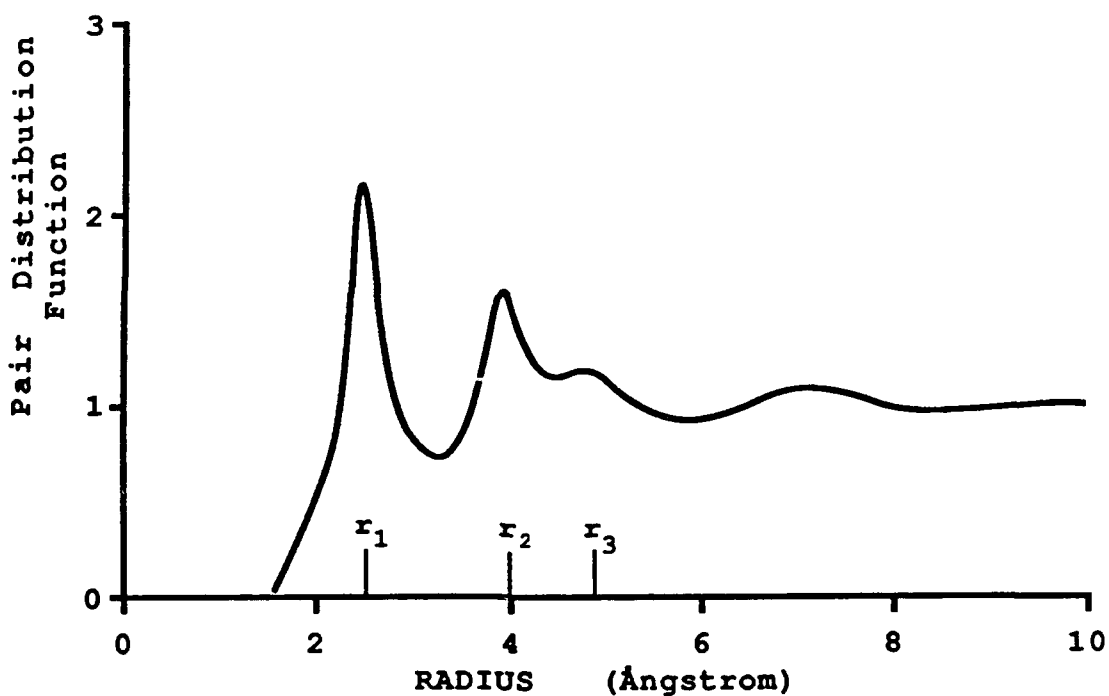
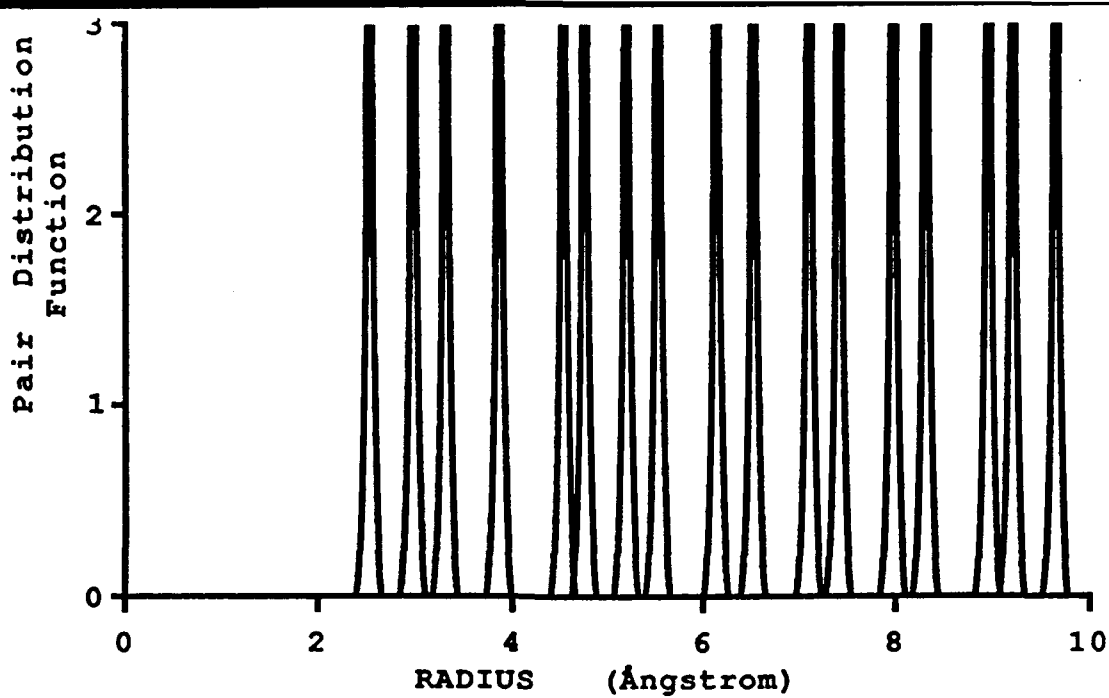


**FIGURE 15**

A) Schematic pair distribution function (PDF), for a crystalline solid, reflecting long range atomic order. B) Schematic PDF for an amorphous solid, showing gradual convergence to unity after approximately 3 units of radius.

which distinguishable peaks, representative of relative atomic order, can typically be found only for the first three radial displacements from the analyzed lattice sight. The ratios of these radii have been fairly well defined in the respective structures: amorphous solids have been shown to exhibit radius ratios of  $r_2/r_1 \approx 1.67$ , and  $r_3/r_1 \approx 1.95$  [53]. As the  $\Delta$  parameter increases, the computed PDF shows increasing convergence toward unity, with apparent similarity to the expected radius ratios mentioned above beginning at a value of  $\Delta \approx 0.200$ . For values of  $\Delta \geq 0.400$ , the radius ratios of the PDF become more characteristic of a liquid structure, for which values of  $r_2/r_1 \approx 1.72$  and  $r_3/r_1 \approx 2.45$  [54].

The simulations referenced herein were performed using values of  $\Delta = 0.000, 0.200, 0.300$ , and  $0.400$ , and initial structures of both ordered equilibrium  $\epsilon$  phase ( $\text{DO}_{20}$  lattice, equilibrium lattice sites for Al and Ni), and disordered  $\epsilon$  (random arrangement of Al and Ni atoms within the  $\text{DO}_{20}$  lattice). Calculated values of  $\Delta H_{m-s}$  used for comparison to experimentally measured data in this study are those computed using  $\Delta = 0.300$ , as this value was found to give the most acceptable approximation to the PDF radius ratios expected for an amorphous solid. The low (absolute) value,  $1.38 \text{ kcal/mole}$ , was computed using the ordered  $\text{DO}_{20}$  starting structure, while the high value,  $5.83 \text{ kcal/mole}$ , was taken from the simulation of the disordered  $\text{DO}_{20}$  starting lattice.

The mean measured value for the  $a \rightarrow \epsilon$  transformation enthalpy falls only 13% short of the predicted value for the disordered amorphous  $\rightarrow \epsilon$  reaction ( $5.023$  vs.  $5.830$ ). When the most well defined thermograms are referenced, the measured value corresponds almost exactly to that predicted ( $5.978, 5.769$ , vs.  $5.830$ ). Thermal analyses performed on samples of varying ion dose, over a dose range of  $1 \frac{1}{2}$  orders of magnitude, did not show a discernible trend toward increasing transformation enthalpies. This last point is an indication that, with reference to the simulation methods, the concept of the "disordered" starting structure-the one whose subsequent amorphization results in the higher transformation enthalpies-is useful for modelling purposes, but in reality would be an

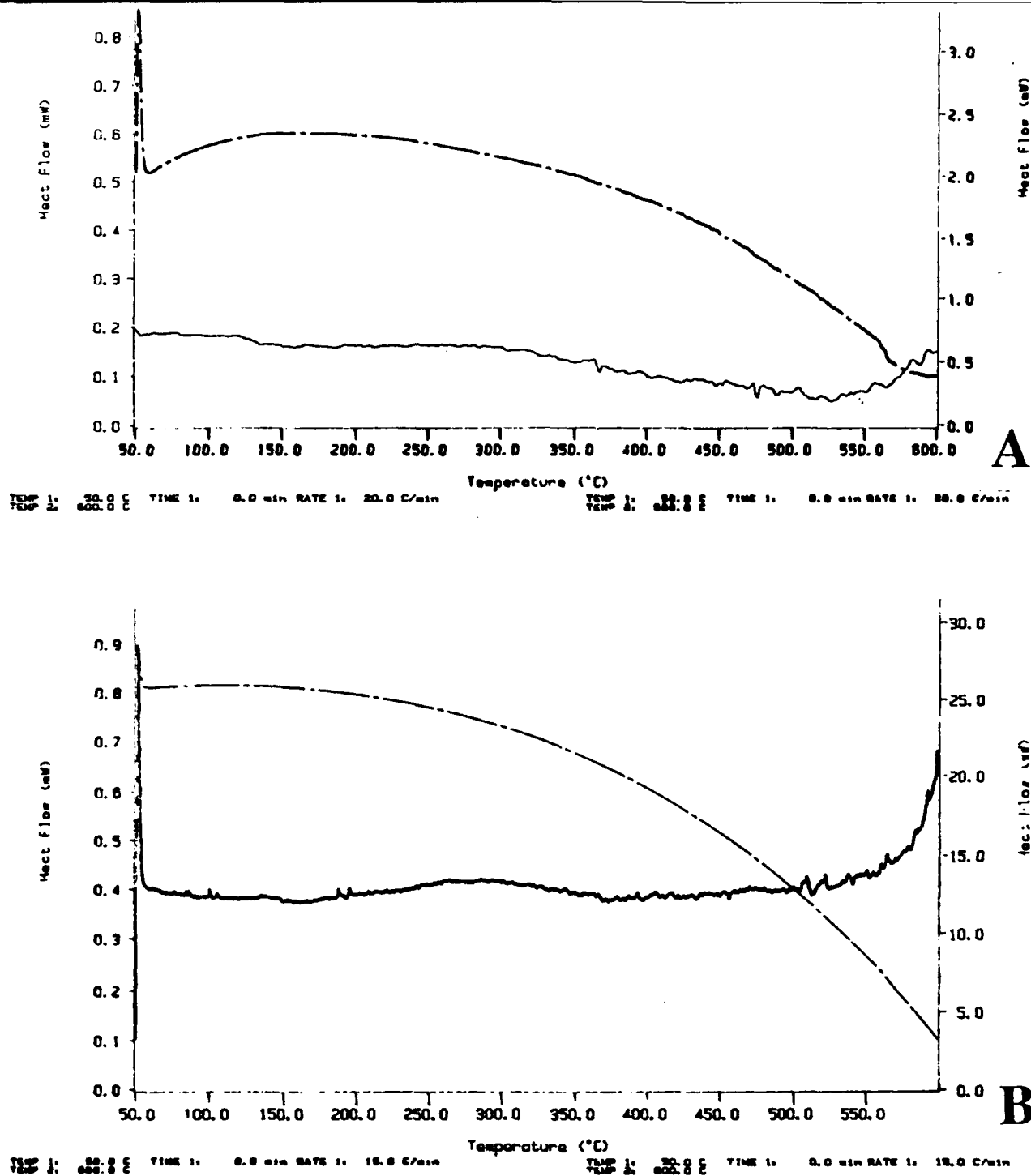


**FIGURE 16**

A) Thermogram recorded for  $\text{Ni}^{++}$  dose of  $3 \times 10^{15}$  ions/cm<sup>2</sup>, showing no discernible thermal reaction. B) Thermogram for  $4 \times 10^{15}$  dose. (Dashed line represents second scan on sample; jagged line represents data from first scan, with second scan subtracted, to indicate net reaction energy).

obvious first step in the lattice disordering sequence resulting from ion irradiation of a sample, and would thus be quite difficult to quantify experimentally. This assertion is supported by the lack of any definable experimental thermograms for measurements performed on samples irradiated below the amorphization threshold of  $5 \times 10^{15}$  ions/cm<sup>2</sup>. For instance, samples irradiated to doses of  $3\text{--}4 \times 10^{15}$  ions/cm<sup>2</sup> showed no discernible evidence of exothermic reaction, as indicated in figure 16.

Overall, experimental data accumulated for the a $\rightarrow$  $\epsilon$  transformation conforms rather well to the values predicted for the disordered a $\rightarrow$  $\epsilon$  transformation using the embedded atom model. This is especially gratifying in light of all the factors influencing the accuracy of both methods, such as variations in pan contact surface, minute sample mass, calorimeter sensitivity, microbalance sensitivity, residual Al, inexact correlation between amorphization parameter and amorphous PDF characteristics, and, in general, all the other considerations regarding use of pair potentials and molecular dynamics simulations in these types of calculations.

#### 4.2 F.C.C. Solid Solution $\rightarrow$ Ordered Orthorhombic Transformation Enthalpy Measurements.

Measurement of the f.c.c. $\rightarrow$  $\epsilon$  transformation was, in a comparative sense, quite straightforward. Electron diffraction patterns of the as-deposited f.c.c. structure are shown in figure 17, with the major Al {hkl} rings indexed. A representative DSC trace is presented in figure 18. Transformation to the equilibrium orthorhombic structure, as a result of the thermal analysis process, is documented in figure 19. Appendix B contains a complete compilation of the DSC analyses performed for this reaction. Of 23 samples initially prepared, all 23 provided thermograms suitable for quantitative analysis. The mean enthalpy value of these 23 measurements is  $-4.157$  kcal/mole, as detailed in table II.

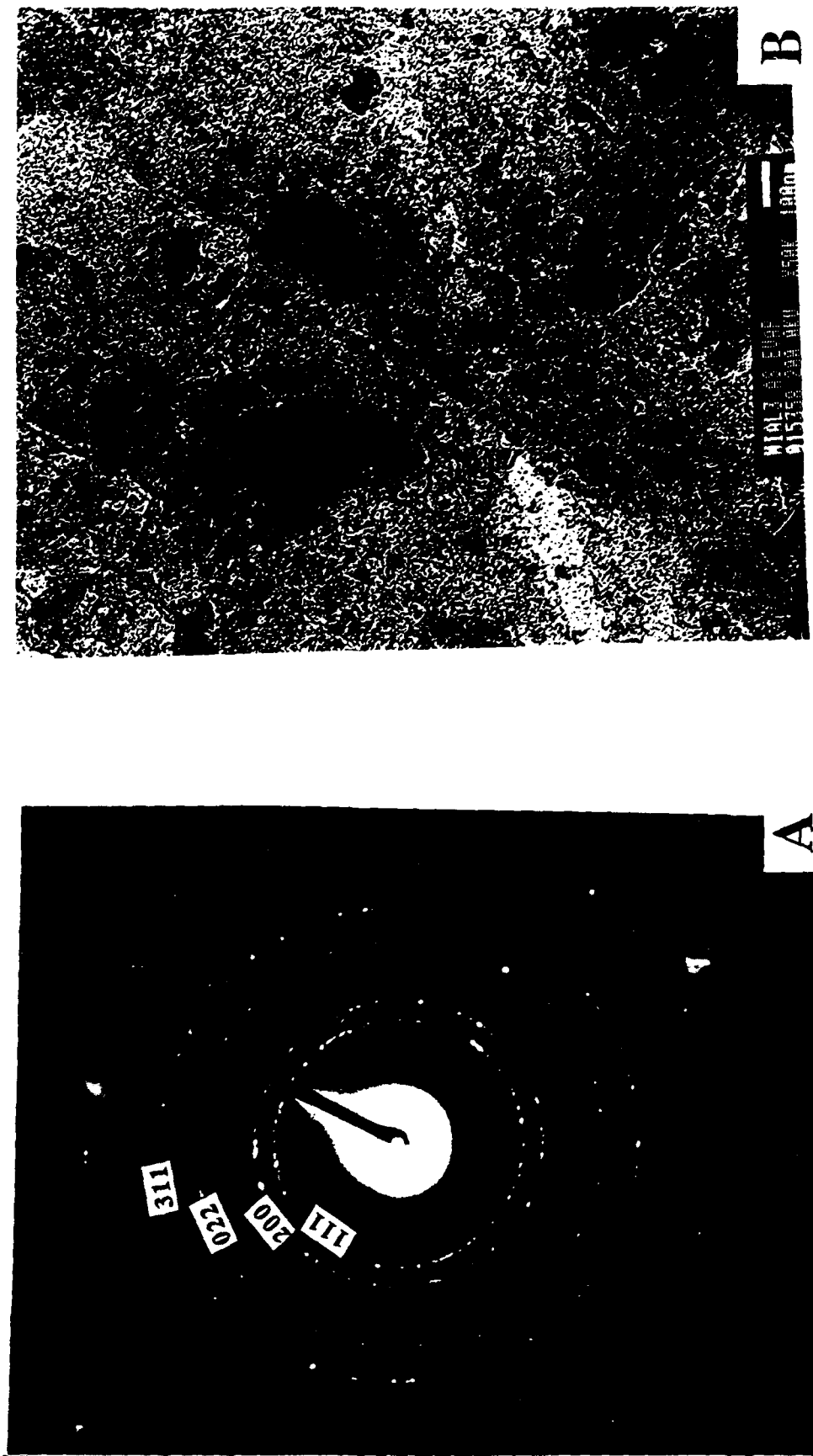


**FIGURE 17**

A) SELECTED AREA DIFFRACTION PATTERN OF AS-DEPOSITED 23Ni-77Al SAMPLE FILM, WITH MAJOR RINGS INDEXED, CORRESPONDING TO F.C.C. LATTICE TYPE. B) TEM SURFACE MICROGRAPH OF (A)

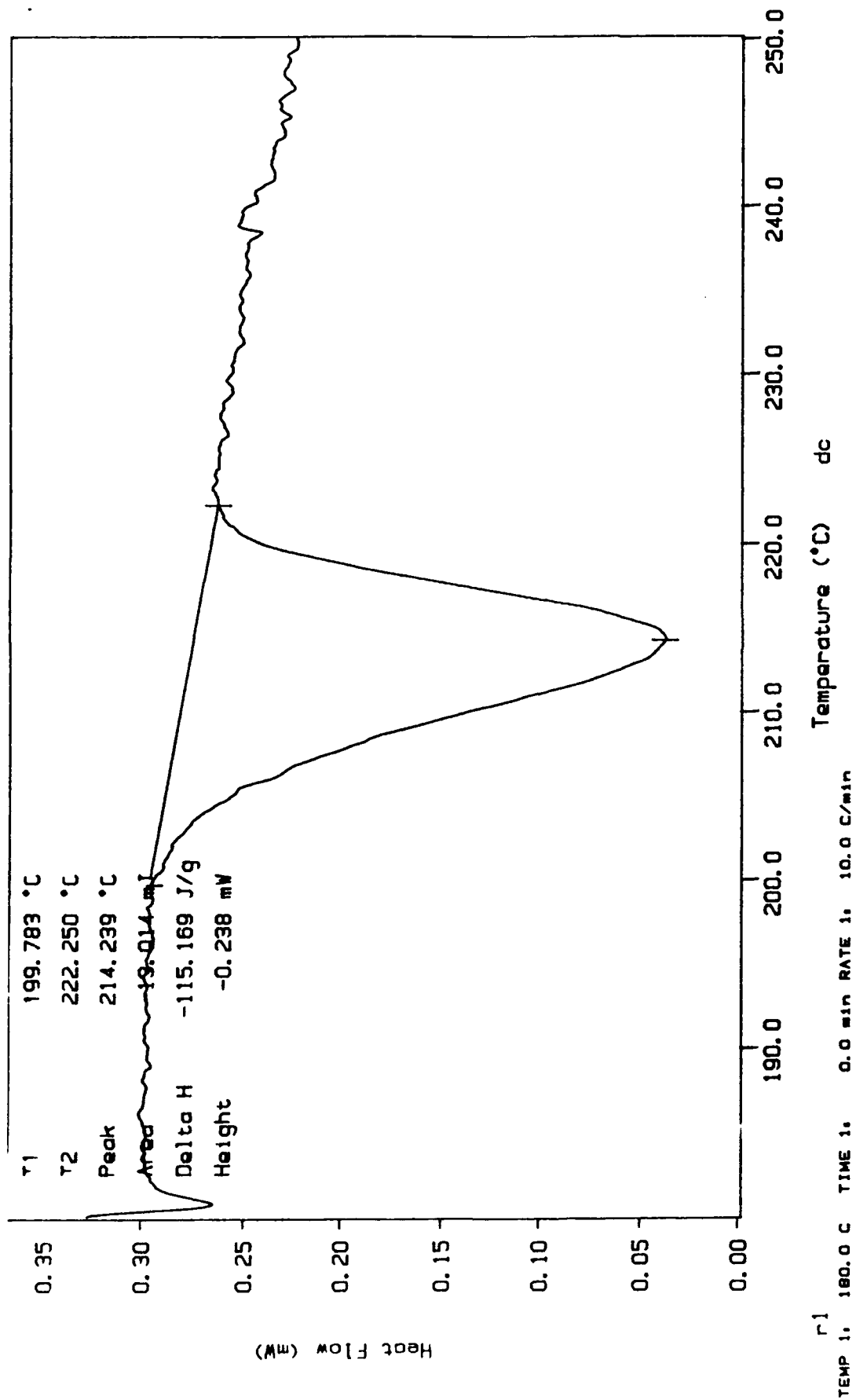


**FIGURE 18**

Representative DSC thermogram for the f.c.c. solid solution-->ordered orthorhombic transformation. Note well-defined exotherm, onset and peak temperatures.

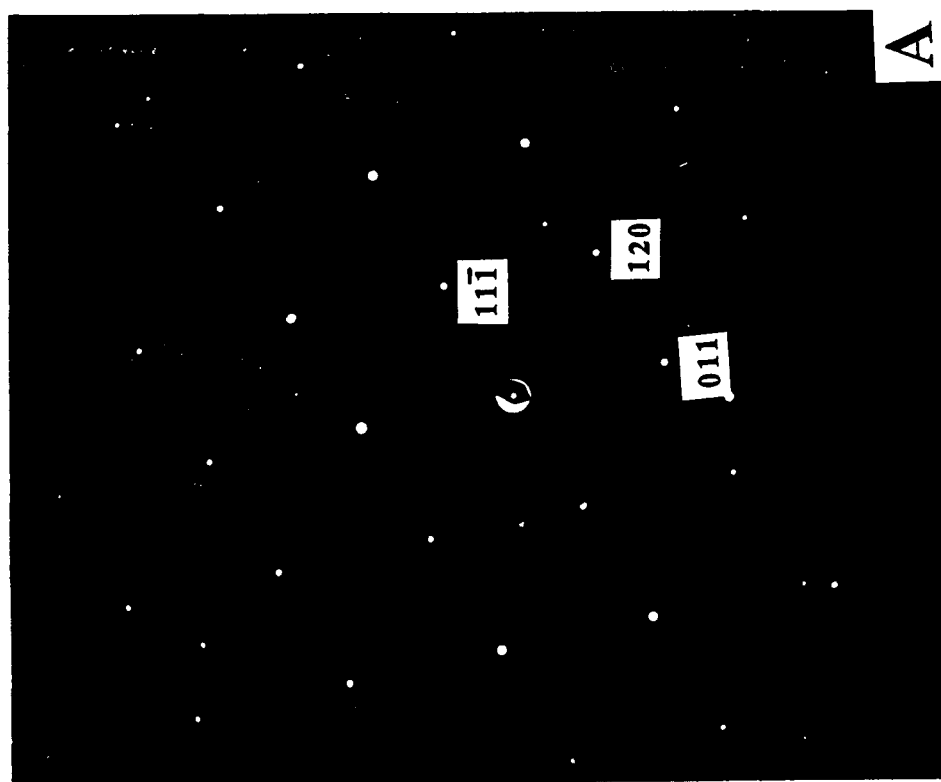


**FIGURE 19**

A) SADP OF DSC-TRANSFORMED F.C.C. SOLID SOLUTION, VERIFYING TRANSFORMATION TO STABLE ORTHORHOMBIC STRUCTURE. B) GRAIN MORPHOLOGY OF (A).

TABLE II

Pertinent data accumulated from thermal analyses of the f.c.c solid solution-->ordered  $\epsilon$  phase transformation.

# DATA POINTS (x)	AVG. SAMPLE MASS (mg)	PEAK TEMP. (°C) (MEAN)	MEAN $\Delta H$ kcal/mole	MASS SENSITIVITY ERROR ( $\pm 5 \mu\text{g}$ ) (kcal/mole)	ERROR DUE TO AVG.RESIDUAL AI OF 2 at.% (kcal/mole)	TOTAL QUANTIFIABLE ERROR DUE TO MASS AND COMPOSITION (kcal/mole)
23	0.090	215	-4.157	$\pm 0.249$	-0.125	+0.249, -0.374

Included in the table are error source contributions similar to those found in the data for the  $a \rightarrow \epsilon$  transformation. Because the basic sample preparation methods, with respect to film deposition and mass measurement, were the same between the two groups, the error contribution values for these two potential sources are the same as well. The higher degree of consistency observed in the thermograms (the higher measurement success rate), can be attributed to much less distortion of sample pan/sample cell contact surface (pan bottom), and thus much more consistent values of  $R_0$ . The relative absence of pan surface distortion in this group is due to a) the limited amount of sample handling required before thermal analysis, and, as a corollary, b) the absence of any thermal treatment cycle during sample preparation. Although both factors contributed to the smoothness of the data, the second is the more important, as the pans remained in a fairly "tough" (as-manufactured), state during the limited amount of handling they received.

It is interesting to note that this latter consideration, while beneficial from the perspective of allowing a higher degree of consistency to be maintained in the thermal analyses, was also a potential source of extraneous noise in the actual DSC traces recorded. The as-manufactured (cold-worked) state of the sample pans used in this portion of the study is one of higher internal energy than that of the annealed pans discussed in the previous section. Indeed, annealing is simply the thermally activated release of this stored energy. As such, work hardened materials are actually in a state of thermodynamic instability, and the exothermic release of this energy with increasing temperature may adversely affect the thermal measurement of the reaction of interest. Therefore, it was necessary to investigate the nature and extent of this possible error in the DSC readings, by thermally analyzing an as-manufactured sample pan with no sample film present. This analysis was performed using exactly the same method as for the TFC studies. The sample pan was analyzed across a temperature range of 50-550°C, using a fully annealed sample pan (500°C, 2 hrs.), as a reference. The resulting thermogram is shown in figure 20.

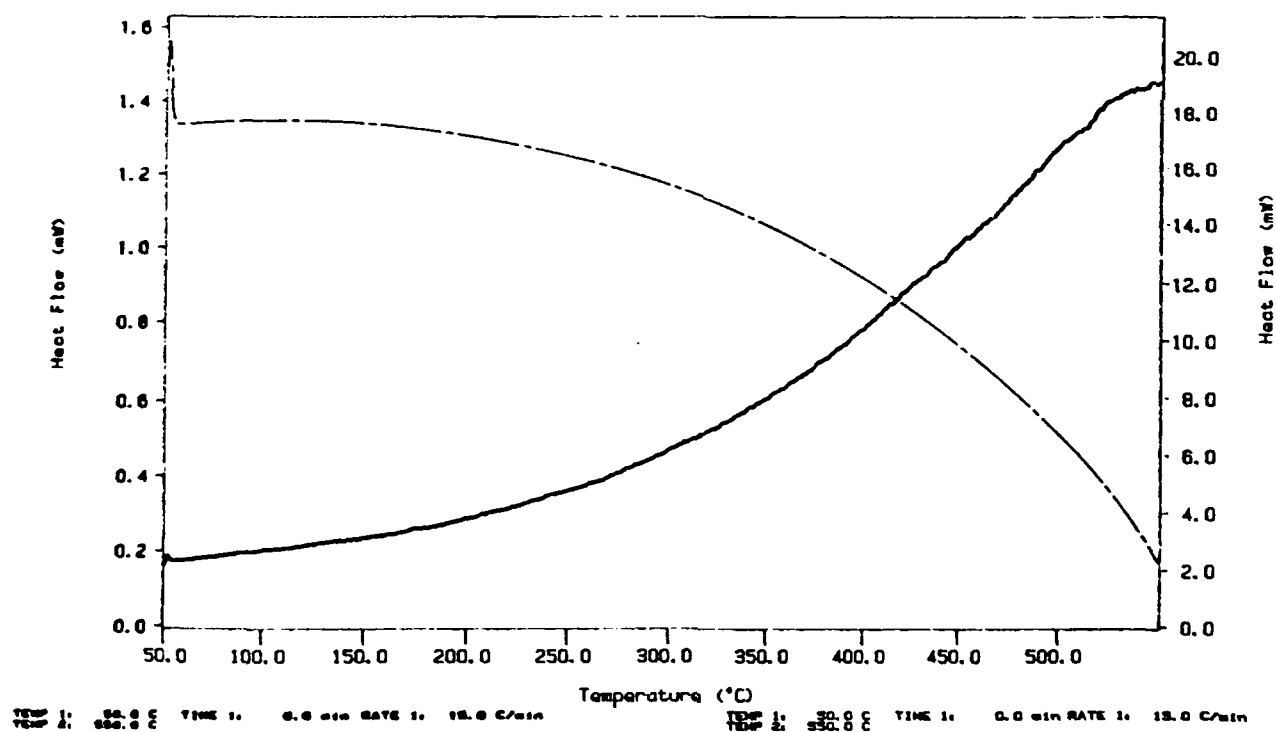


**FIGURE 20**

Thermogram from scan of as-manufactured DSC sample pan (no film). No significant thermal activity due to recovery from drawing process is evident.

There is no visible exothermic signal across the entire temperature range scanned, and it was thus concluded that any release of energy stored in the sample pans, as a result of the manufacturing process, was not of a magnitude measurable within the sensitivity limits of the instrument.

Unfortunately, no computer-simulated data was available to compare with the experimentally determined enthalpy value for this transformation. However, simulations have been performed for the transformation from a disordered orthorhombic  $\text{DO}_{20}$  lattice, to the ordered structure, and the results are interestingly similar to the measured values for the f.c.c.-->  $\epsilon$  transition. The computed enthalpy for the disordered-->ordered  $\text{DO}_{20}$  reaction is -4.310 kcal/mole, as compared to the measured f.c.c.--> $\epsilon$  reaction enthalpy of -4.157 kcal/mole.

Since evidence of ordering, in the form of superlattice rings, is totally absent from the as-deposited SADP's, this structure is assumed to be disordered f.c.c. Hence, the transformation of this structure to the orthorhombic, equilibrium ordered structure is, by definition, a disorder-->order reaction, analagous to the disorder-->order reaction for the  $\text{DO}_{20}$  structure, for which simulations have been performed. Although it is not possible, given the lack of comparative data, to conclude that the two transformations are entirely similar, it is interesting to note that the two starting structures have close similarities in terms of nearest neighbor distances, and as such could very well have similar transformation heats.

Each atom in an f.c.c. structure has 12 nearest neighbors. All of the indexed rings in the as-deposited diffraction pattern correspond to the major Al {hkl} planes. Since the Ni atoms are small relative to the Al host atoms, the Al lattice constant is not measurably altered. In the pure metal (Al, f.c.c.), the distance of closest approach is  $2.86\text{\AA}$  [56]. For the ordered orthorhombic,  $\text{NiAl}_3$  structure, each Al atom has 11 neighbors, each Ni atom has 9. The average Al-Al distance in this structure,  $2.76\text{\AA}$ , is very similar to that of the pure metal [57]. Thus, very little difference exists between the interatomic distances for Al

in the configurational change from the disordered f.c.c. to the ordered orthorhombic, and those associated with the transformation from the disordered to ordered orthorhombic structure. Due to the fact that Al and Ni have a very strong interaction in a number of different atomic configurations, as evidenced by the relatively high melting temperatures of their various compounds, it is perhaps legitimate to infer that the transformation enthalpies associated with the two different disorder-->order reactions discussed here would have very similar values. Indeed, the measured enthalpy for the f.c.c.--> $\epsilon$  transformation, -4.157 kcal/mole, differs from the computed enthalpy for the disordered --> ordered  $\epsilon$  reaction, -4.310 kcal/mole, by only 3.5%. Thus, theoretical considerations, coupled with experimental observation, indicate that the two different reactions, from a thermodynamic perspective, are closely associated.

A summary of measured versus calculated data for the measurements performed in this study is presented in table III. Calculated values in column 3 of the table are those taken from the embedded atom calculations discussed previously. Measured values, shown in column 4, represent the arithmetic mean of all measurements made for the respective reactions, save for the exclusion of sample group A1 data from the a--> $\epsilon$  reaction enthalpy measurements. Measured values are followed in parentheses by standard deviation values ( $\sigma$ ), determined using standard counting statistics. Column 5 shows the standard deviation ( $\sigma$ ), as a percentage of mean measured enthalpy.

**TABLE III**  
 **$\Delta H_{m-s}$  (Measured vs. Calculated) For Metastable to Stable Phase**  
**Transformations in NiAl<sub>3</sub>**

<i>TRANSFORMATION</i>		$\Delta H$ (kcal/g-atom)		$\sigma_x/\Delta H$ $\times 100\%$
<i>STARTING</i> <i>STRUCTURE</i>	<i>ENDING</i> <i>STRUCTURE</i>	<i>CALC.</i>	<i>MEASURED</i> ( $\sigma$ )	
<i>amorph.</i>	$\epsilon$	-1.38 to -5.83	-5.023 (0.489)	9.70%
<i>f.c.c. solid</i> <i>solution</i>	$\epsilon$	-4.310*	-4.157 (0.35)	8.40%

\*this value represents  $\Delta H$  for the simulated transformation from disordered DO<sub>20</sub>->ordered DO<sub>20</sub>.

## 5. CONCLUSIONS

Thermal analysis measurements performed on ion irradiated, 0.78-0.90  $\mu\text{m}$  amorphous thin films of nominal composition 75Al-25Ni indicate a mean transformation enthalpy value of  $-5.023 \pm 0.489$  kcal/mole, for the amorphous to ordered orthorhombic ( $\epsilon$ ) phase transition. This compares favorably with the highest (in absolute value), quantity predicted for this reaction, using the Embedded Atom computer simulation model, -5.83 kcal/mole. Thermal measurements performed on as-deposited, 1.0-1.2  $\mu\text{m}$  thin films of the same nominal composition indicate a mean transformation enthalpy of  $-4.157 \pm 0.35$  kcal/mole. Although computer simulated values are not available for this transformation, this quantity compares closely to the enthalpy calculated for the disordered-->ordered DO<sub>20</sub>

transformation, -4.310 kcal/mole. This experimental data, combined with similarities in the atomic structures of the two metastable starting phases, is a strong indication that the reactions are closely related thermodynamically.

## 6. FUTURE WORK

The studies presented in the body of this work have established thin film calorimetry as a viable technique for thermodynamic characterization of samples which had previously been quite difficult to thermally analyze. Having already applied the technique to one of the intermetallics in the Ni-Al system, it would be interesting to investigate the two more technologically important alloys in that system, NiAl and Ni<sub>3</sub>Al, with respect to the enthalpies associated with the  $\beta \rightarrow \beta'$  and  $\gamma \rightarrow \gamma'$  reactions, respectively. The increasing utilization of both of these alloys in high temperature-high stress applications requires intimate knowledge of the thermodynamics governing their stability.

Additionally, a host of metastable phases, exclusive to ion beam processing, can be easily prepared and analyzed, lending valuable insight into the thermodynamics and kinetics of these previously inaccessible alloys. The list of possible systems and compounds requiring more distinctive thermodynamic characterization is much too lengthy to discuss here, but it is readily apparent that TFC is a powerful tool with which to perform the studies needed to further extend man's basic knowledge of metastable phase materials.

## 7. REFERENCES

- [1] Easterling, K.E., and Porter, D.A., "Phase Transformations in Metals and Alloys", (1981), p. 3, Van Nostrand Reinhold, Berkshire, England
- [2] Gambino, R.J., MRS Bulletin 4 (1990) 20.
- [3] Anderson, B., Hentzell, H.T.G., Karlsson, S.E., Acta Metall. 7 (1983) 1131.
- [4] Cantor, B., Cahn, R.W., Acta Met., 24 (1976) 845.
- [5] Anderson, B., Hentzell, H.T.G., Karlsson, S.E., Acta Metall. 7 (1983) 1136.
- [6] Ibid., 1134.
- [7] Cahn, R.W., Cantor, B., Acta Metall. (1976) 845.
- [8] Grant, W.A., Nucl. Instr. and Meth. 182/183 (1981) 809.
- [9] Sood, D.K., Radiation Effects 63 (1982) 141.
- [10] Davies, J.A., in "Ion Implantation and Beam Processing", eds. J.S.Williams and J.S. Poate, Academic Press, 1984.
- [11] Averbach, R.S., and Kirk, M.A., in "Surface Alloying by Ion, Electron, and Laser Beams", eds. L.E.Rehn, S.T.Picraux, H.Wiedersich, American Society for Metals, 1985.
- [12] Easterling, K.E., and Porter, D.A., "Phase Transformations in Metals and Alloys", Van Nostrand Reinhold 1981.
- [13] Picraux, S. T., Physics Today 11 (1984) 38.
- [14] Eridon, J.M., Was, G.S., Nucl. Instr. and Meth. in Phys. Res. B24/25 (1987) 557.
- [15] Hung, L.S., Lilienfeld, D.A., Mayer, J.W., Nucl Instr. and Meth. in Phys. Res. B19/20 (1987) 1-7.
- [16] Gyulai, J., Hung, L.S., Mayer, J.W., Nastasi, M., Appl. Phys. Lett. 42 (1983) 672.
- [17] Mader, S., J. Vac. Sci. Technol. 2 (1965) 35.

- [18] Brimhall, J.L., Charlot, L.A., Kissinger, H.E., Radiat. Eff. 77 (1983) 273.
- [19] Follstaedt, D.M., Nucl. Instr. and Meth. in Phys. Res. B7/8 (1985) 11-19.
- [20] Brimhall, J.L., Charlot, L.A., Kissinger, H.E., Radiat. Eff. 77 (1983) 273.
- [21] Gyulai, J., Hung, L.S., Mayer, J.W., Nastasi, M., Appl. Phys. Lett. 42 (1983) 672.
- [22] Lupis, C.H.P., "Chemical Thermodynamics of Materials", North-Holland, 1983.
- [23] Omar, M.A. "Elementary Solid State Physics", Addison-Wesley, 1975.
- [24] Lupis, C.H.P., "Chemical Thermodynamics of Materials", North-Holland, 1983.
- [25] Ibid.
- [26] Machlin, E.S., Acta Metallurgica 22 (1974) 109.
- [27] Baskes, M.I., Daw, M.S., Physical Rev. B 29 (1984) 6443.
- [28] Ansara, I., Sundman, B., Willemin, P., Acta Metall. 4 (1988) 977.
- [29] Ibid.
- [30] Baskes, M.I., Daw, M.S., Physical Rev. B 29 (1984) 6443.
- [31] Voter, A.F., Chen, S.P., in "MRS Symposium I Proceedings", Volume 82, 1986.
- [32] Ibid.
- [33] Eridon, J.M., Was, G.S., Nuc. Instr. and Meth. in Phys. Res., B24/25 (1987) 559.
- [34] Anderson, C.H., Fan, J.C.C., J. Appl. Phys. 52(6) 1981 4003.
- [35] Kissinger, H.E., Anal. Chem., 29 (1957) 1703.
- [36] Altounian, Z., Strom-Olsen, J.O., Walter, J.L., J. Appl. Phys. 6 (1984) 1566.
- [37] Atzmon, M., in "Solid State Powder Processing", eds. A.H. Clauer and J.J. deBarbadillo, The Minerals, Metals, & Materials Society, 1990.
- [38] Richardson, B.C., Risbud, S.H., Speyer, R.F., Met. Trans A, 17A (1986) 1479.

- [39] Roorda, S., Poate, J.M., Jacobson, D.C., Eagleshan, D.J., Dennis, B.S., Dierker, S., Phys. Res. Lett., (to be submitted, 1990).
- [40] Donovan, E.P., Spaepen, F., Turnbull, D., Poate, J.M., Jacobson, D.C., Appl. Phys. Lett. 42 (1983) 698.
- [41] Eridon, J.M., private communication.
- [42] Cavašin, D., Army Research Office progress report, 1988.
- [43] Gyulai, J., Hung, L.S., Mayer, J.W., Nastasi, M., Appl. Phys. Lett. 42 (1983) 672.
- [44] Brimhall, J.L., Simonen, E.P., Nucl. Instrum. Methods B, 16 (1986) 187
- [45] Thornton, J.A., Metallurgy Dept. Project Summary, The Telic Corp., Technical Report no. SR-79-135, 1979.
- [46] Fisher, R.M., Duan, J.Z., Fox, A.G., Mat Sci. and Eng. A117 (1989) 3.
- [47] Barbour, J.C., Liu, J.C., Mayer, J.W., J. Appl. Phys. 64 (1988) 656.
- [48] Barbour, J.C., Liu, J.C., Mayer, J.W., J. Appl. Phys. 64 (1988) 651.
- [49] Nicolet, M.A., Yang, H.Y., Zhao, X.A., J. Appl. Phys. 62 (1987) 1821.
- [50] McNaughton, J.L., Mortimer, C.T., "Differential Scanning Calorimetry", Perkin-Elmer Corp. Technical Publication L-604.
- [51] Gray, A.P., in "Proc. Amer. Chem. Soc. Symp. Analytical Chlorimetry", eds. R.S. Porter and J.F. Johnson, Plenum Press, 1968.
- [52] McKinley, J., private communication.
- [53] Pelton, A.R., Moine, P., Nack, M.A., Sinclair, R., in "Proceedings of the Materials Research Society", Symposium Q, Fall, 1985.
- [54] Ibid.
- [55] Ziegler, J.F., IBM Research Report RC9250, (1982)
- [56] Doolittle, L.R., Nuc. Inst. and Meth., B9 (1985) 344
- [57] Bradley, A.J., Phil. Mag., 23 (1937) 1049.

## APPENDIX A

DSC Subtraction

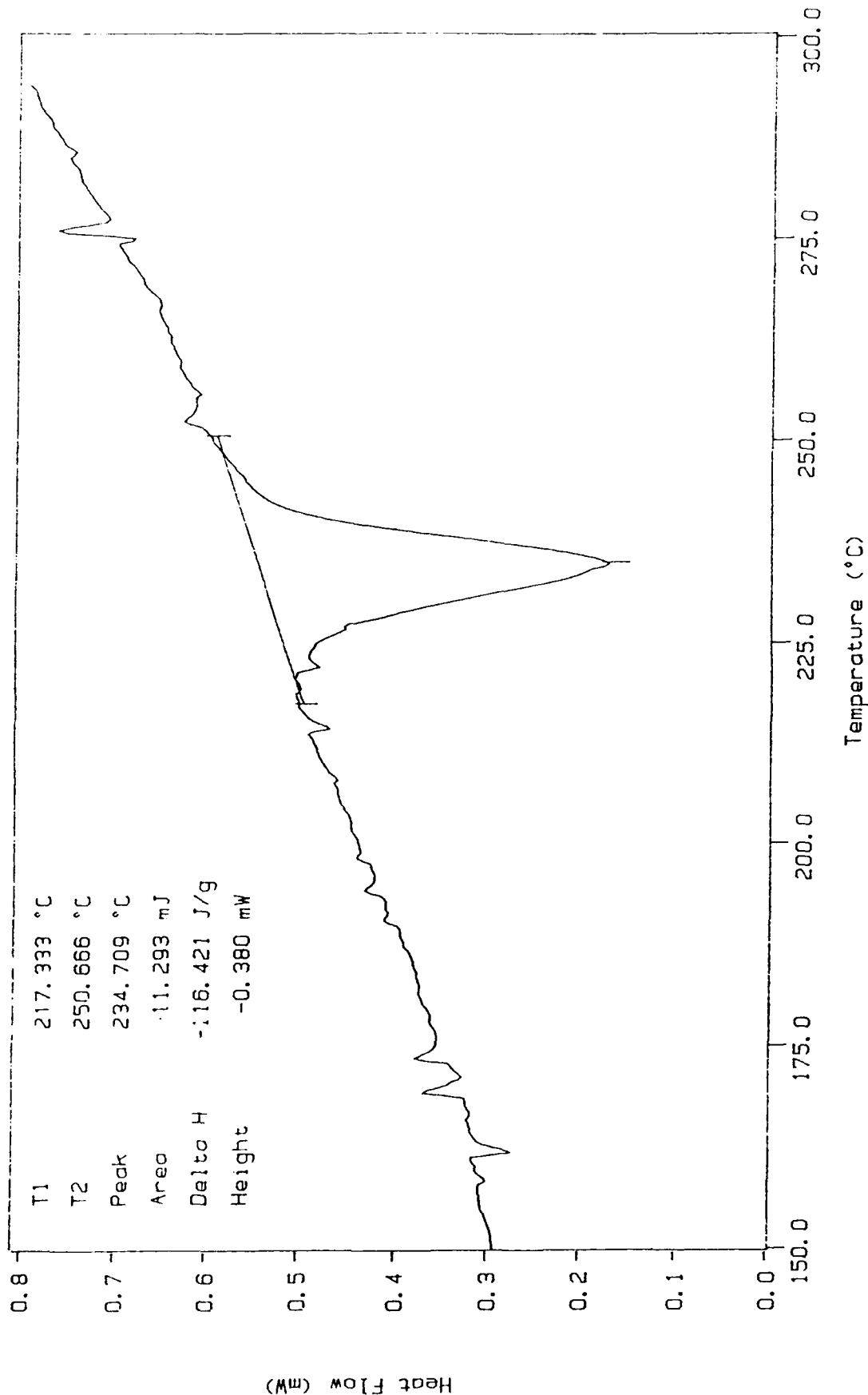
Sample Weight: 0.097 mg

Wed Apr 08 15:06:13 1987

dan09 600C 1hr. 5e15 run 1 4/27/90

(Subtracted) P1A09

PERKIN LLMER  
7 Series Thermal Analysis System



TEMP 1: 50.0 °C TIME 1: 0.0 min RATE 1: 20.0 °C/min  
TEMP 2: 600.0 °C

DSC Subtraction

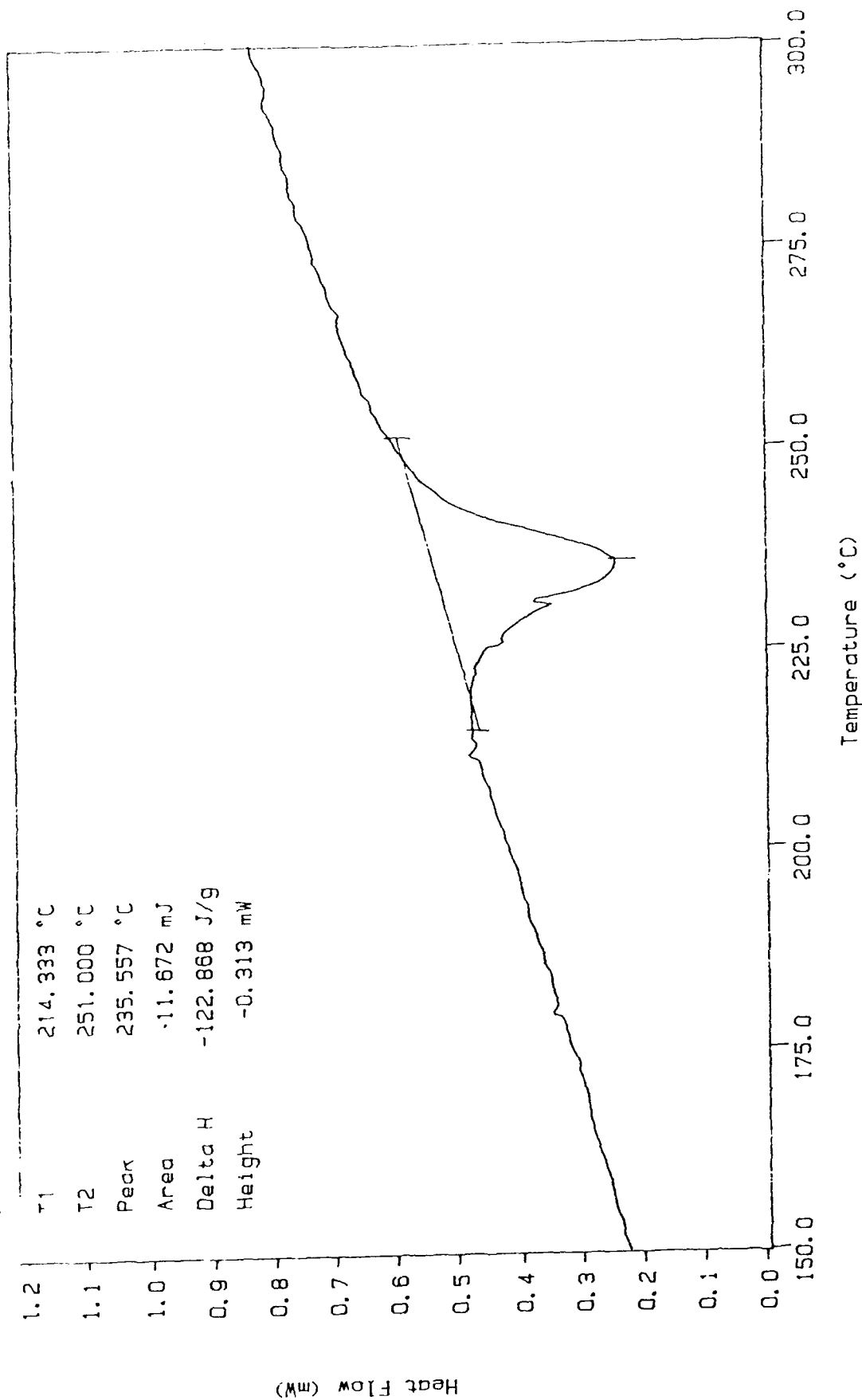
Sample Weight: 0.095 mg

Wed Apr 08 17:34:26 1987

Jan09 pan3 run1 4/27/90

(Subtracted) P3A09

PERKIN-ELMER  
7 Series Thermal Analysis System



TEMP 1: 50.0 °C TIME 1: 0.0 min RATE 1: 20.0 °C/min  
TEMP 2: 600.0 °C

DSC Subtraction

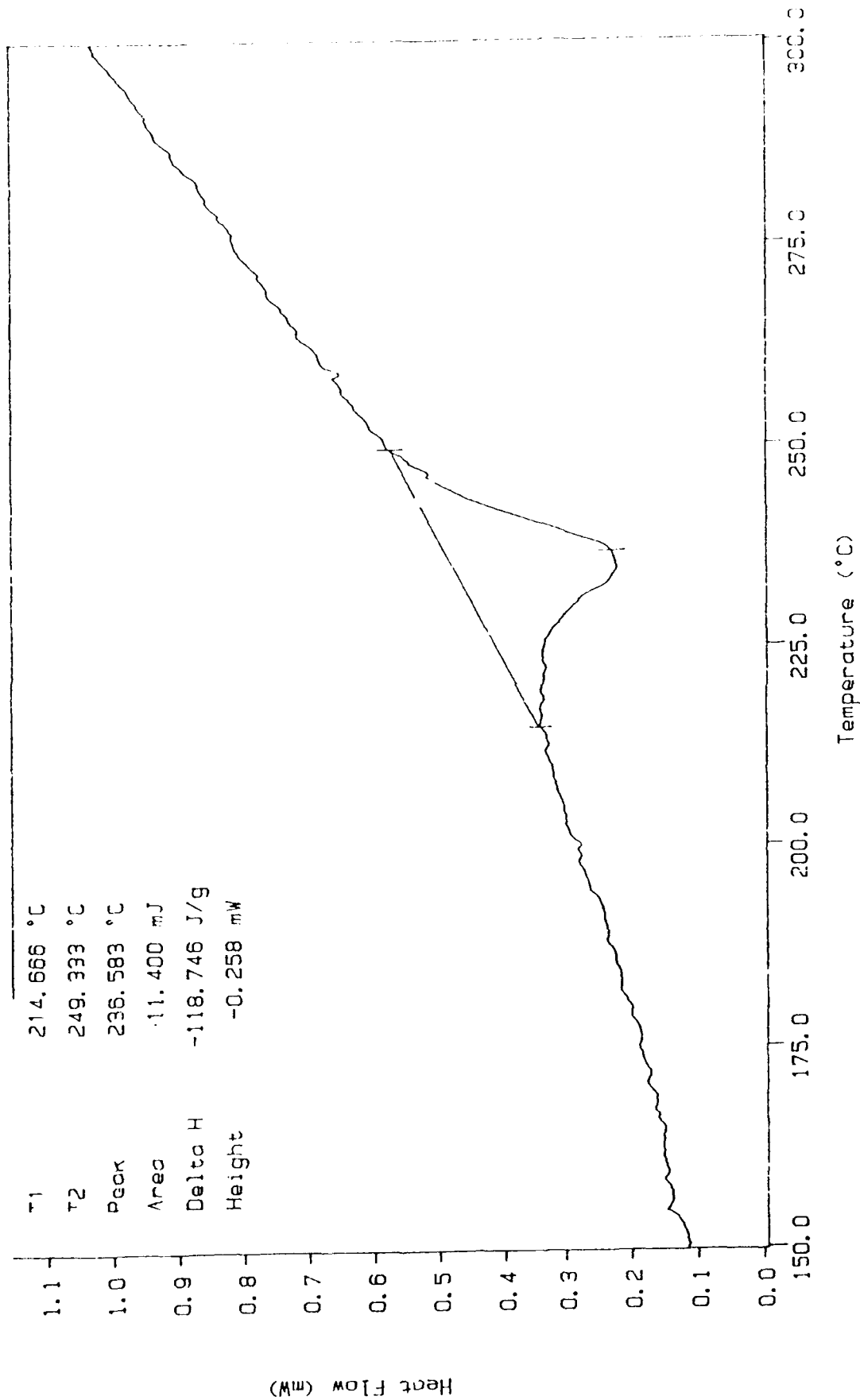
Sample Weight: 2.096 mg

Wed Apr 08 18:43:51 1987

Jan09 pan4 run1 4/27/90

(Subtracted) P4A09

PERKIN-ELMER  
7 Series Thermal Analysis System



TEMP 1: 50.0 °C TIME 1: 0.0 min RATE 1: 20.0 °C/min  
TEMP 2: 800.0 °C

DSC Subtraction

Sample Weight: 0.072 mg

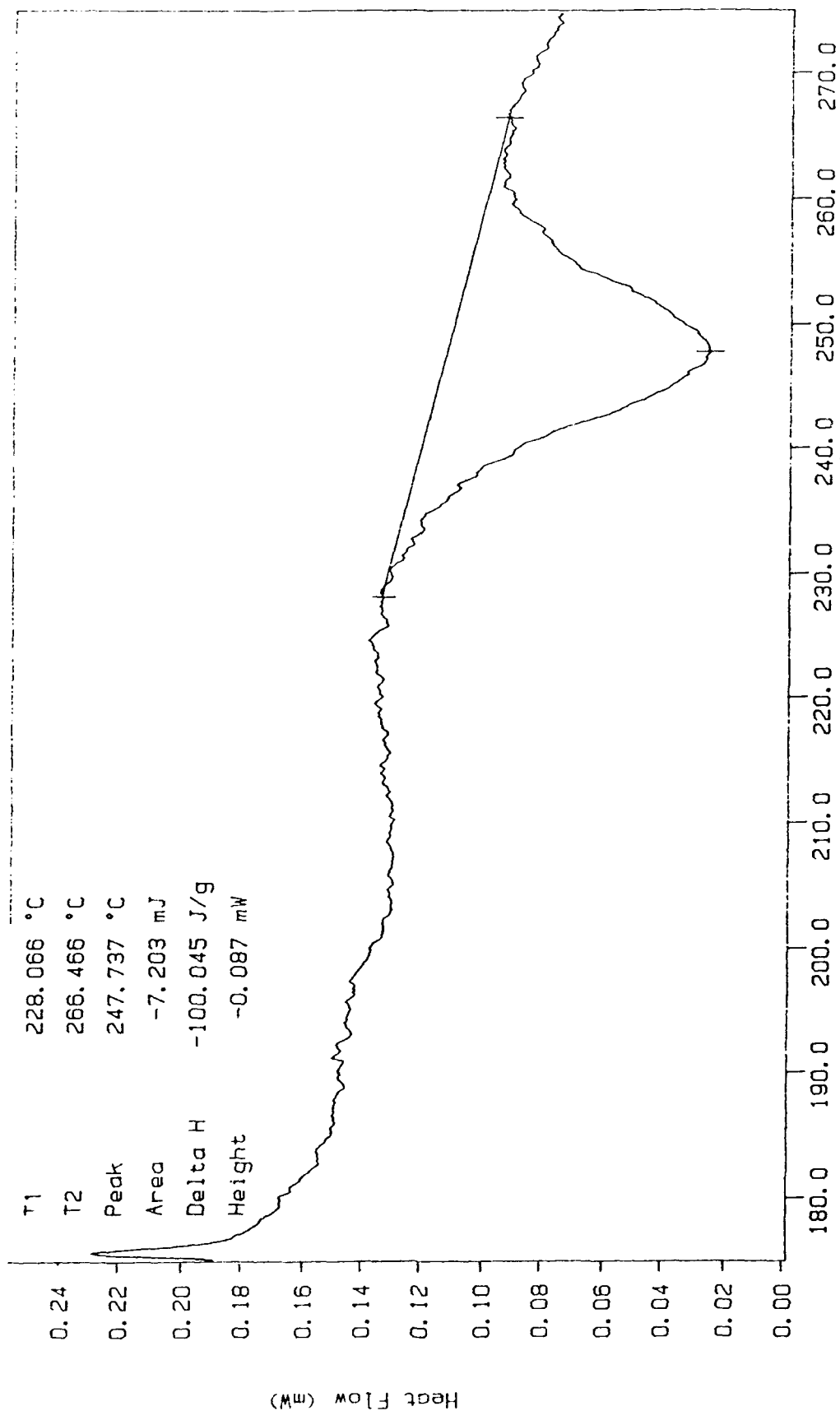
Thu Apr 09 07:57:00 1987

Jan10 p1 vs p10 ~~5/13/90~~ 5/13/90

(Subtracted)

PLR KIN-ELMER

7 Series Thermal Analysis System



Run 1

TEMP 1: 175.0 °C

TEMP 2: 275.0 °C

TIME 1: 0.0 min RATE 1: 10.0 °C/min

Temperature (°C) 110

DSC Subtraction

Sample Weight: 0.074 mg

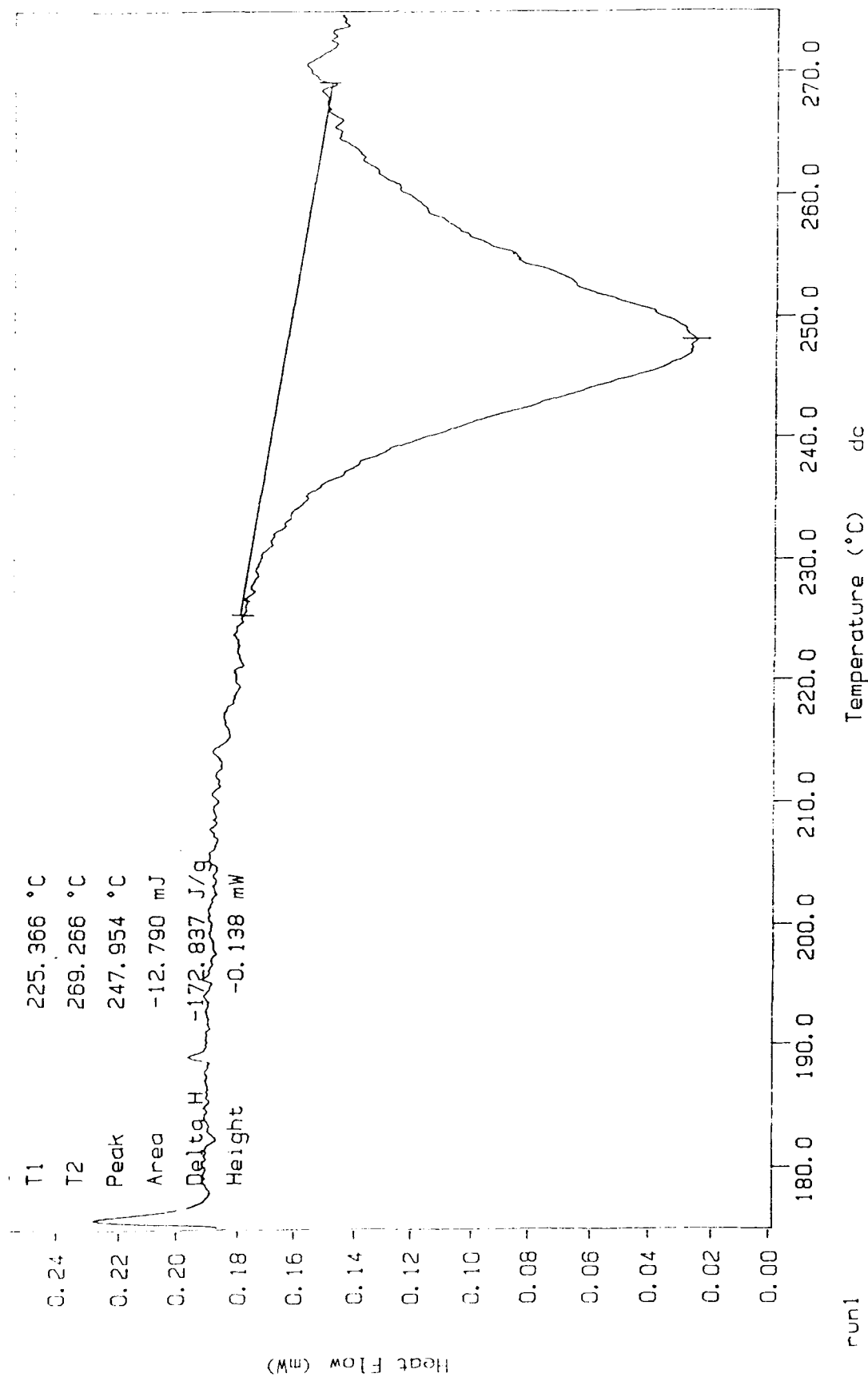
Thu Apr 09 08:40:58 1987

p2 vs p10 5/13/90

(Subtracted)

PERKIN-ELMER

7 Series Thermal Analysis System



run1

TEMP 1: 175.0 °C

TEMP 2: 275.0 °C

TIME 1:

0.0 min

RATE 1:

10.0 °C/min

DSC Subtraction

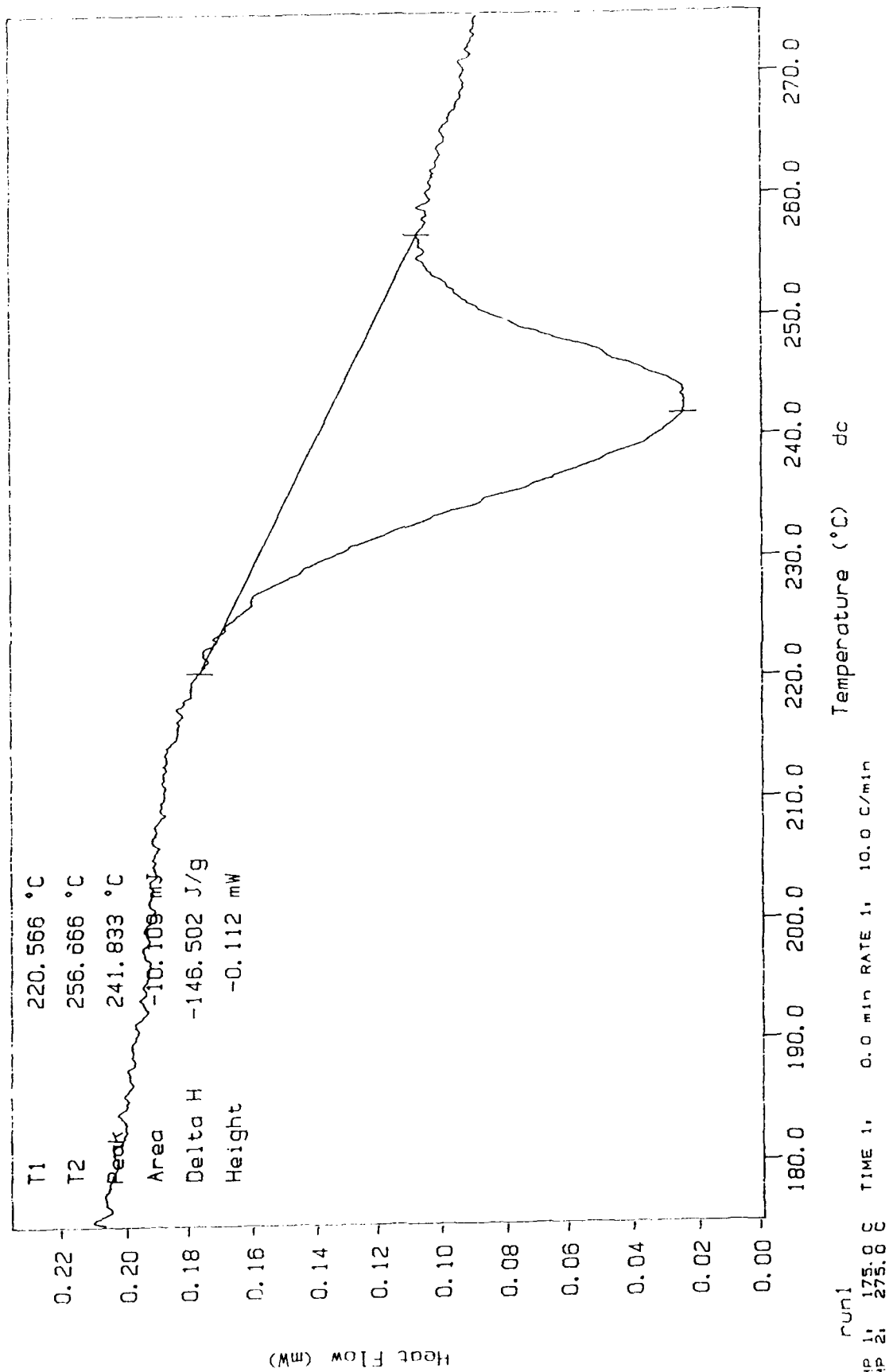
Sample Weight: 0.069 mg

Thu Apr 09 09:23:19 1987

p3 vs p10 5/13/90

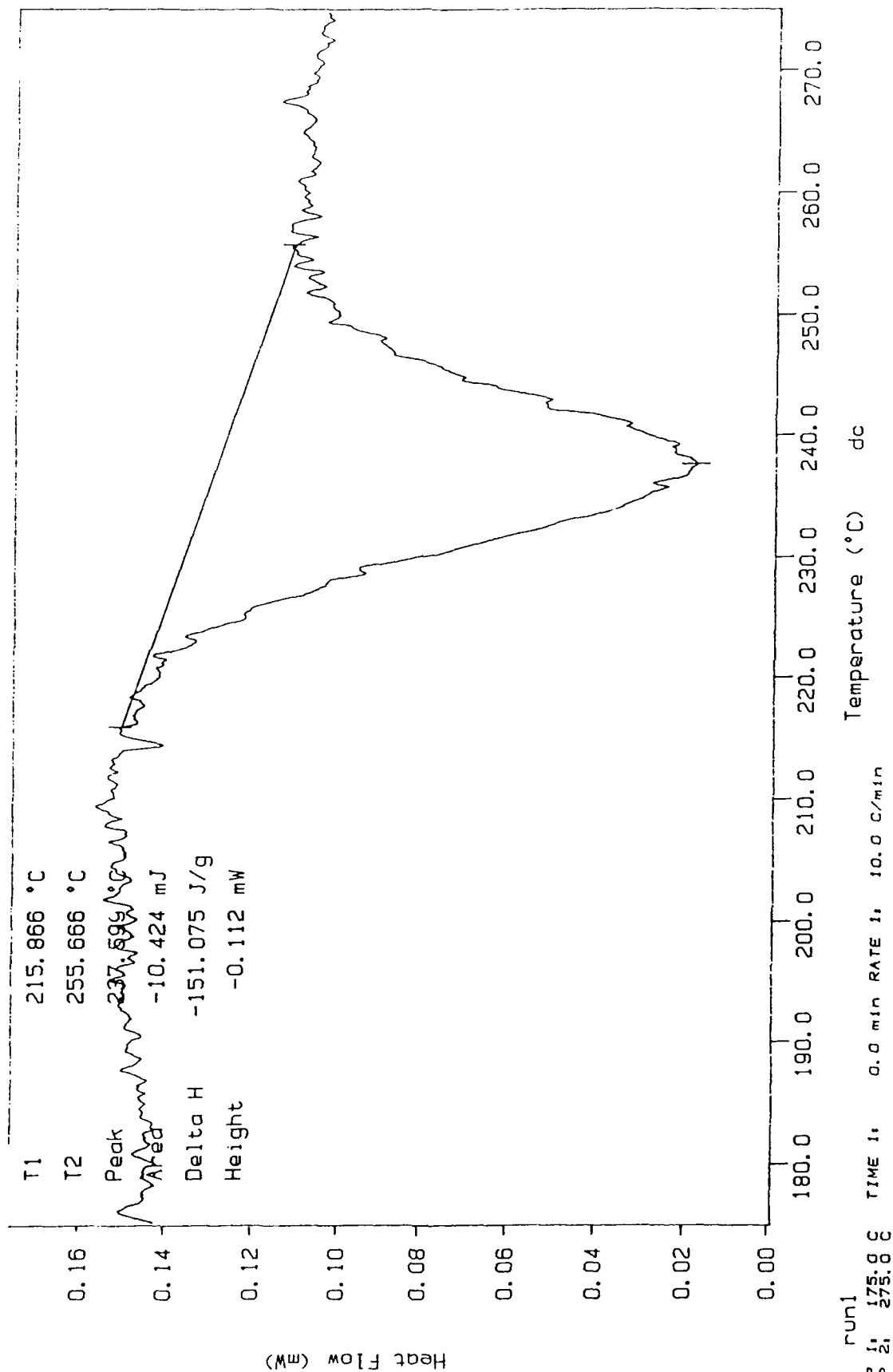
(Subtracted)

PERKIN-ELMER  
7 Series Thermal Analysis System



DSC Subtraction  
Sample Weight: 0.069 mg  
Thu Apr 09 10:06:31 1987  
p4 vs p10 1e16 5/13/90  
(Subtracted)

PERKIN-ELMER  
7 Series Thermal Analysis System



DSC Subtraction

Sample Weight: 0.072 mg

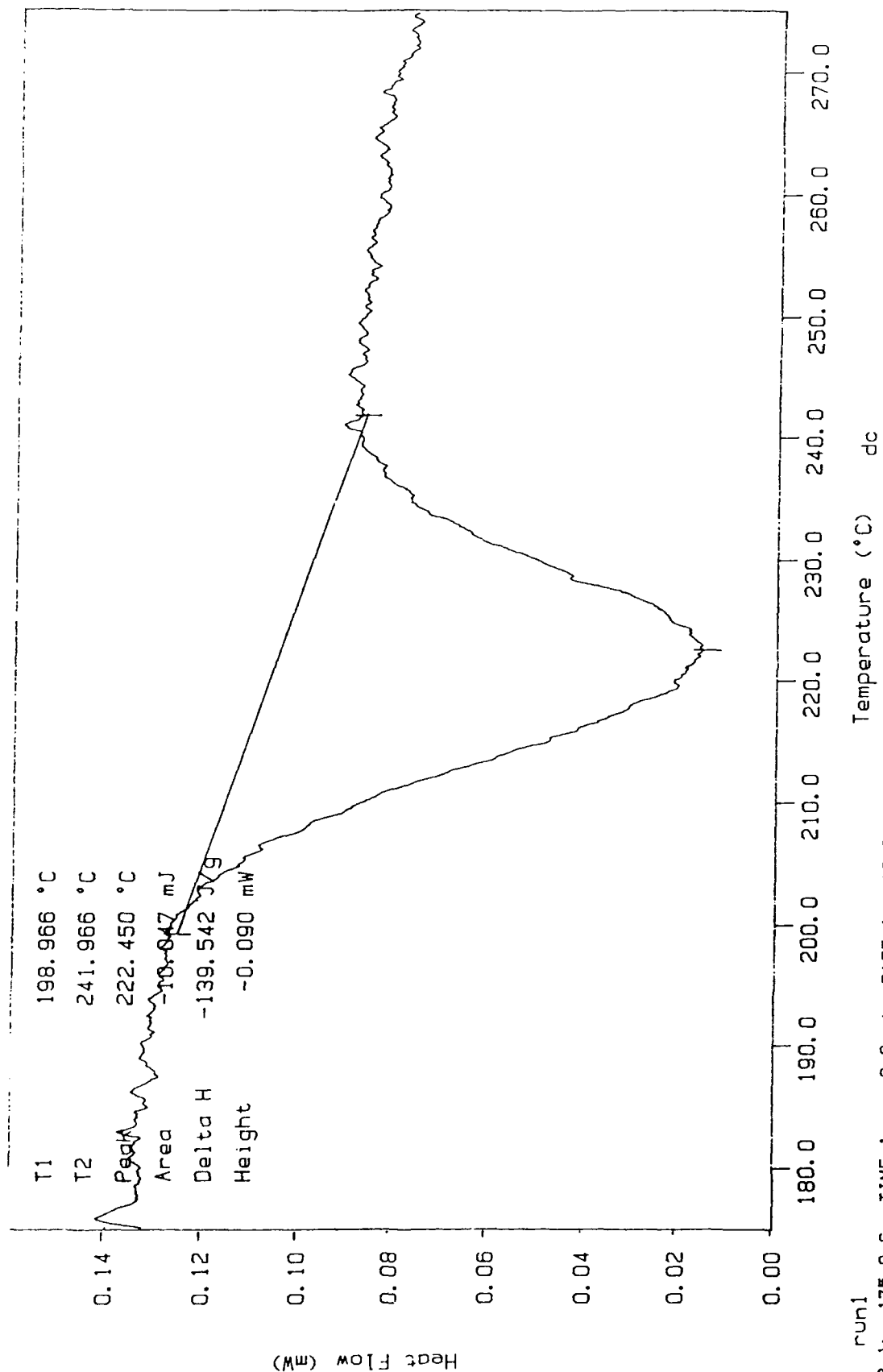
Thu Apr 09 10:51:00 1987

p5 vs p10 1E16 5/13/90

(Subtracted)

PERKIN-ELMER

7 Series Thermal Analysis System



DSC Subtraction

Sample Weight: 0.074 mg

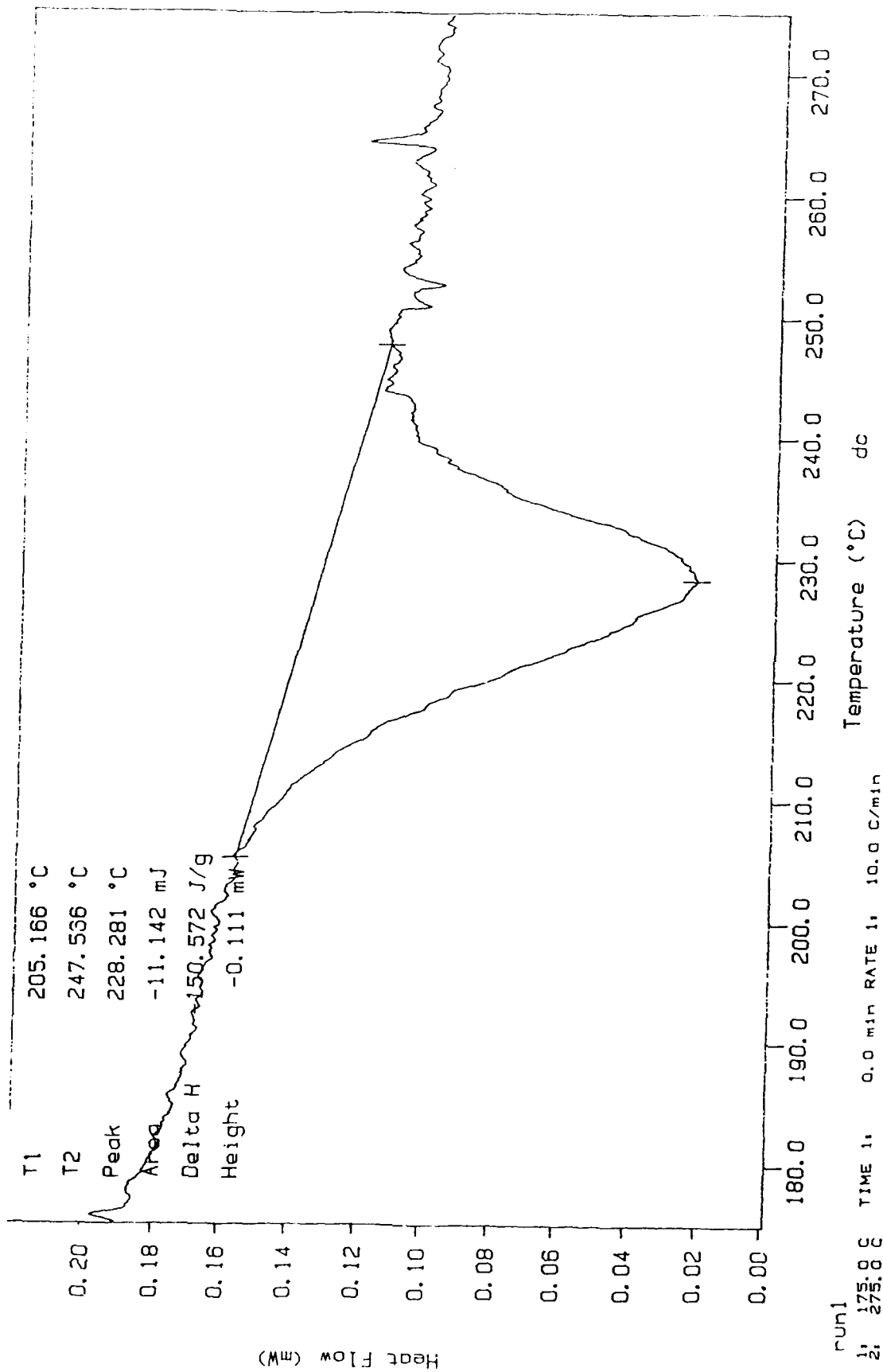
Thu Apr 09 11:35:41 1987

p6 /s p9 8e15 5/13/90

(Subtracted)

PERKIN-ELMER

7 Series Thermal Analysis System



DSC Subtraction

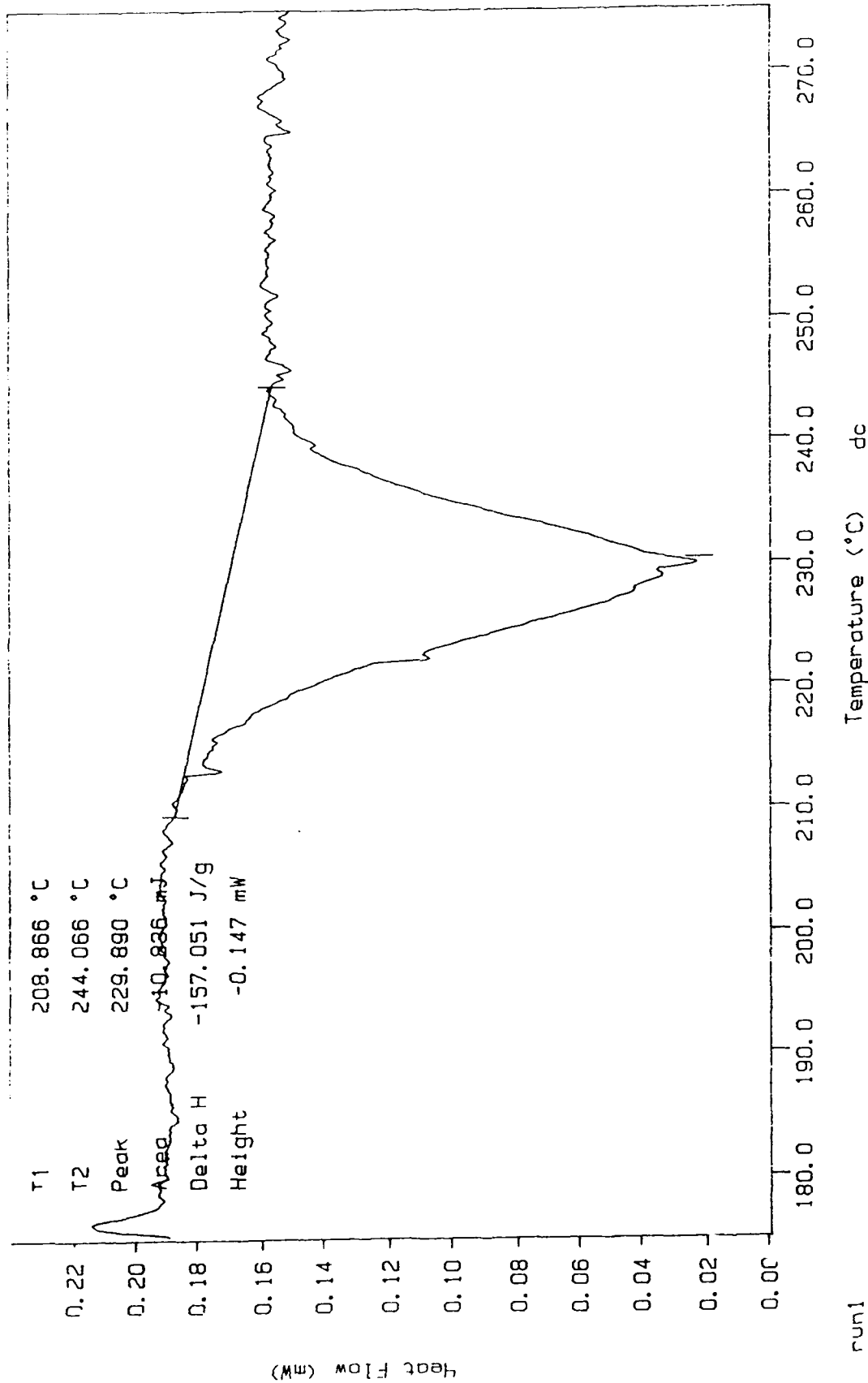
Sample Weight: 0.069 mg

Thu Apr 09 12:18:21 1987

p7 /s p14 8L15 5/13/90

(Subtracted)

PERKIN-ELMER  
7 Series Thermal Analysis System



run1  
TEMP 1: 175.0 °C  
TEMP 2: 275.0 °C  
TIME 1: 0.0 min RATE 1: 10.0 °C/min

DSC Subtraction

Sample Weight: 0.085 mg

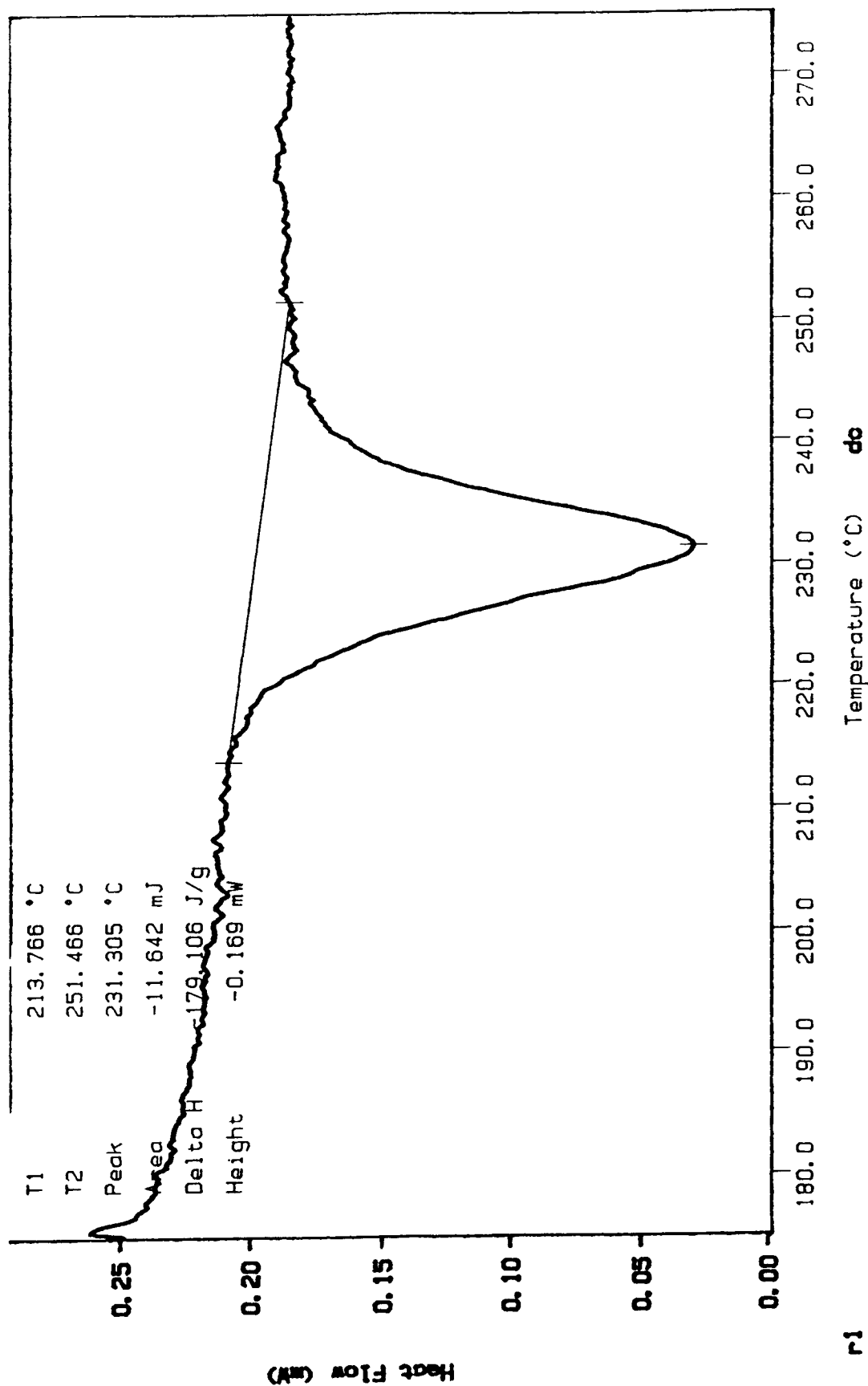
Wed Apr 08 17:40:22 1987

dan12 7e15 run1 pan1 5/17/90

(Subtracted)

PERKIN-ELMER

7 Series Thermal Analysis System



177.8 °C TIME: 0.0 min RATE: 10.0 C/min

DSC Subtraction

Sample Weight: 0.069 mg

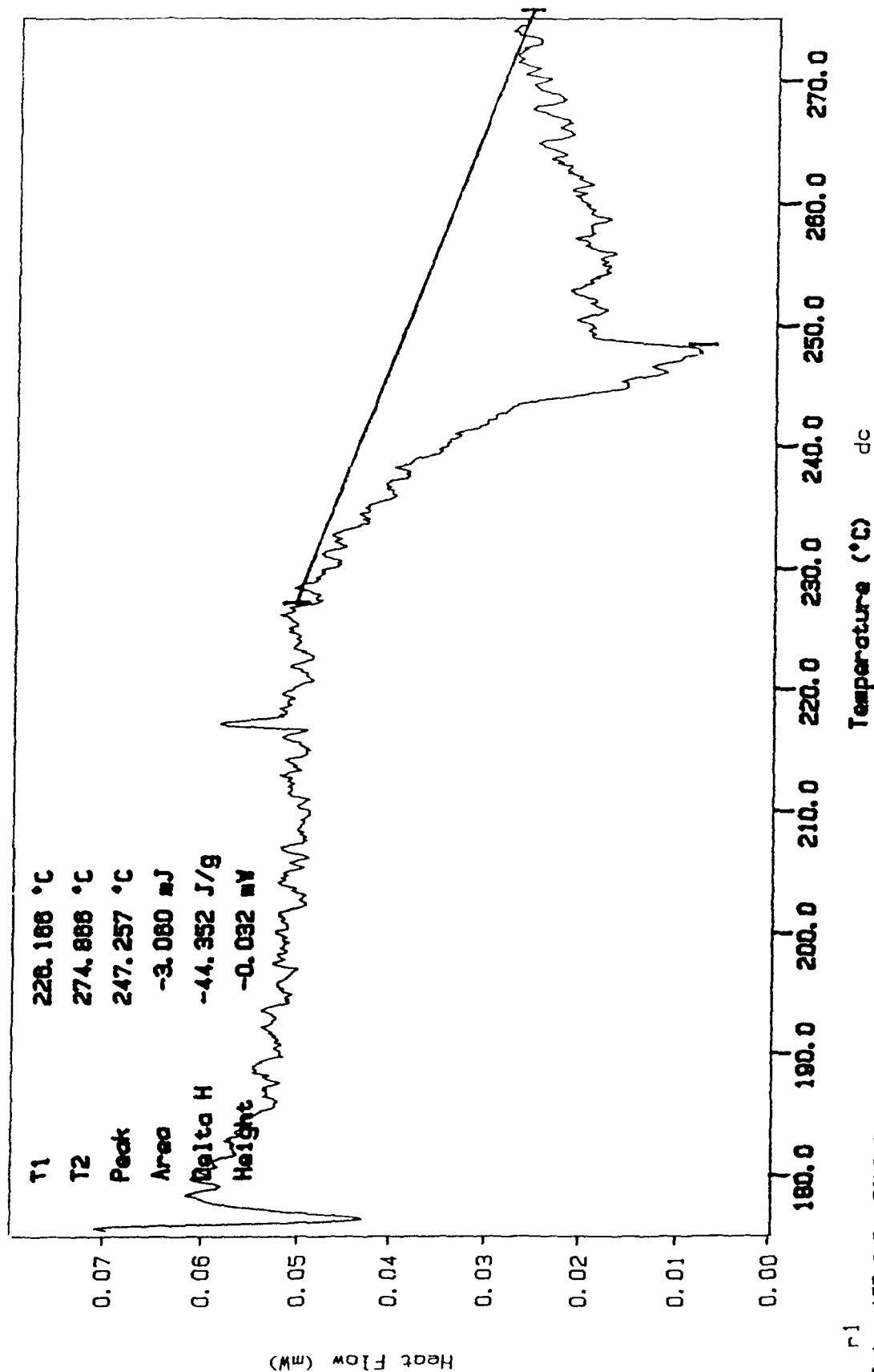
Wed Apr 08 19:04:34 1987

p3 5/17/90

(Subtracted)

PERKIN-ELMER

7 Series Thermal Analysis System



DSC Subtraction

Sample Weight: 0.074 mg

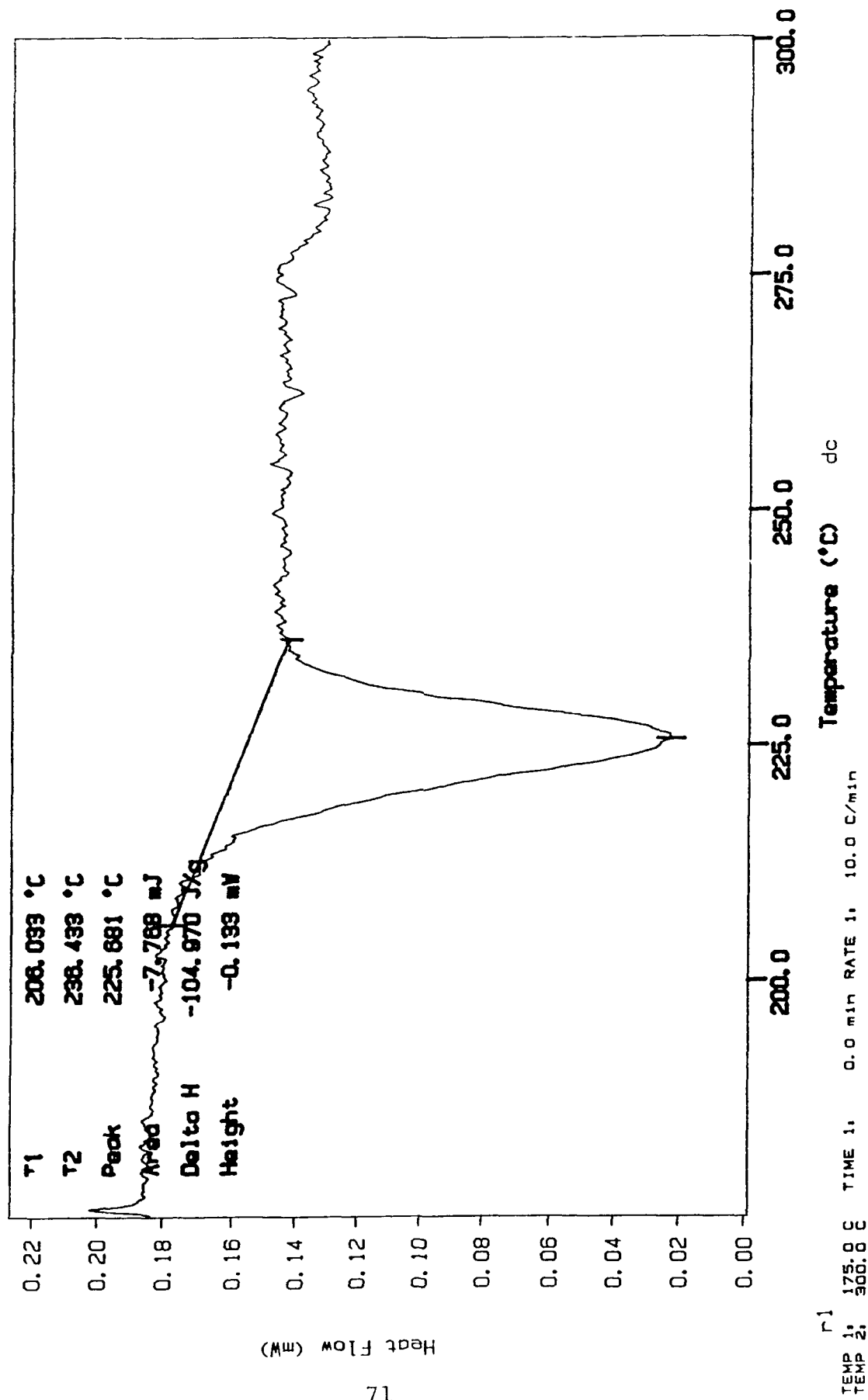
Wed Apr 08 19:48:39 1987

p1 5/17/90

(Subtracted)

PERKIN-ELMER

7 Series Thermal Analysis System



DSC Subtraction

Sample Weight: 0.069 mg

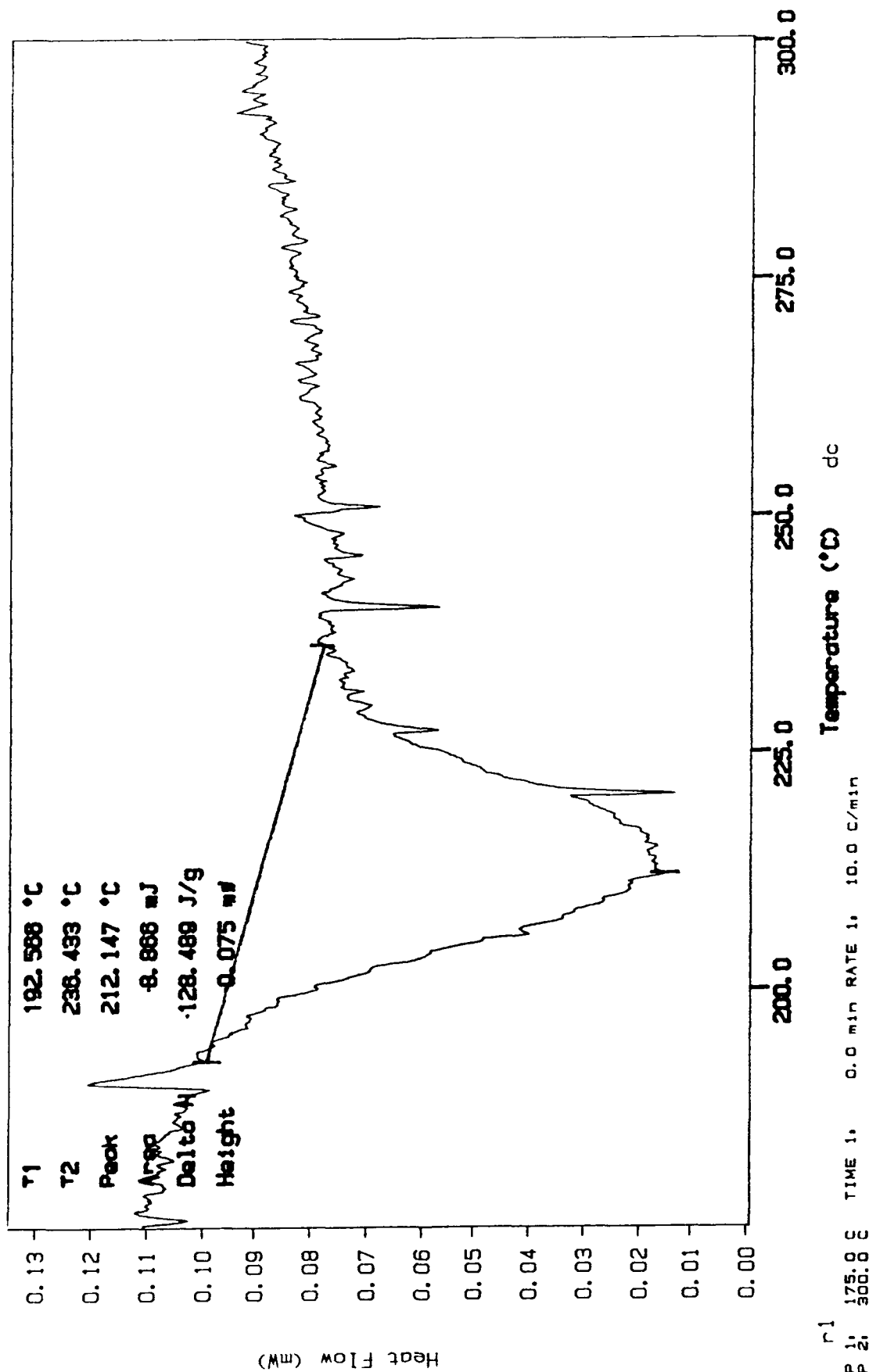
Wed Apr 08 20:34:55 1987

p5-2e16 5/17/90

(Subtracted)

PURKIN LMER

# 7 Series Thermal Analysis System



DSC Subtraction

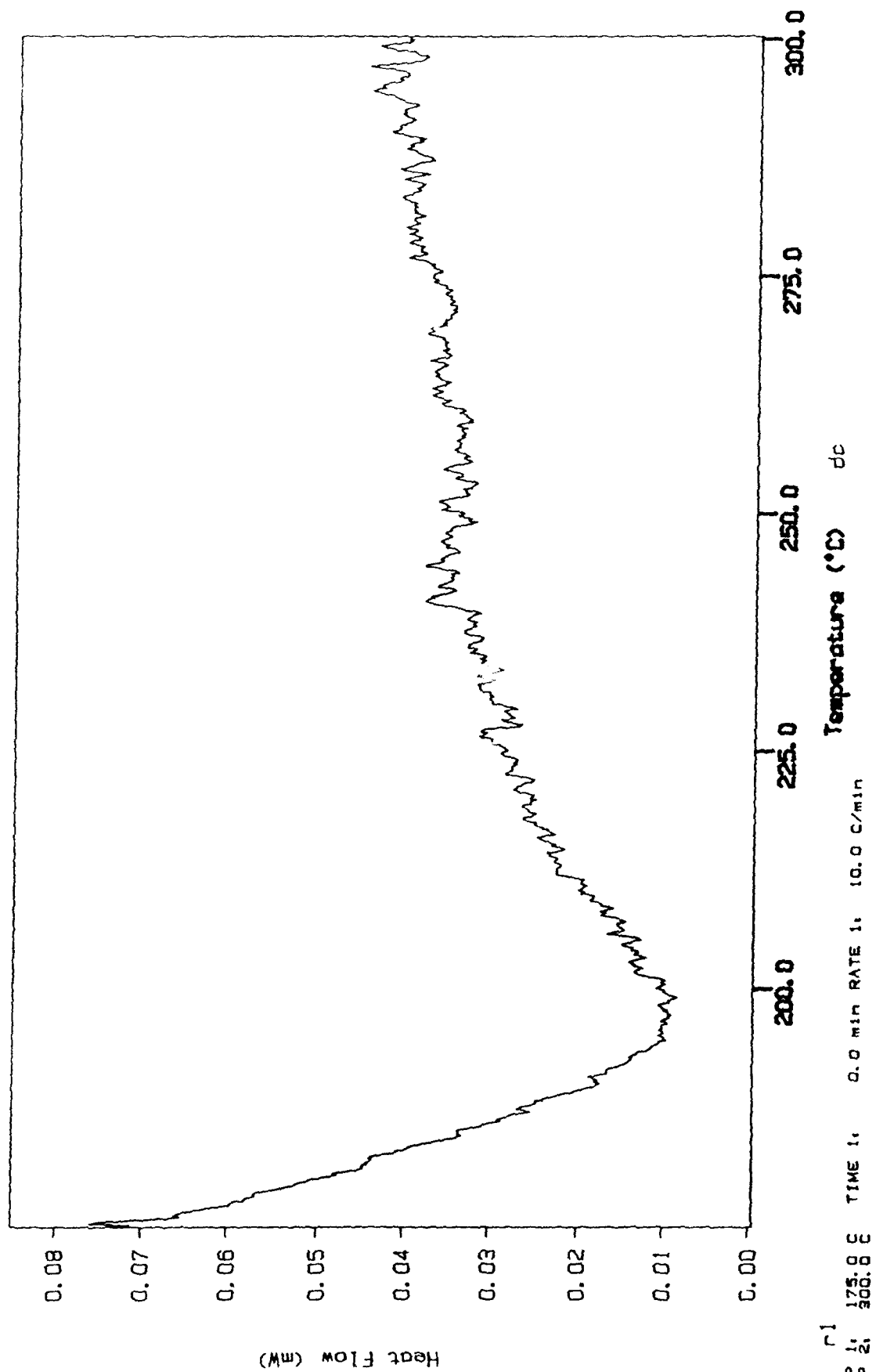
Sample Weight: 0.070 mg

Wed Apr 08 21:23:02 1987

PG 2e16 5/17/90

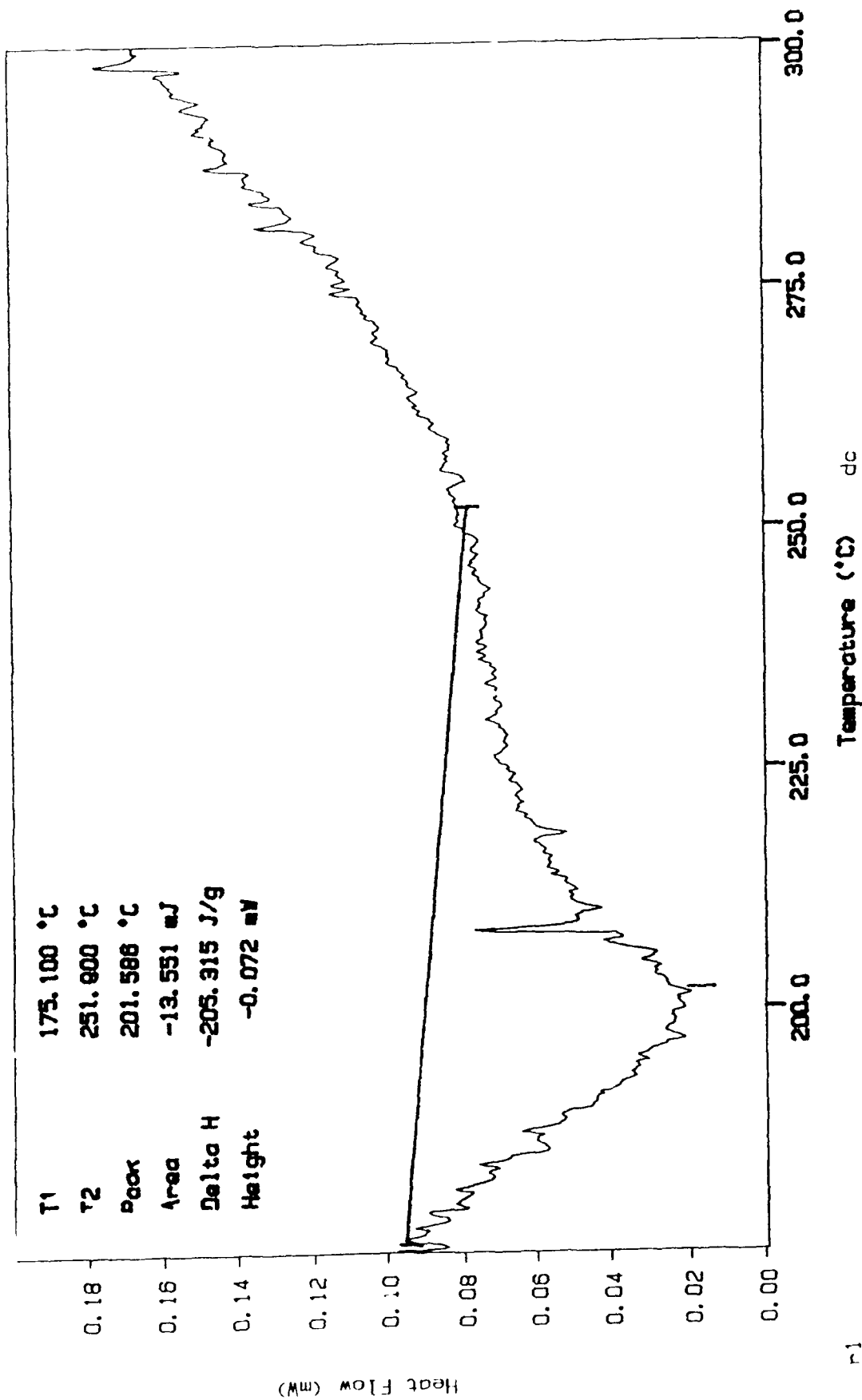
(Subtracted)

P\_RKIN \_M\_R  
7 Series Thermal Incl/919 S/9tem



# PERKIN-ELMER 7 Series Thermal Analysis System

DSC Subtraction  
Sample Weight: 0.066 mg  
Wed Apr 08 22:11:43 1987  
p7 2e16 5/17/90  
(Subtracted)

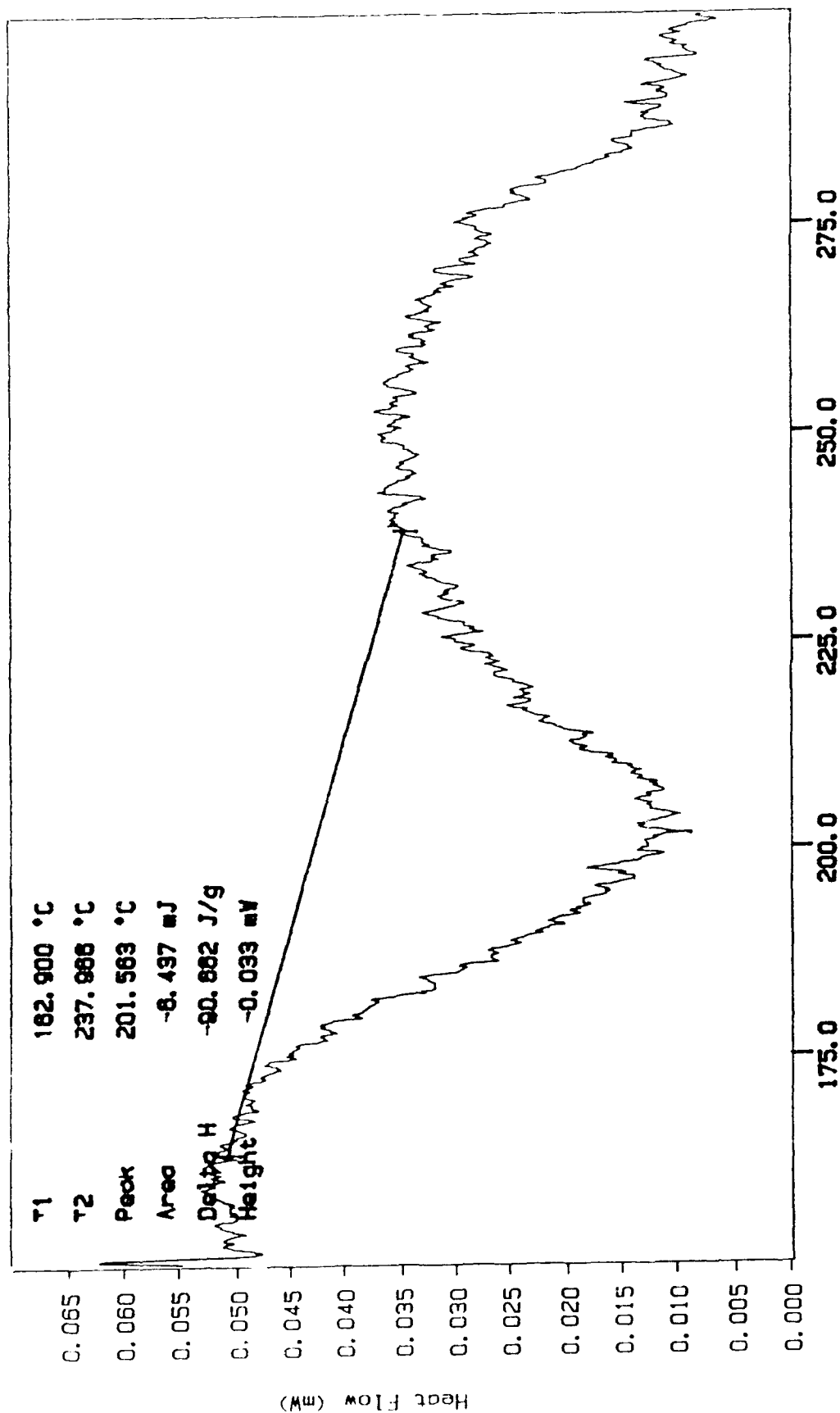


r1  
TEMP 1: 175.0 °C  
TEMP 2: 300.0 °C  
TIME 1: 0.0 min  
RATE 1: 10.0 °C/min  
dc

DSC Subtraction  
 Sample Weight: 0.071 mg  
 Wed Apr 08 23:04:20 1987  
 p8 2e16 5/17/90  
 (Subtracted)

PERKIN-ELMER

# 7 Series Thermal Analysis System



r1  
 TEMP 1: 150.0 °C  
 TEMP 2: 300.0 °C  
 TIME 1: 0.0 min  
 RATE 1: 10.0 °C/min

dc

DSC Subtraction

Sample Weight: 0.071 mg

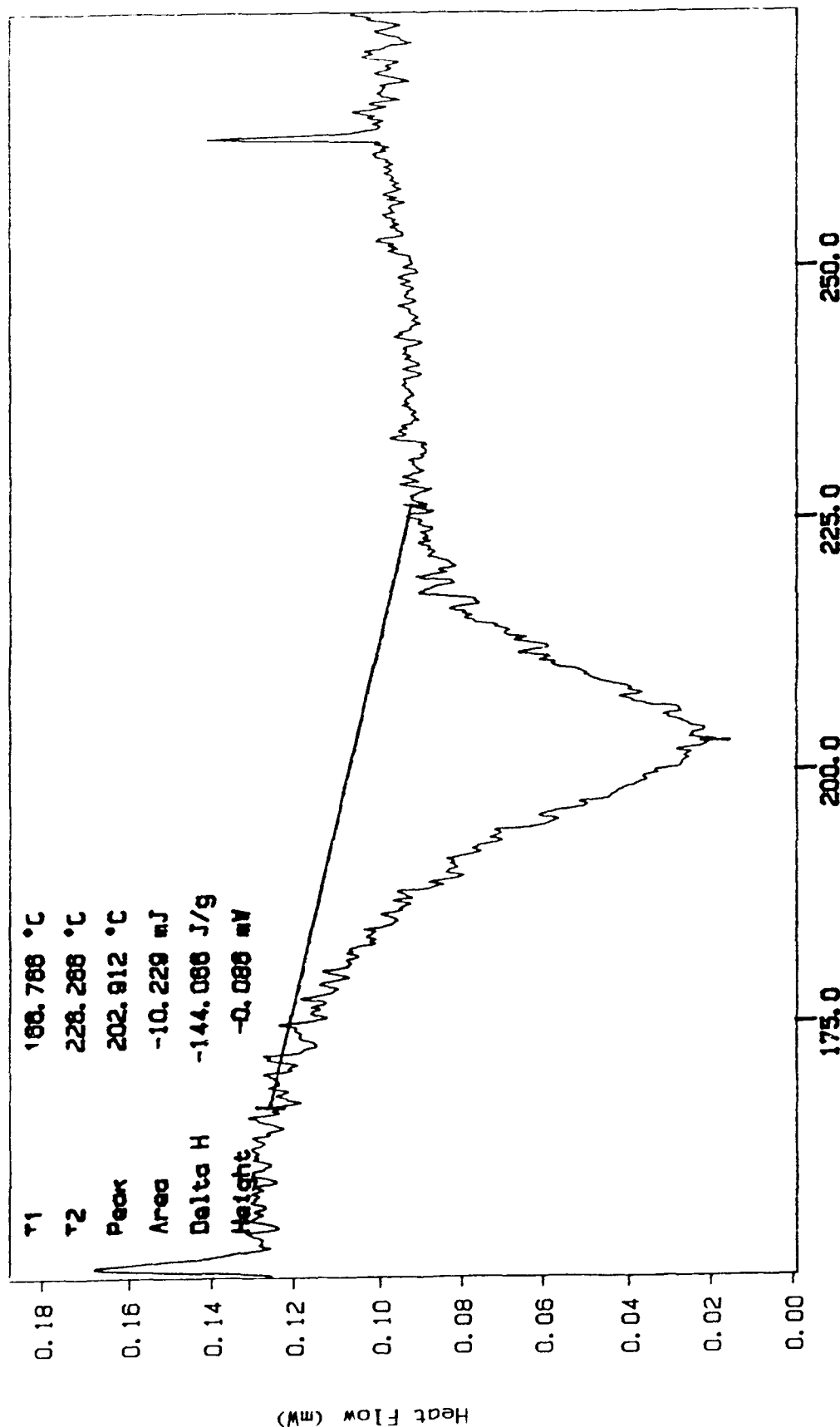
Wed Apr 08 23:53:49 1987

p9 2e16 5/17/90

(Subtracted)

PLRKN LLMR

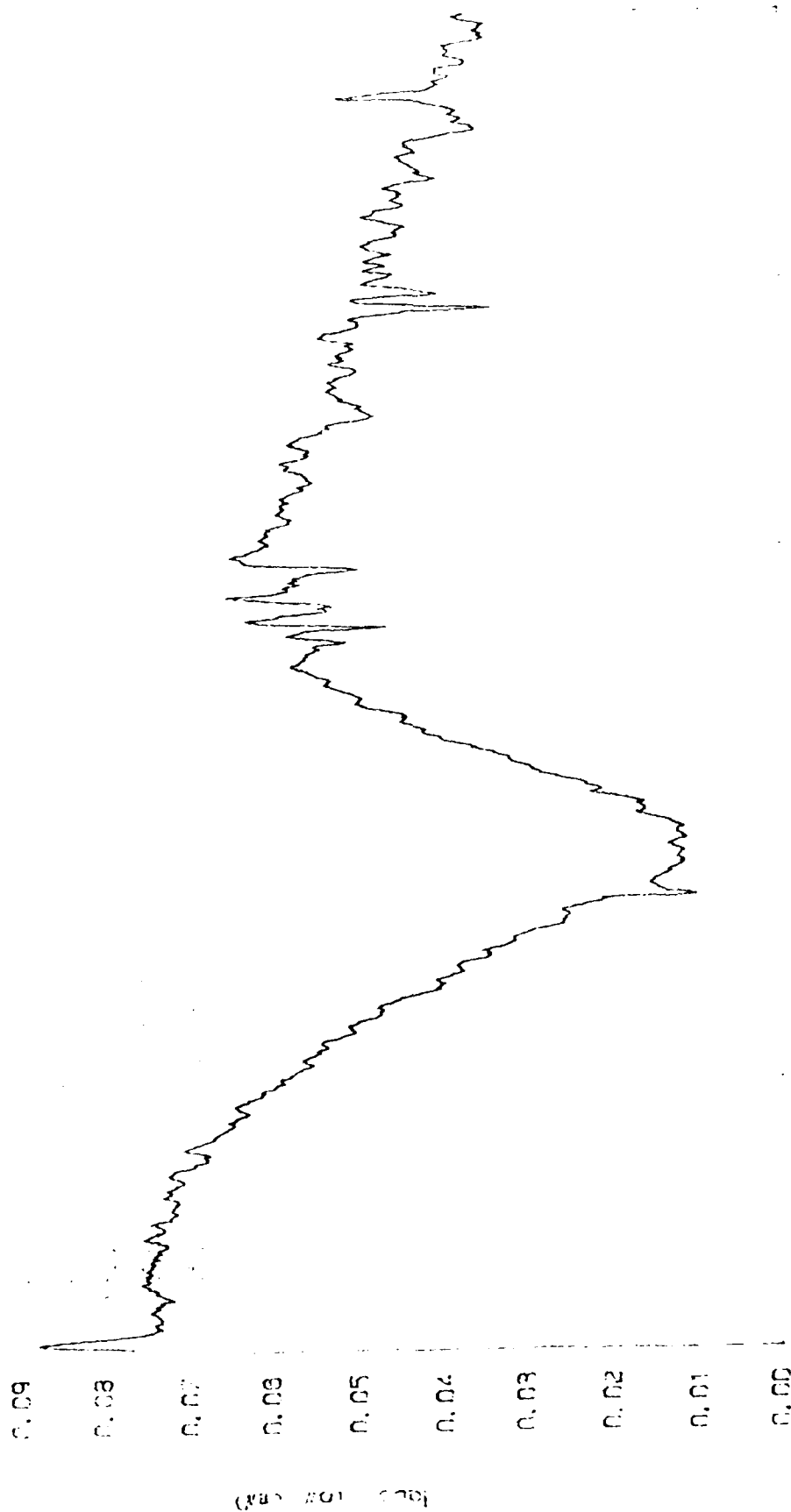
7 Series Thermal Analysis S/9.0M



Temperature (°C) dc

r1  
TEMP 1: 190.0 °C TIME 1: 0.0 min RATE 1: 10.0 °C/min  
TEMP 2: 275.0 °C

22. Subtraction  
 Sample Weight: 0.073 mg  
 Run Date: 09/09/2008 11:22:19  
 Run Time: 01:55:00  
 (continued)



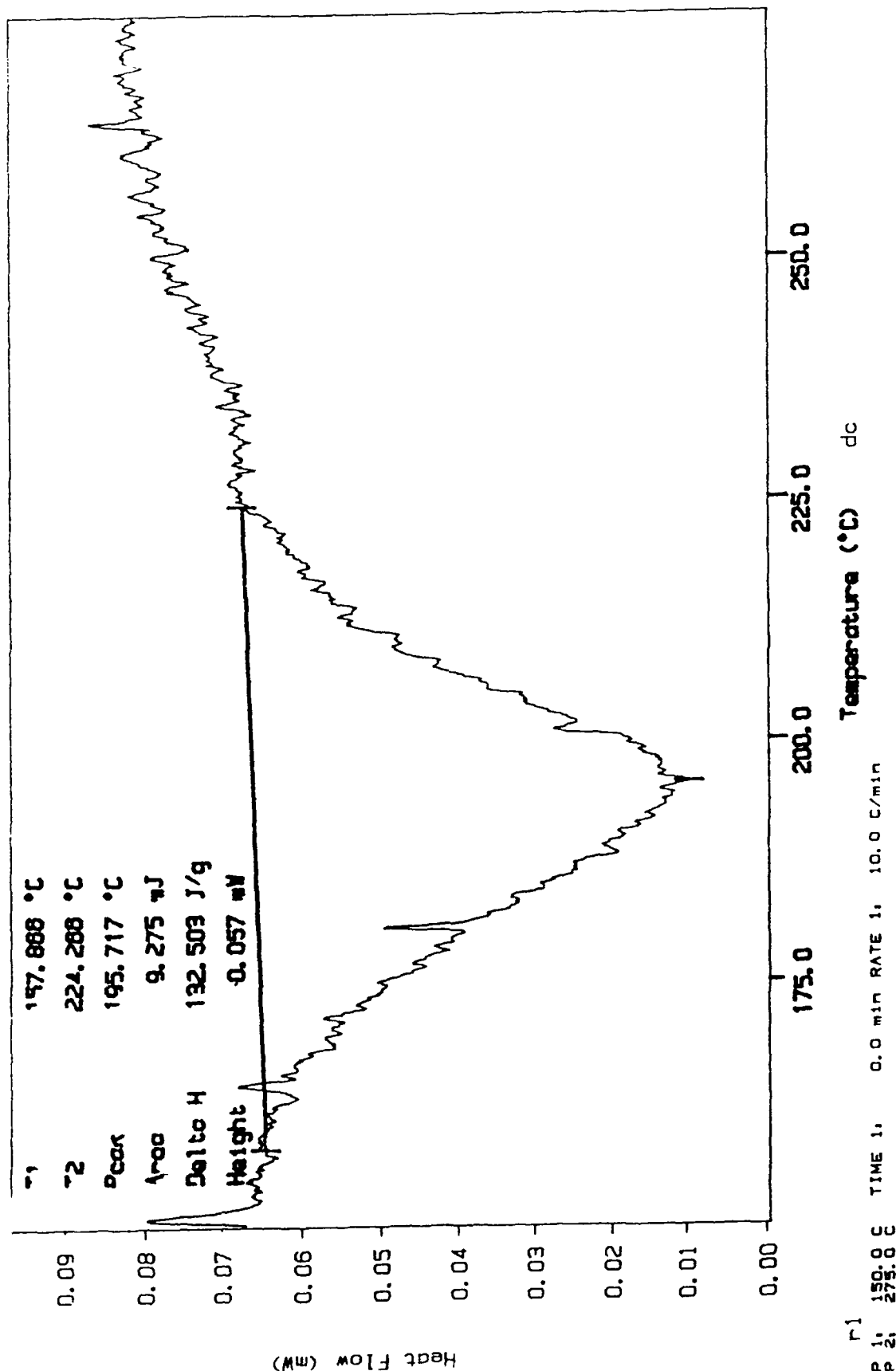
dc

TEMP 1: 150.0 C  
 TEMP 2: 275.0 C  
 TIME 1: 0.0 min RATE 1: 10.0 C/min

DSC Subtraction  
 Sample Weight: 0.070 mg  
 Thu Apr 09 01:21:58 1987  
 pl1 7a15 5/17/90  
 (Subtracted)

PERKIN ELMER

7 Series Thermal Analysis System



DSC Subtraction

Sample Weight: 0.063 mg

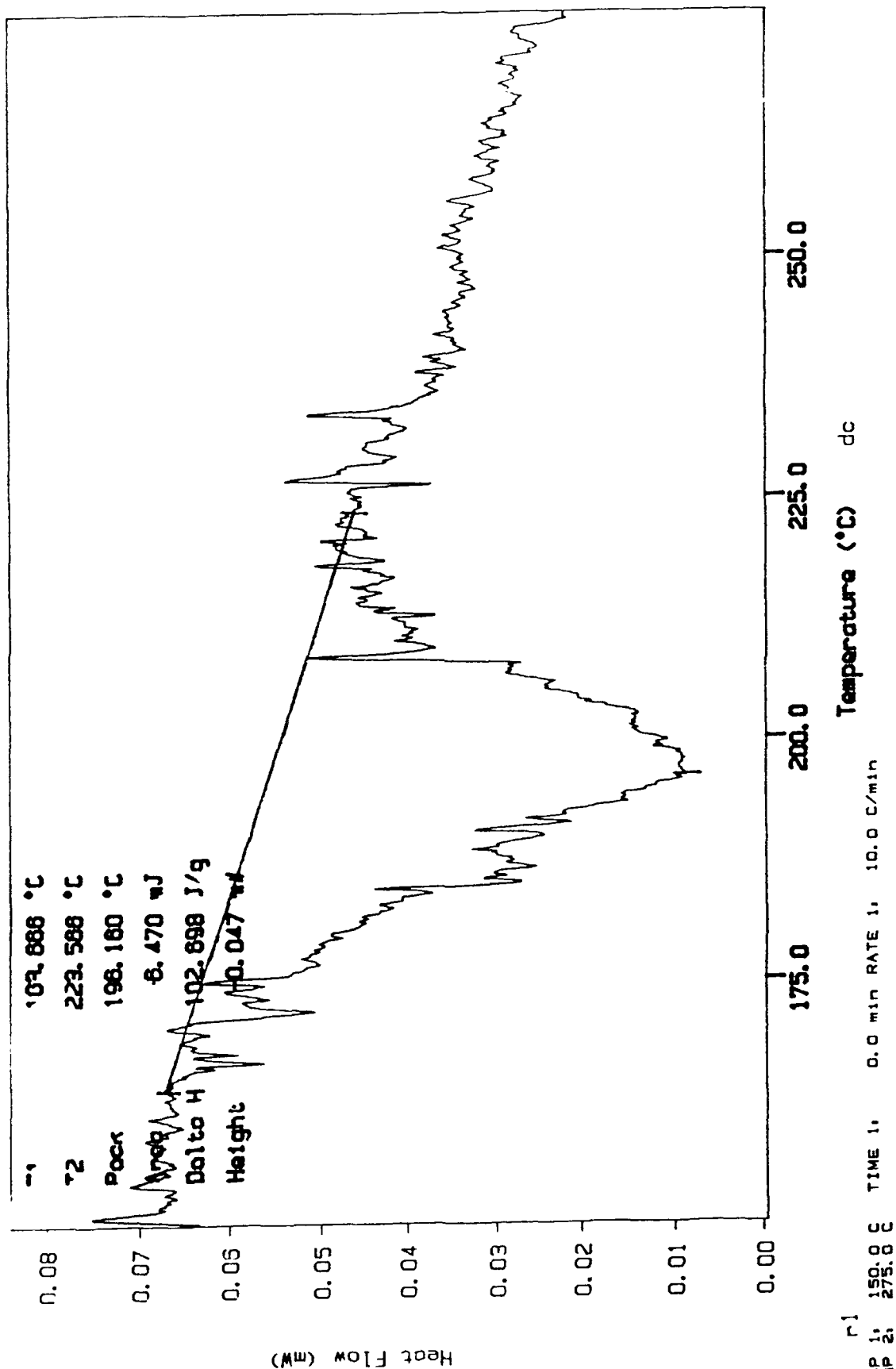
Thu Apr 09 02:05:19 1987

n12 7e15 5/17/90

(Subtracted)

PURIN LMLR

7 Series Thermal Analysis System



DSC Subtraction

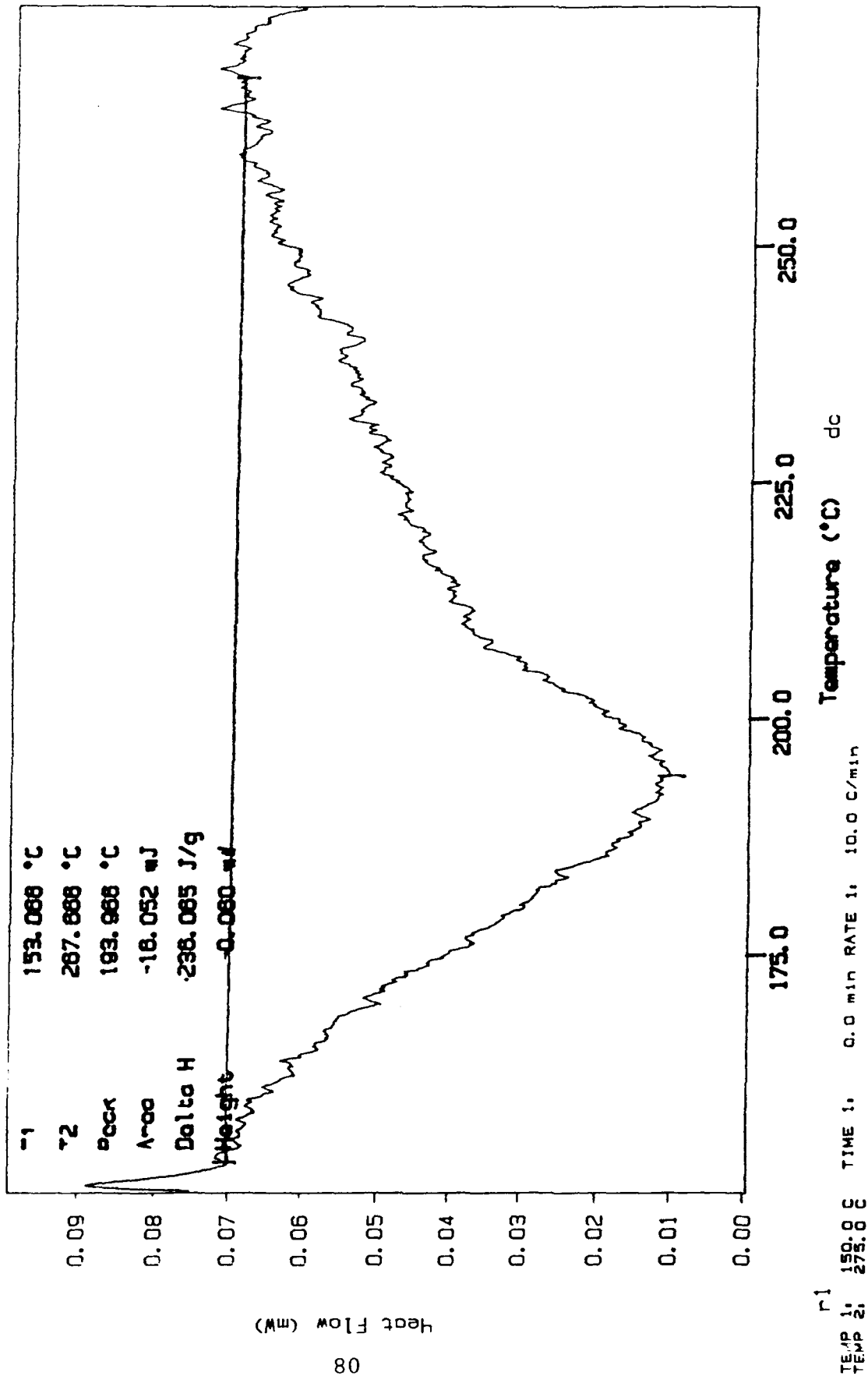
Sample Weight: 0.068 mg

Thu Apr 09 02:49:43 1987

pl3 2a16 5/17/90

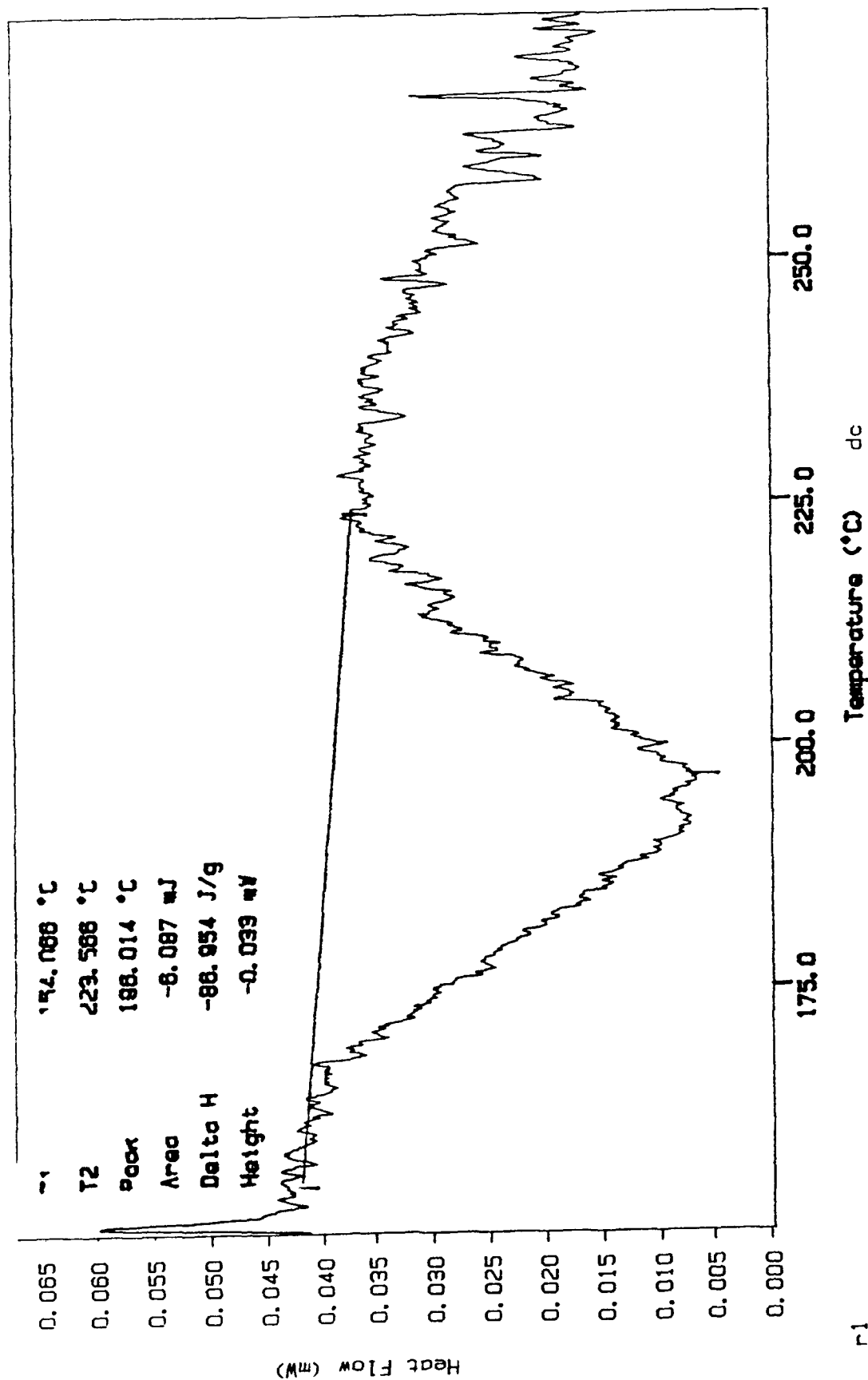
(Subtracted)

P\_RAIN\_MLR  
7 Series Thermal 1mcl/sis 9/scom



DSC Subtraction  
 Sample Weight: 0.070 mg  
 Thu Apr 09 03:32:35 1987  
 p14 2e16 5/17/90  
 (Subtracted)

PLRIN LMLR  
 7 Series Thermal Analysis System



r1  
 TEMP 1: 150.0 °C  
 TEMP 2: 275.0 °C  
 TIME 1: 0.0 min  
 RATE 1: 10.0 °C/min

DSC Subtraction

Sample Weight: 0.065 mg

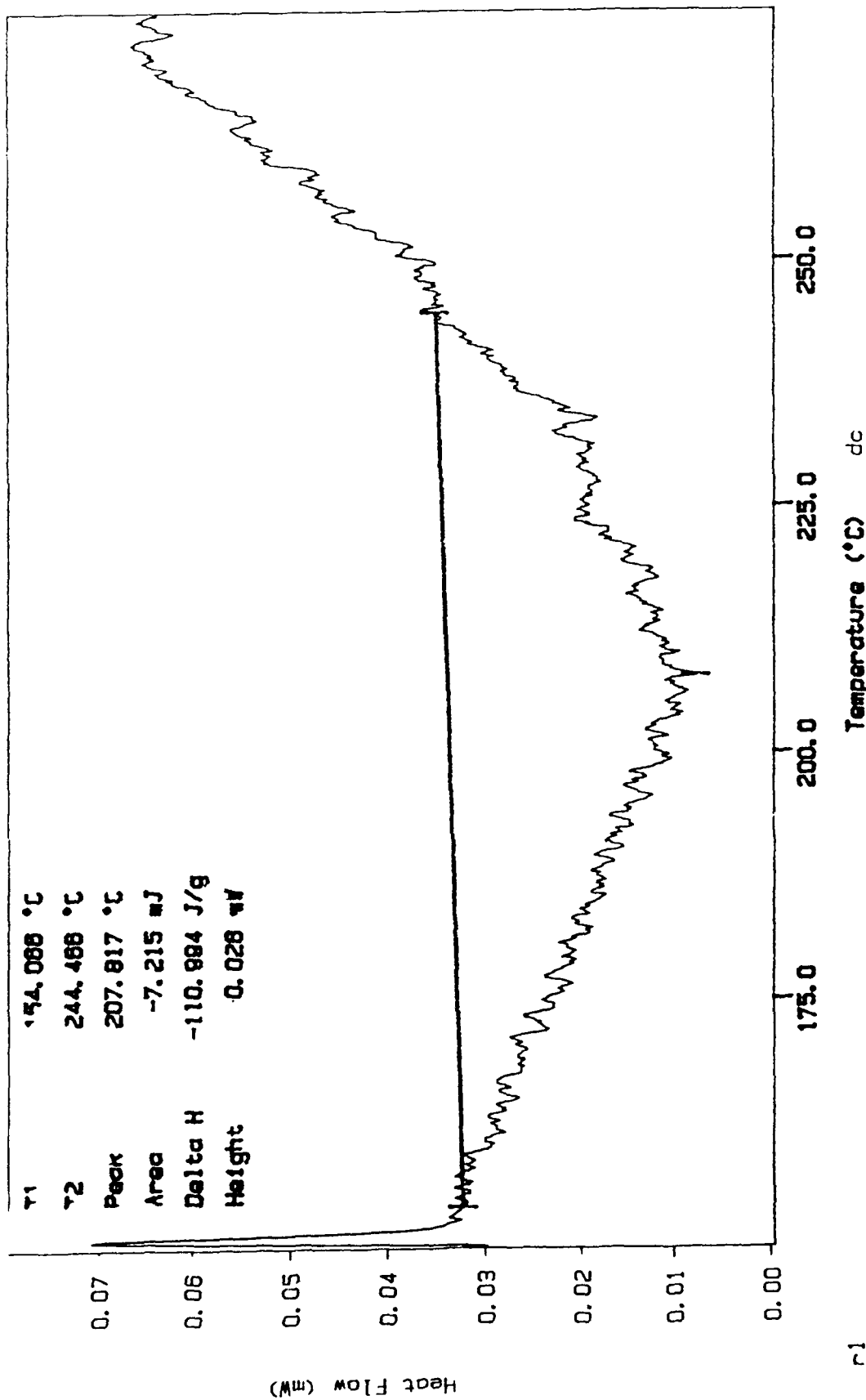
Thu Apr 09 04:15:20 1987

PL5 2e16 5/17/90

(Subtracted)

PERKIN LELMER

7 Series Thermal Analysis System



r1

TEMP 1: 150.0 °C TIME 1: 0.0 min RATE 1: 10.0 °C/min

TEMP 2: 275.0 °C

## APPENDIX B

DSC Subtraction

Sample Weight: 0.088 mg

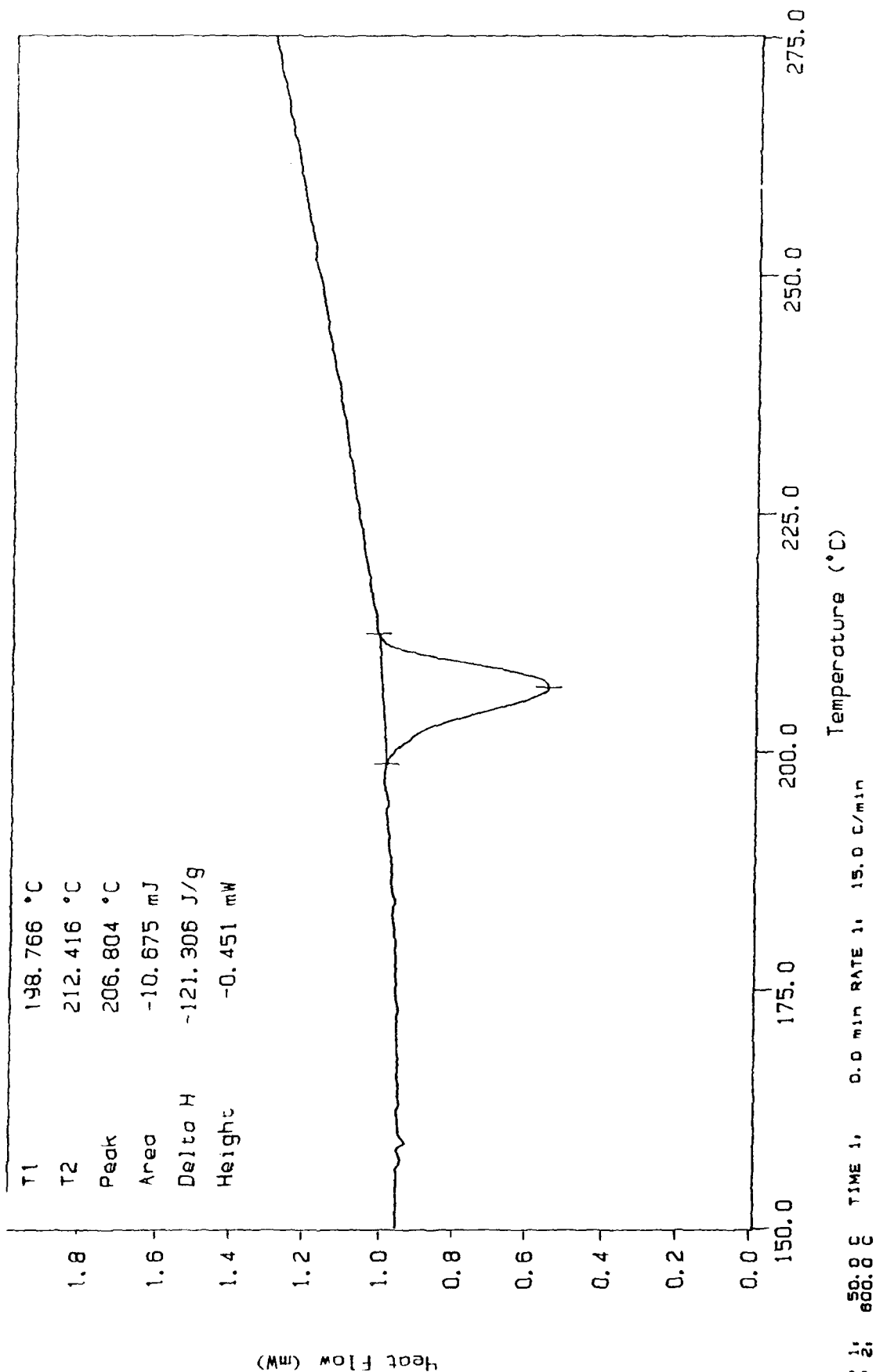
Wed Apr 08 14:31:18 1987

don09 pan9 vs pan5 run1 4/28/90

(Subtracted)

PERKIN-ELMER

7 Series Thermal Analysis System



DSC Subtraction

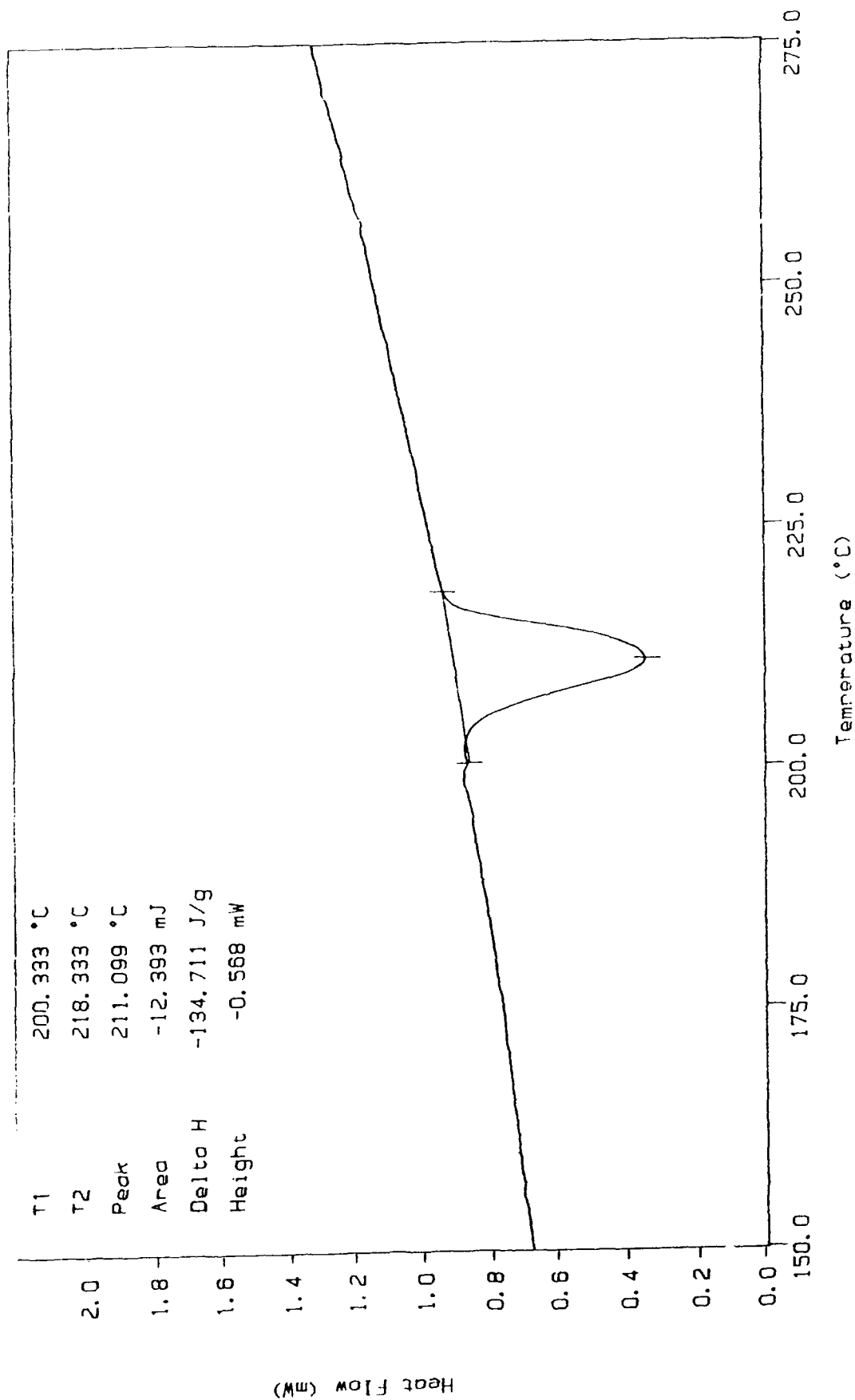
Sample Weight: 0.092 mg

Wed Apr 08 20:07:14 1987

Don09 pan10 vs pan6, run1 4/27/90

(Subtracted)

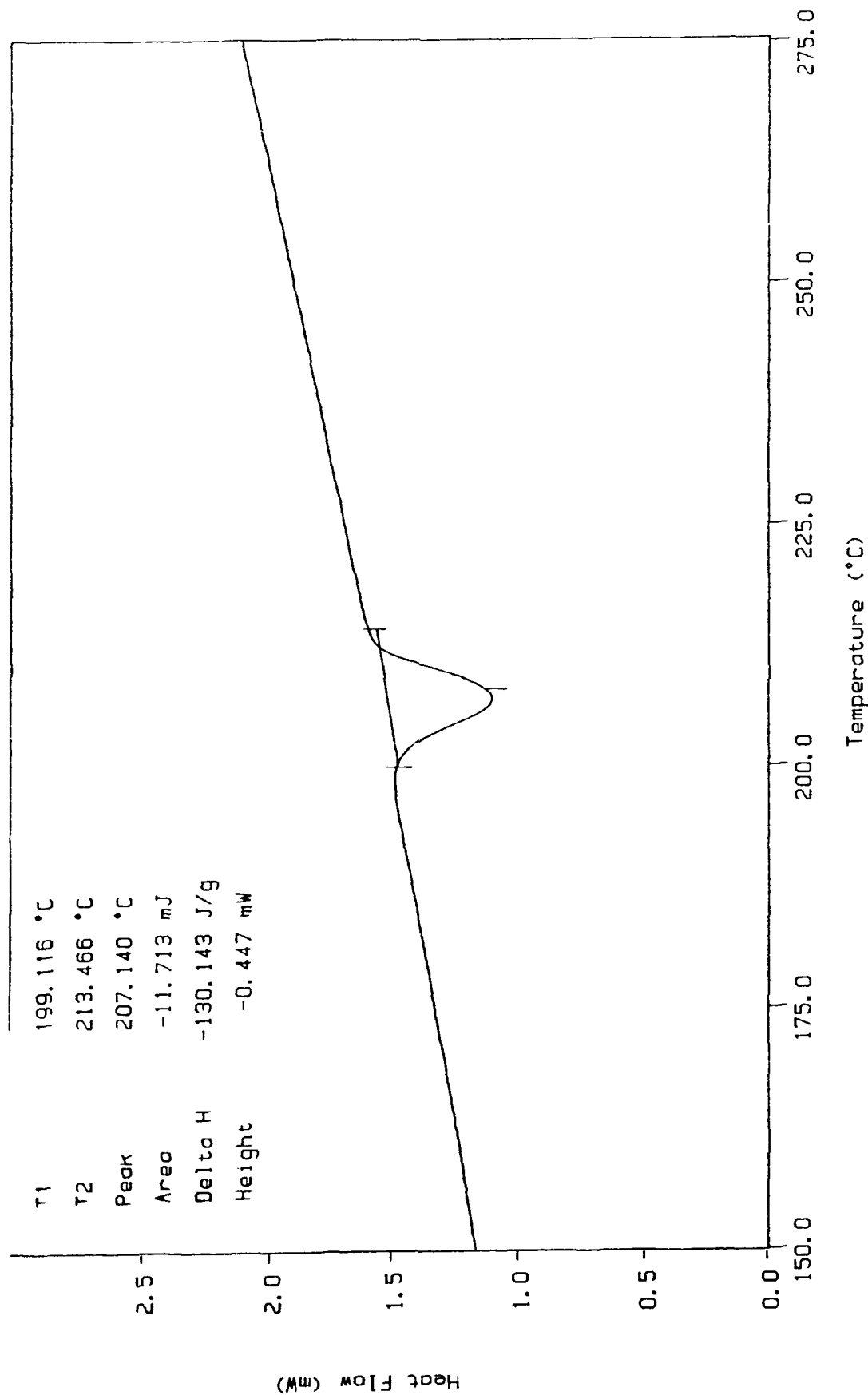
PERKIN-ELMER  
7 Series Thermal Analysis System



TEMP 1: 50.0 °C    TIME 1: 0.0 min    RATE 1: 20.0 °C/min  
TEMP 2: 800.0 °C

DSC Data File: pl109  
 Sample Weight: 0.090 mg  
 Mod Apr 08 16:07:37 1987  
 Jan09 pan11 vs pan7 run1 4/28/90

# PERKIN-ELMER 7 Series Thermal Analysis System



TEMP 1: 50.0 °C TIME 1: 0.0 min RATE 1: 15.0 °C/min  
 TEMP 2: 600.0 °C

DSC Subtraction

Sample Weight: 0.093 mg

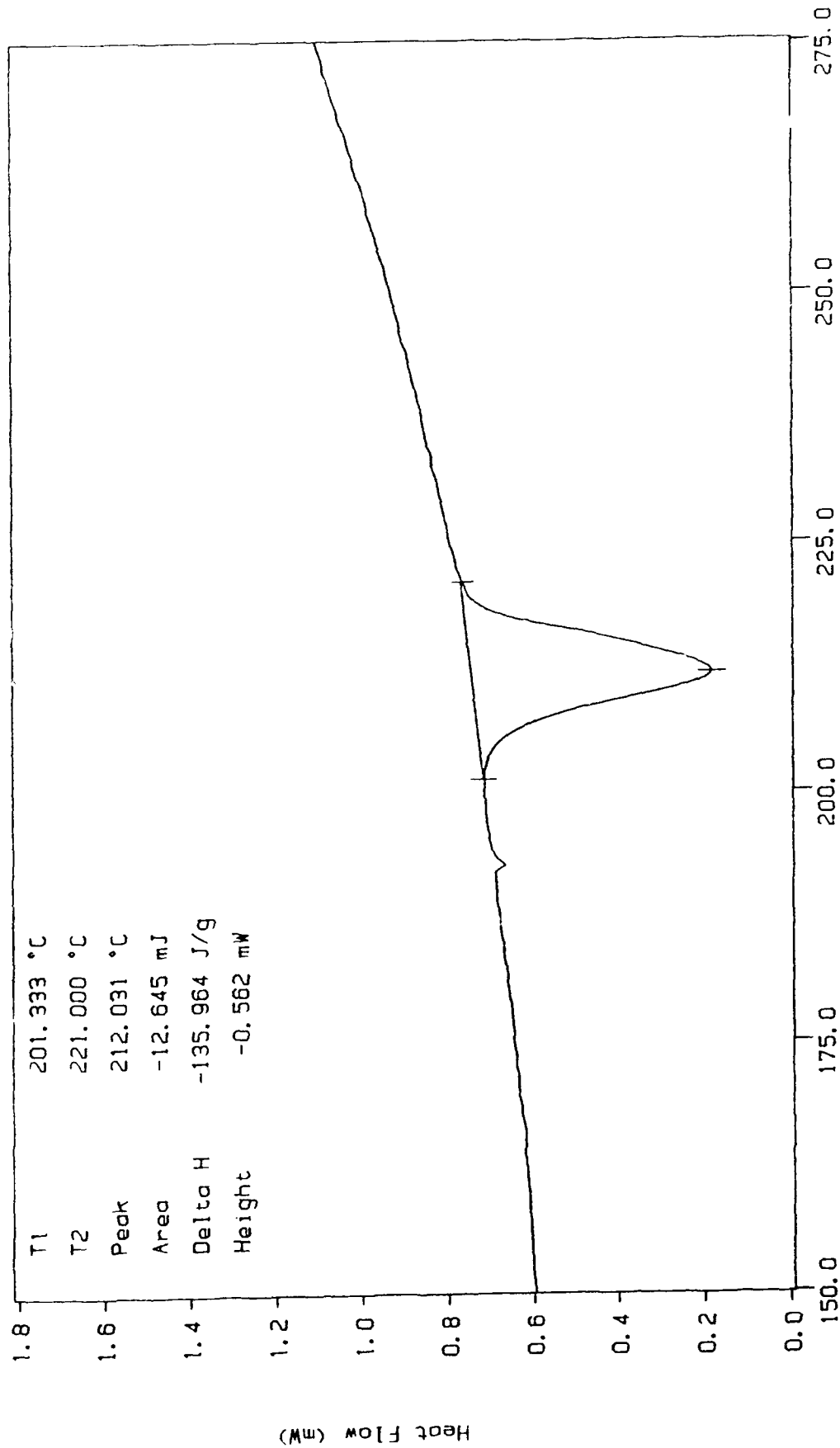
Wed Apr 08 17:38:32 1987

Jan09 p12 /s p8 run1 4/28/90

(Subtracted)

PLRKN LLMER

7 Series Thermal Analysis System



TEMP 1: 50.0 °C TIME 1: 0.0 min RATE 1: 20.0 °C/min

TEMP 2: 600.0 °C

DSC Subtraction

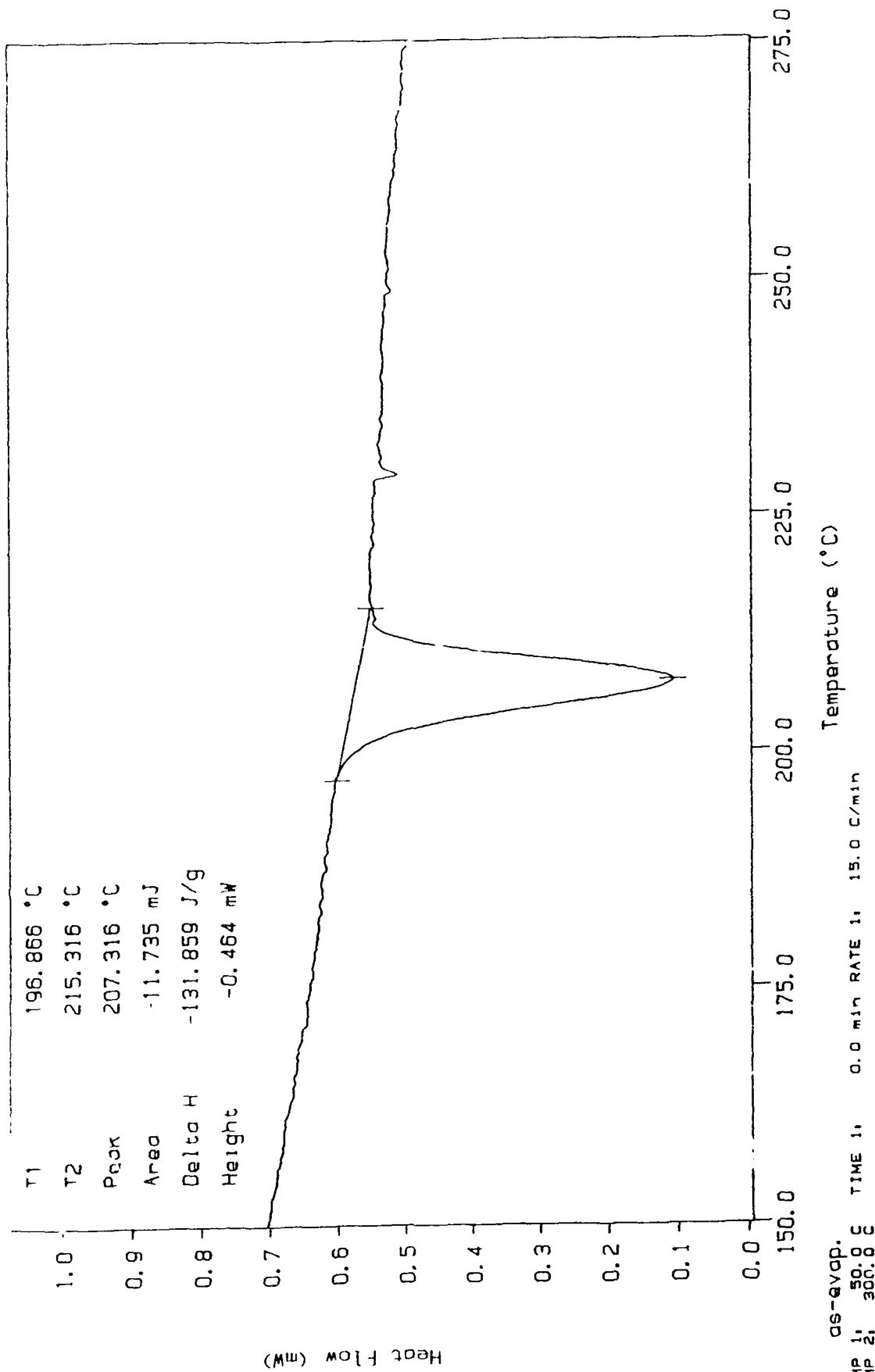
Sample Weight: 0.089 mg

Wed Apr 08 14:35:19 1987

Jan09 pl3 vs p5 run1 5/1/90

(Subtracted)

PERKIN-ELMER  
7 Series Thermal Analysis System



DSC Subtraction

Sample Weight: 0.090 mg

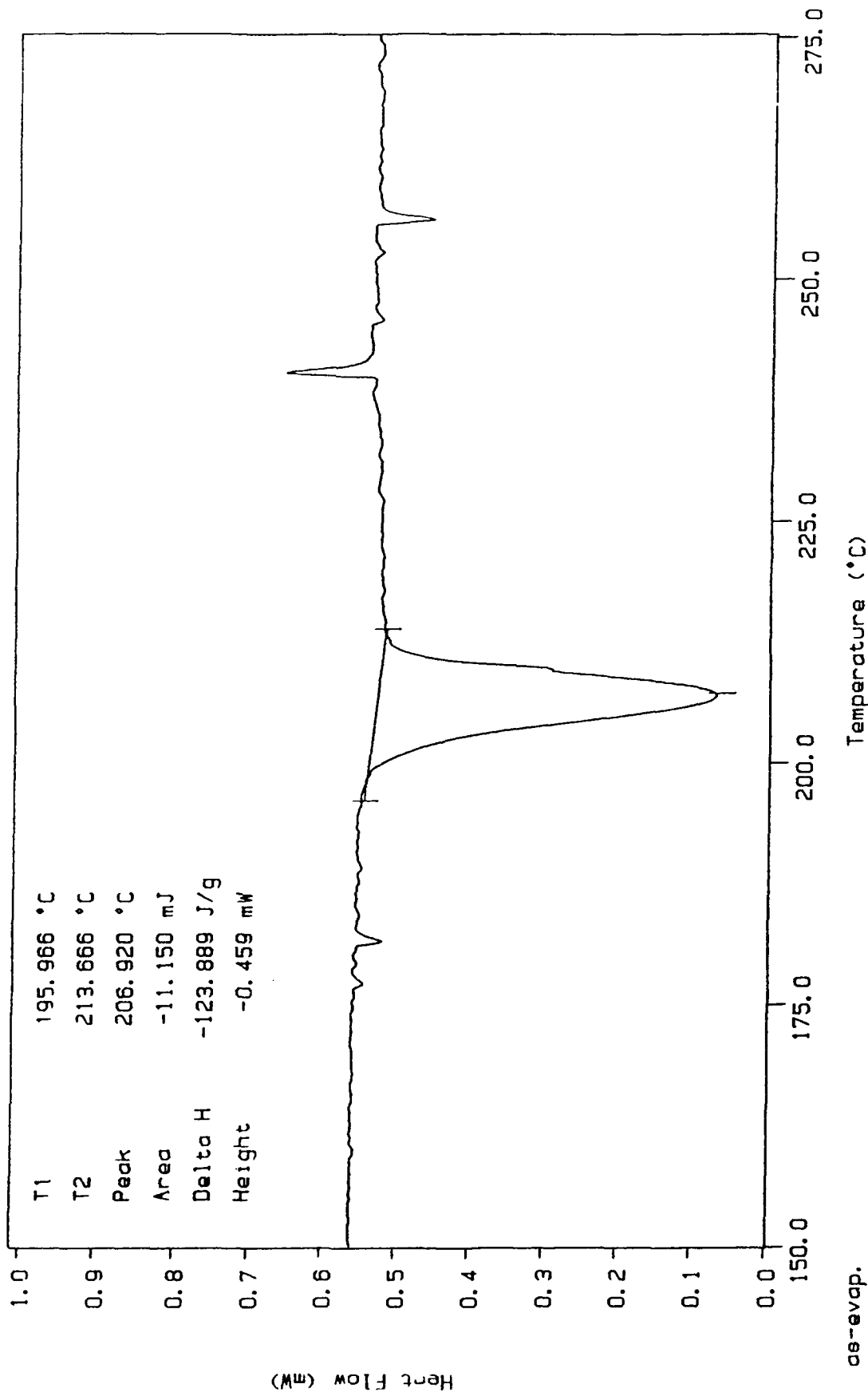
Wed Apr 08 15:22:49 1987

Don09 p14 vs p6 run1 5/1/90

(Subtracted)

PERKIN-ELMER

7 Series Thermal Analysis System



08-evap.

TEMP 1: 50.0 °C

TEMP 2: 300.0 °C

TIME 1: 0.0 min

RATE 1: 15.0 °C/min

DSC Subtraction

Sample Weight: 0.090 mg

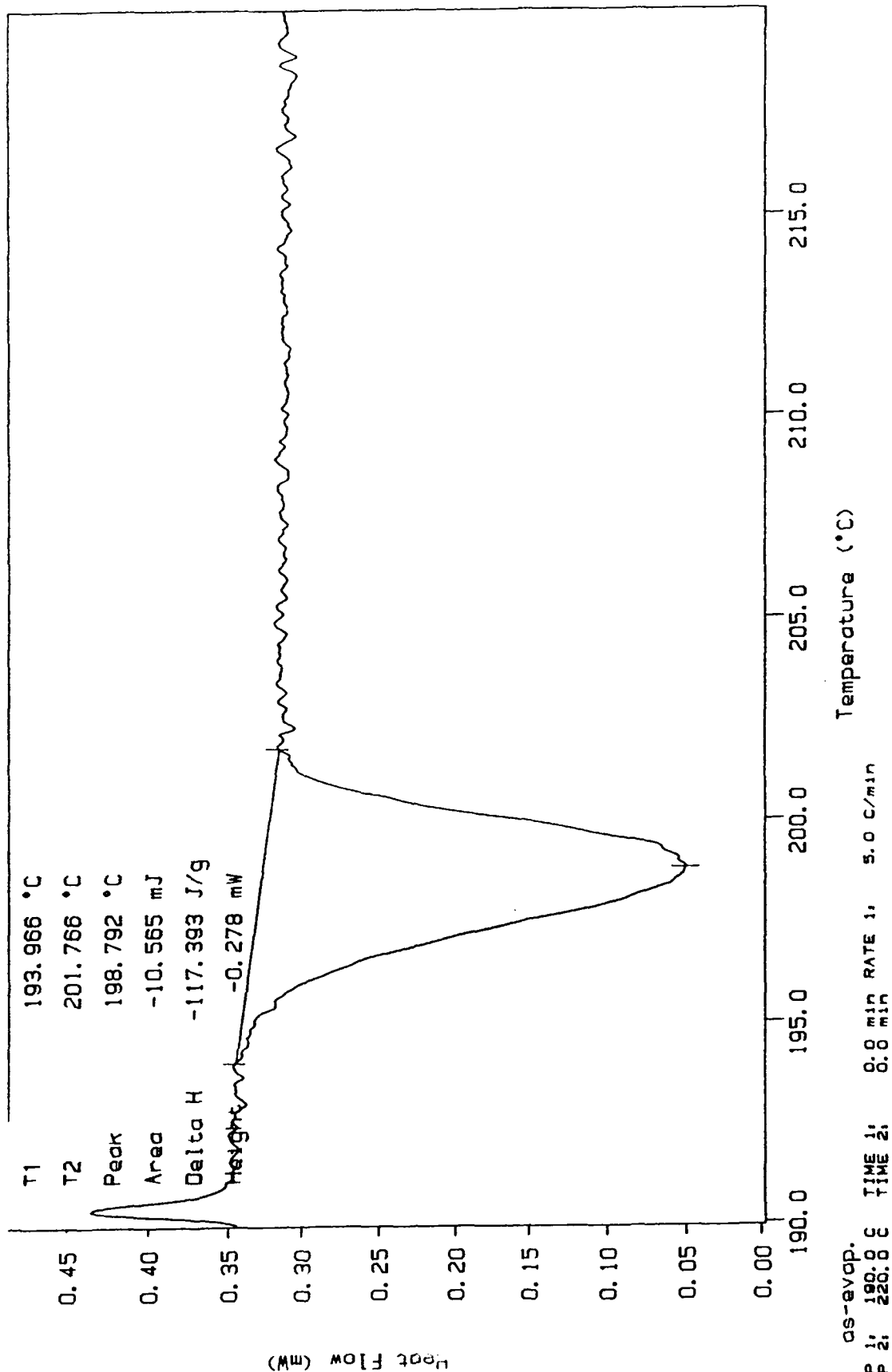
Wed Apr 08 16:05:47 1987

Jan09 p15 vs p7 run1 5/1/90

(Subtracted)

PLRK IN-ELMER

7 Series Thermal Analysis System



DSC Subtraction

Sample Weight: 0.122 mg

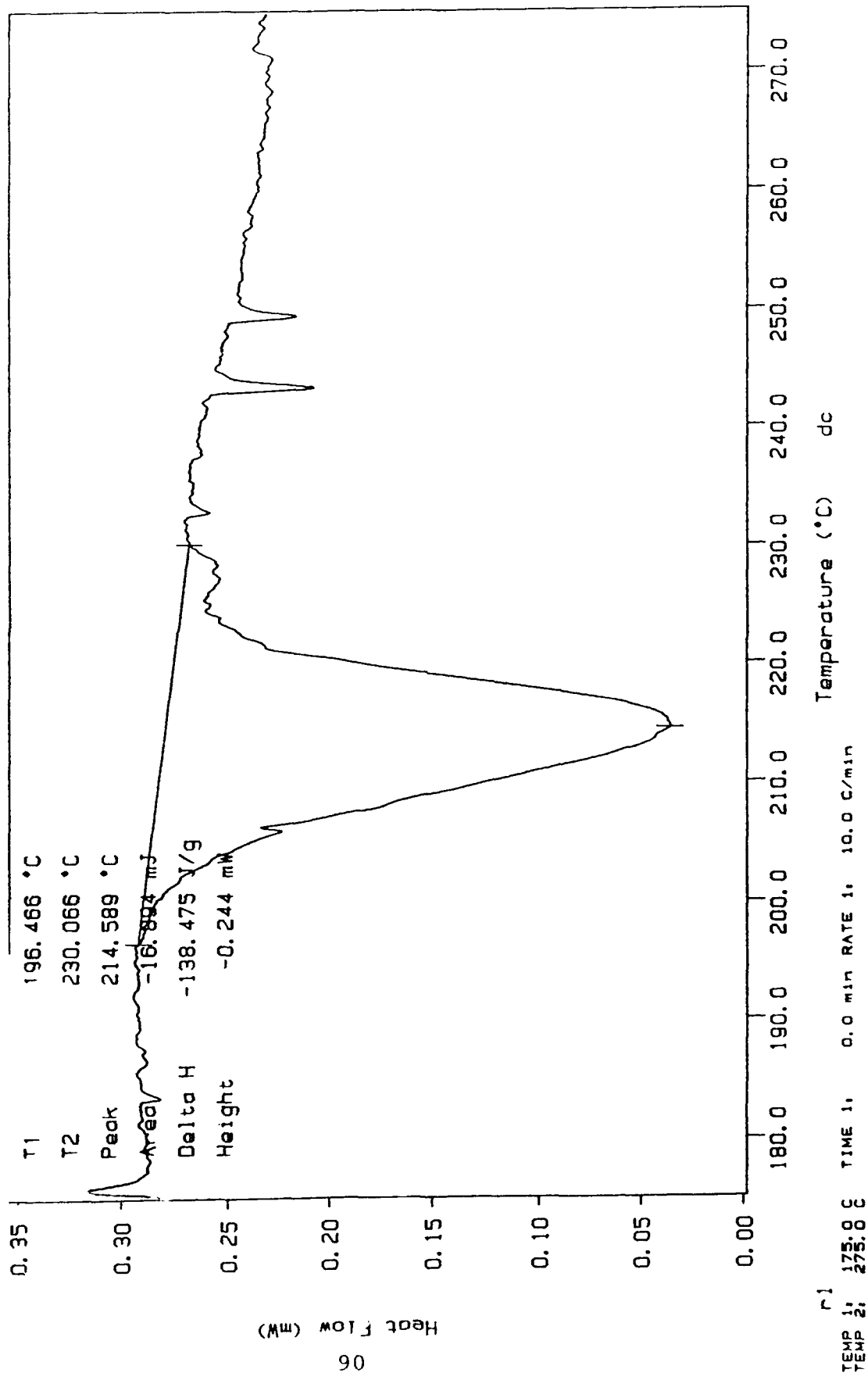
Thu Apr 09 18:51:49 1987

don11 pl asevap 5/18/90

(Subtracted)

PERKIN-ELMER

7 Series Thermal Analysis System



USL Subtraction

Sample Weight: 0.122 mg

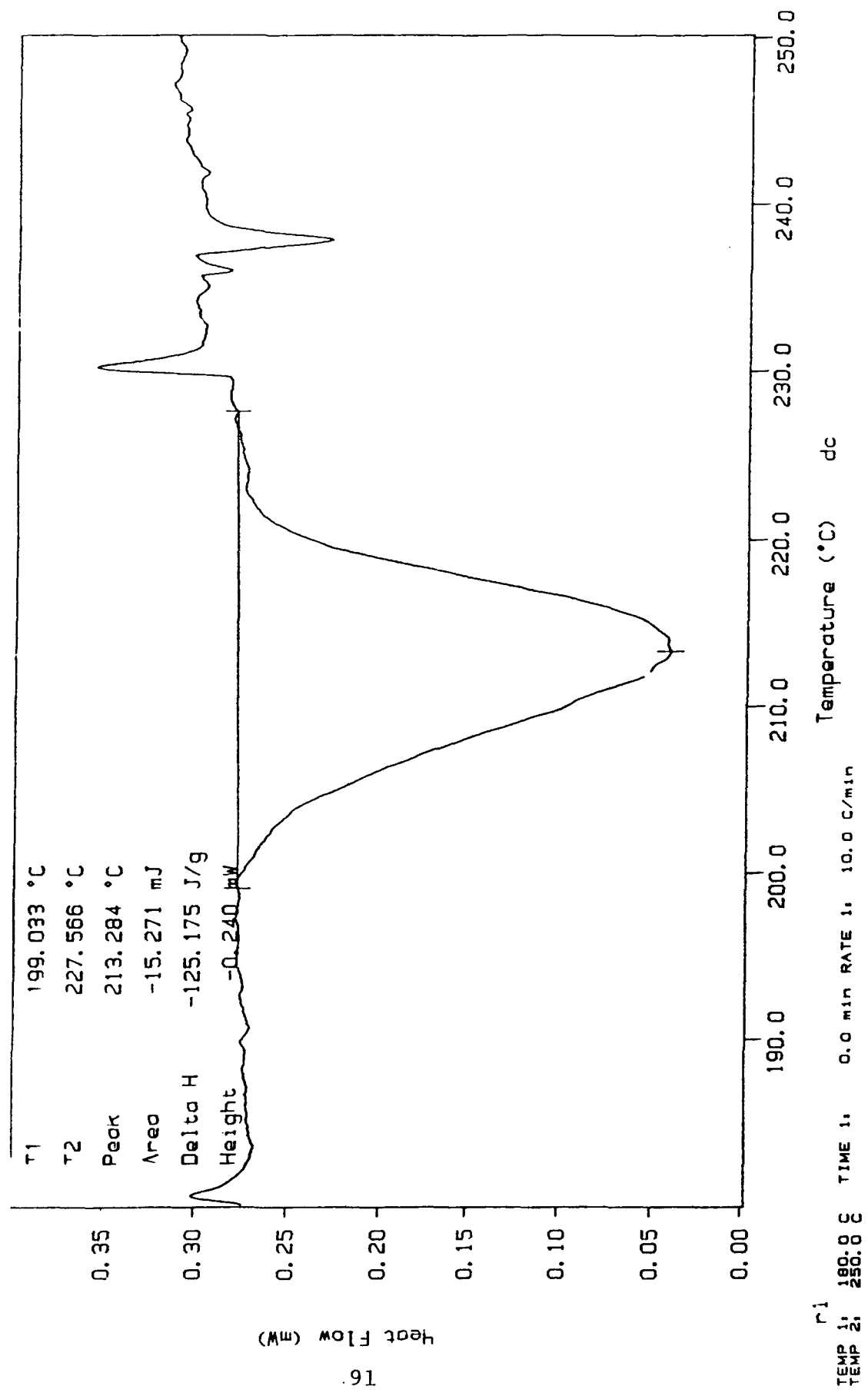
Thu Apr 09 19:33:03 1987

p2 osevap 5/18/90

(Subtracted)

PERKIN LLMR

7 Series Thermal Analysis System



DSC Subtraction

Sample Weight: 0.119 mg

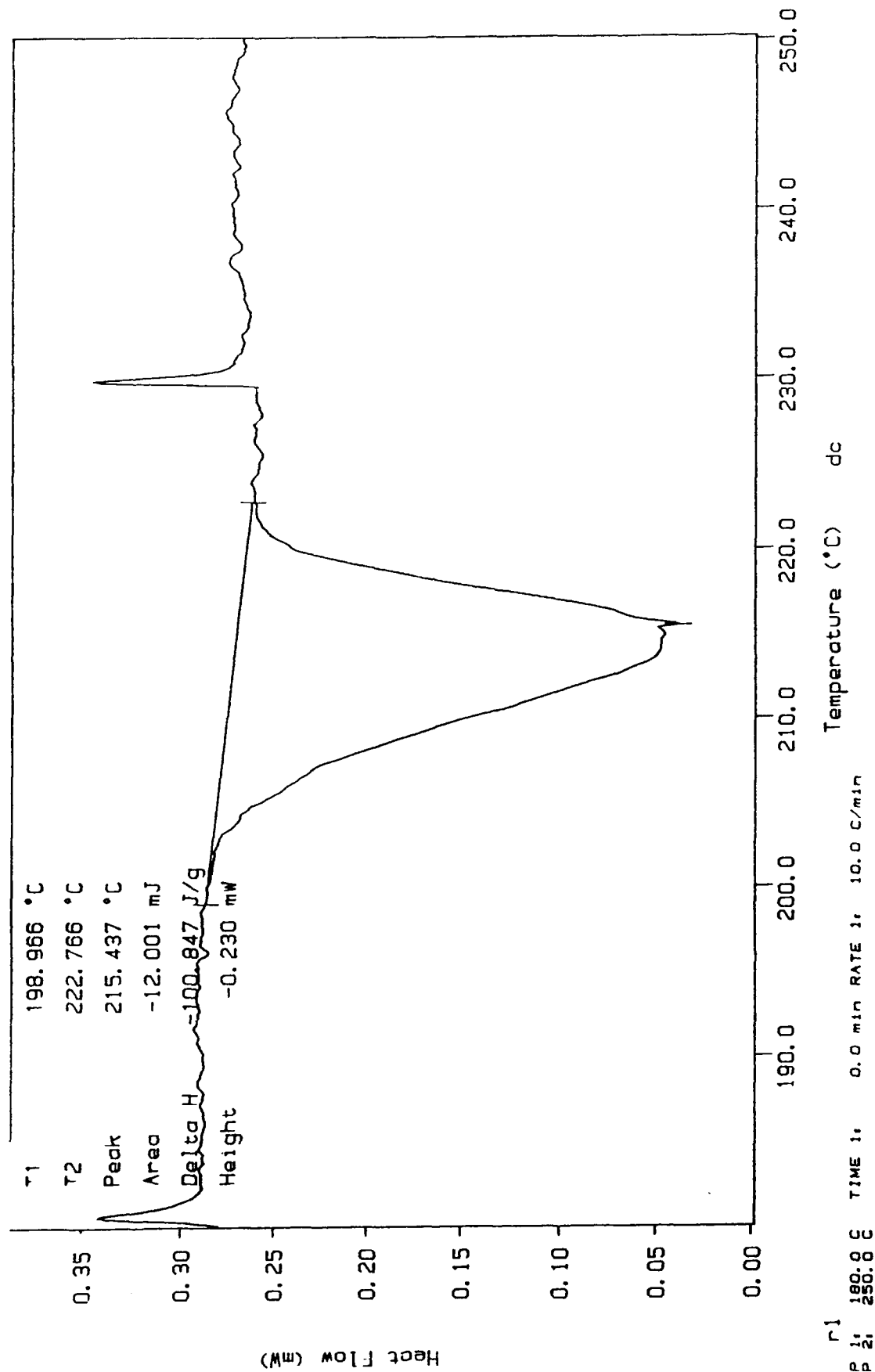
Thu Apr 09 20:04:47 1987

r3 csevap 5/18/90

(Subtracted)

PERKIN-ELMER

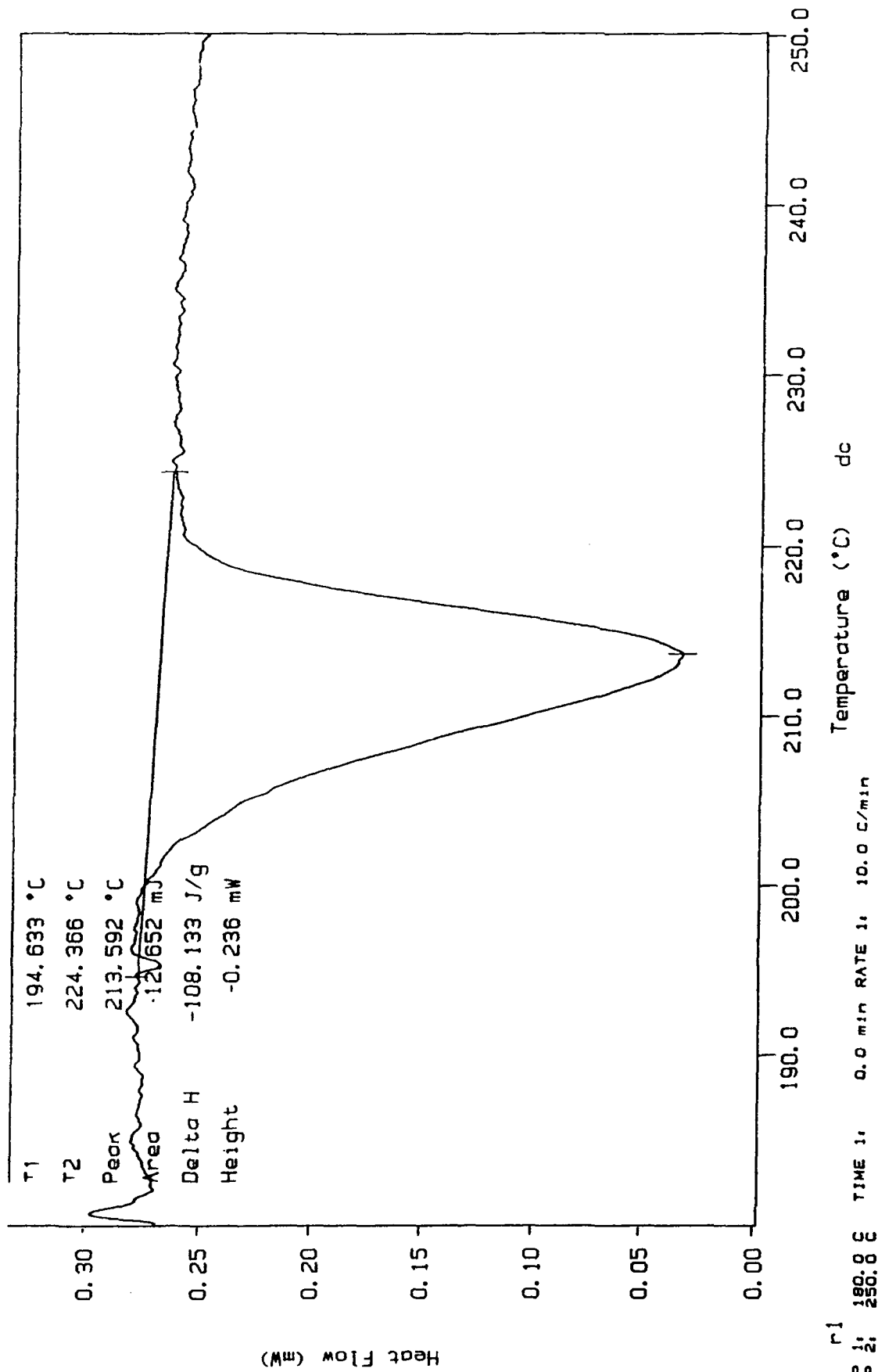
7 Series Thermal Analysis System



Sample Weight: 0.117 mg  
 Thu Apr 09 20:35:01 1987  
 p4 osevap 5/18/90  
 (Subtracted)

PERKIN-ELMER

7 Series Thermal Analysis System



DSC Subtraction

Sample Weight: 0.119 mg

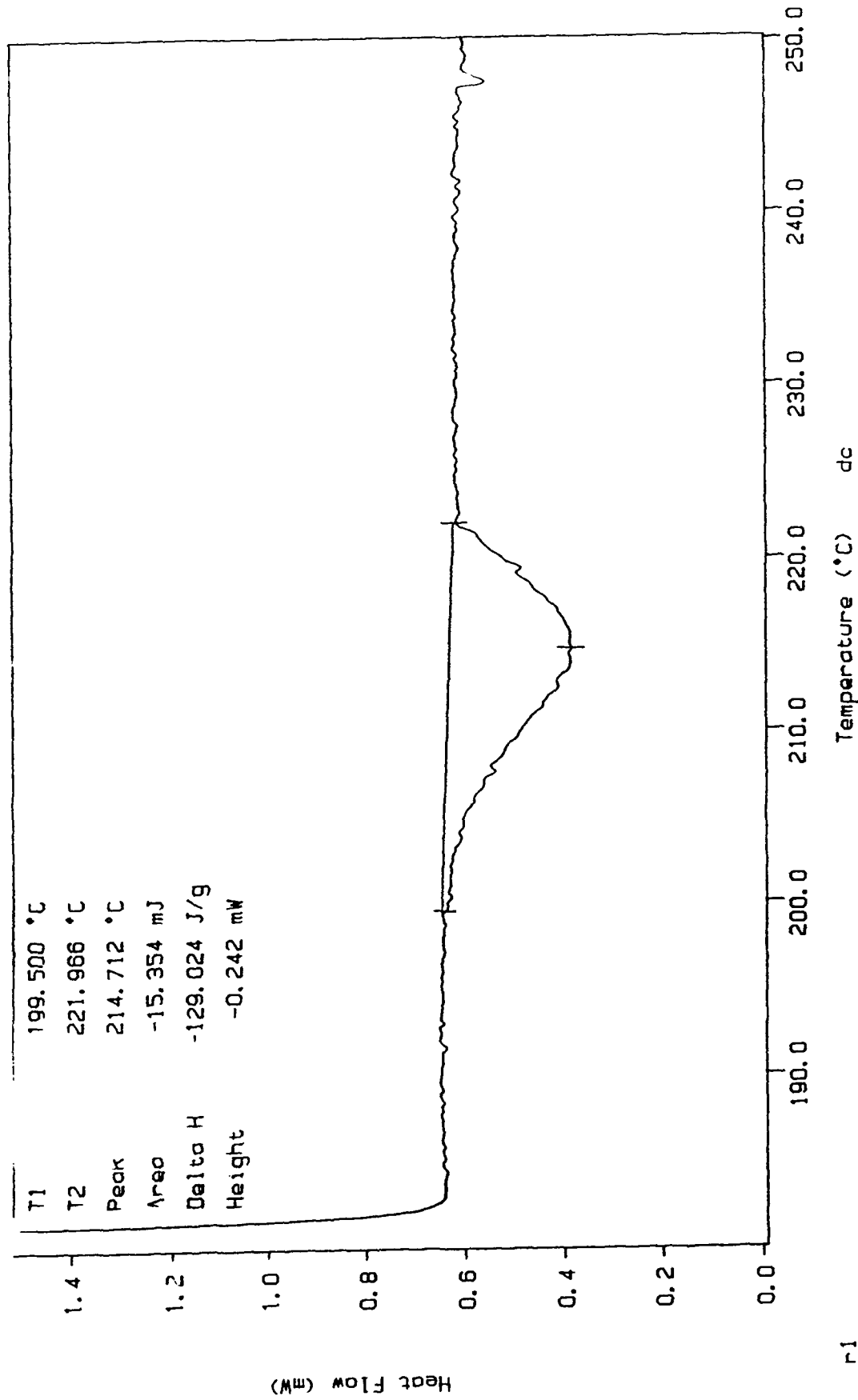
Thu Apr 09 21:37:24 1987

p6 osavap 5/18/90

(Subtracted)

PERKIN-ELMER

7 Series Thermal Analysis System



DSC Subtraction

Sample Weight: 0.118 mg

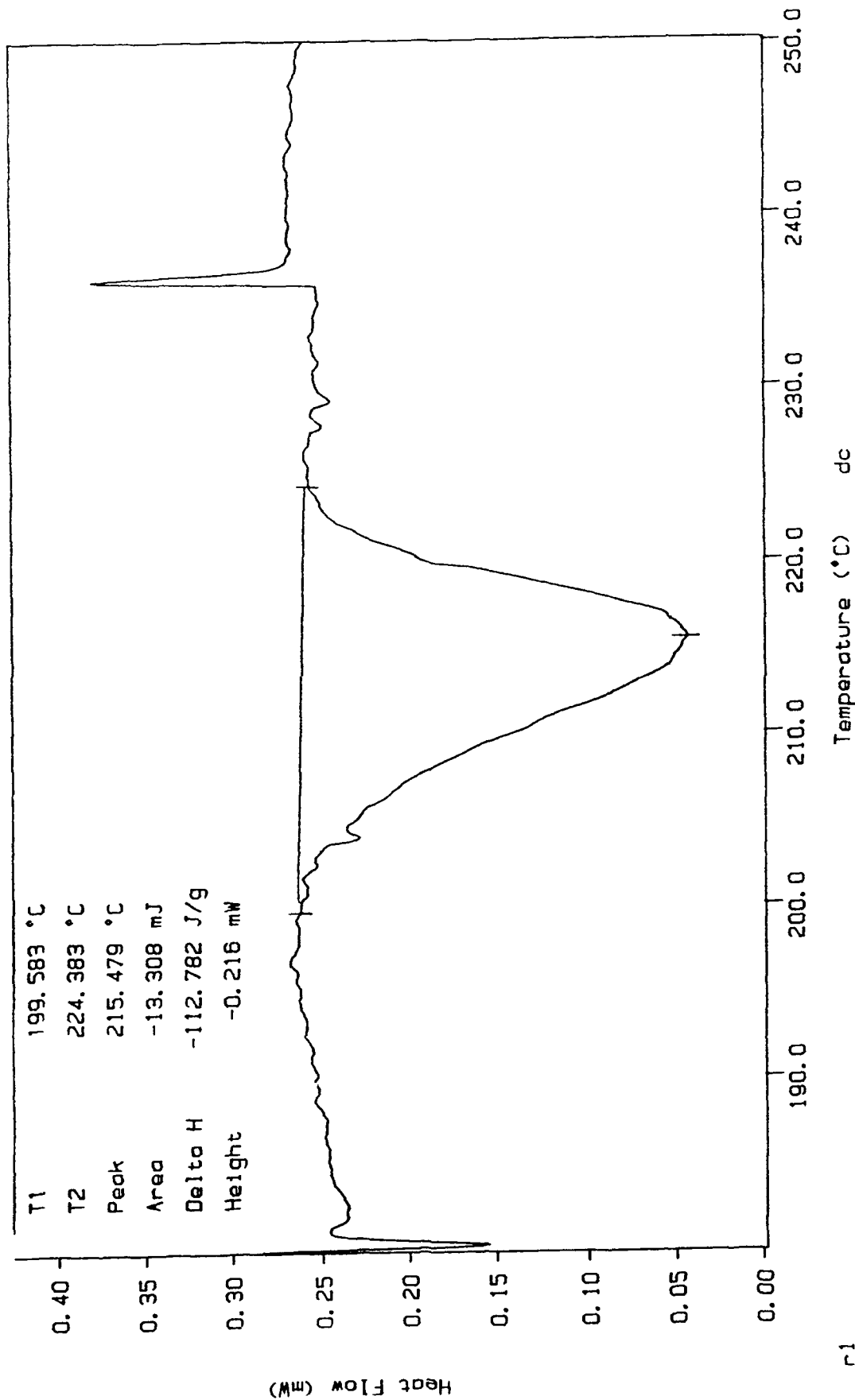
Thu Apr 09 22:03:18 1987

p7 cseavap 5/18/90

(Subtracted)

PERKIN-ELMER

7 Series Thermal Analysis System



r1

TEMP 1: 180.0 C  
TEMP 2: 250.0 C

TIME 1: 0.0 min RATE 1: 10.0 C/min

DSC Subtraction

Sample Weight: 0.113 mg

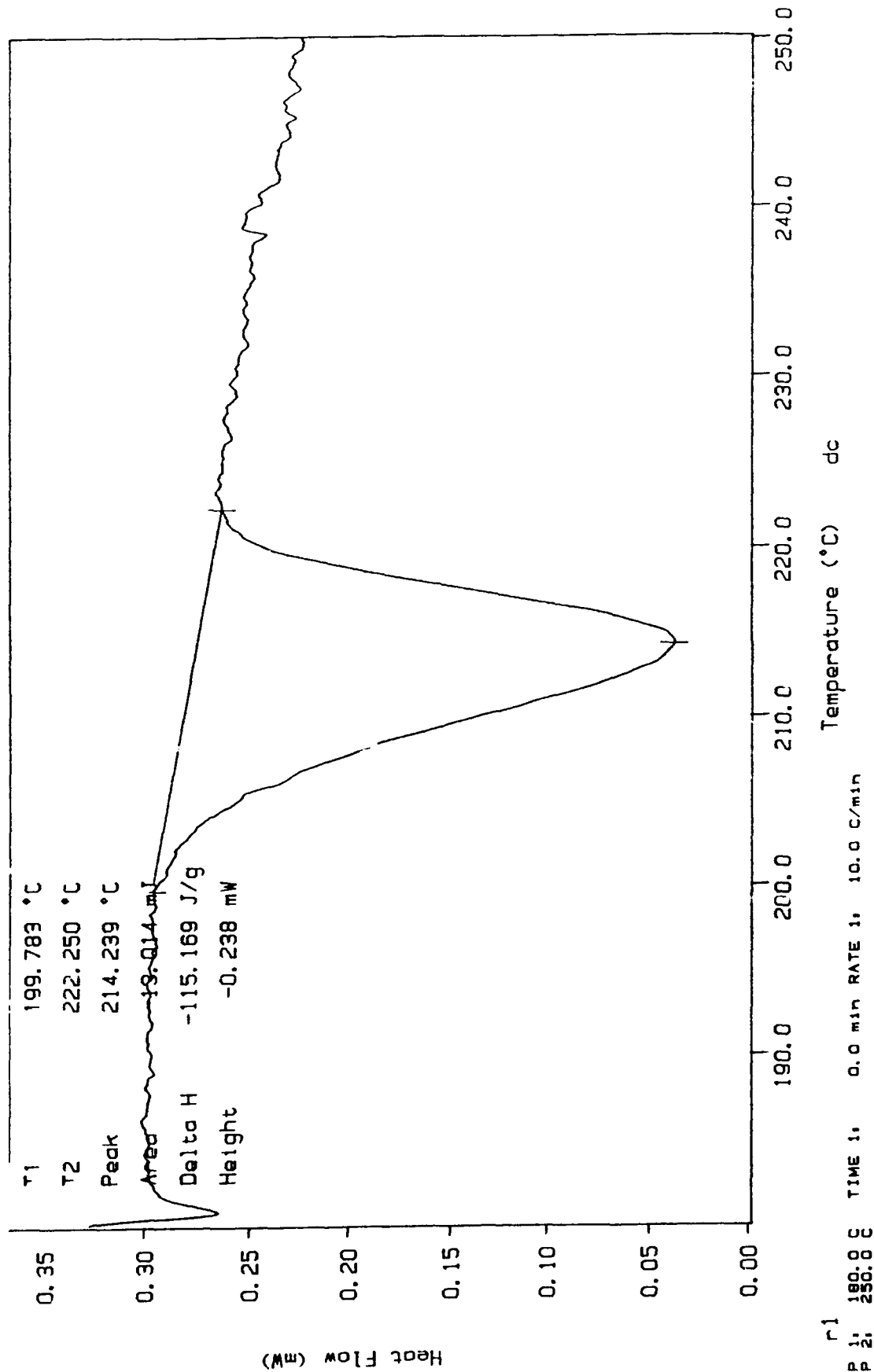
Thu Apr 09 22:30:46 1987

p8 osevap 5/18/90

(Subtracted)

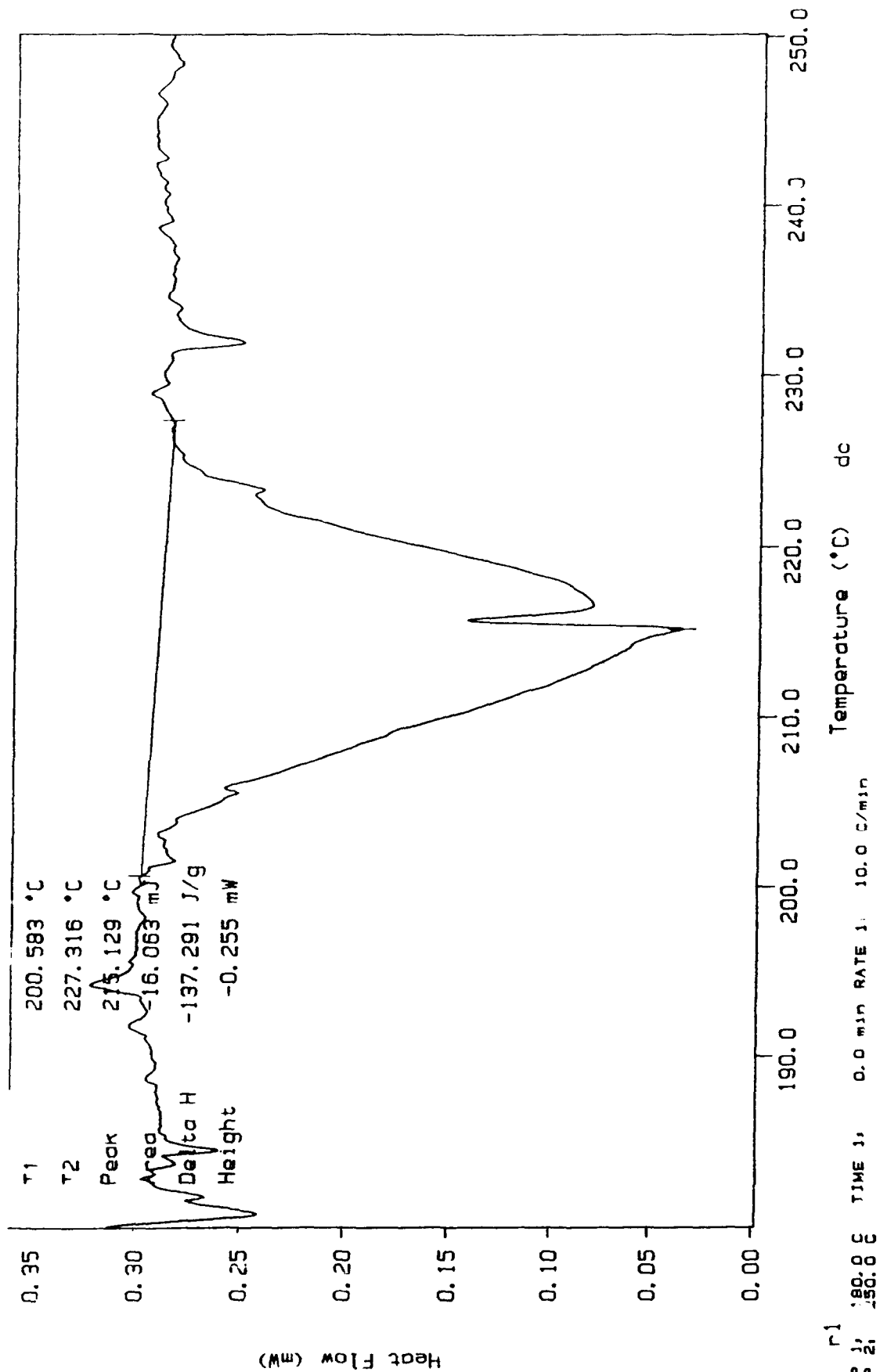
PLRWIN-ELMER

7 Series Thermal Analysis System



DSC Subtraction  
 Sample Weight: 0.117 mg  
 Thu Apr 09 22:57:51 1987  
 pg 05evcp 5/18/90  
 (Subtracted)

PLRIN-ELMLR  
 7 Series Thermal Analysis System



DSC Subtraction

Sample Weight: 0.118 mg

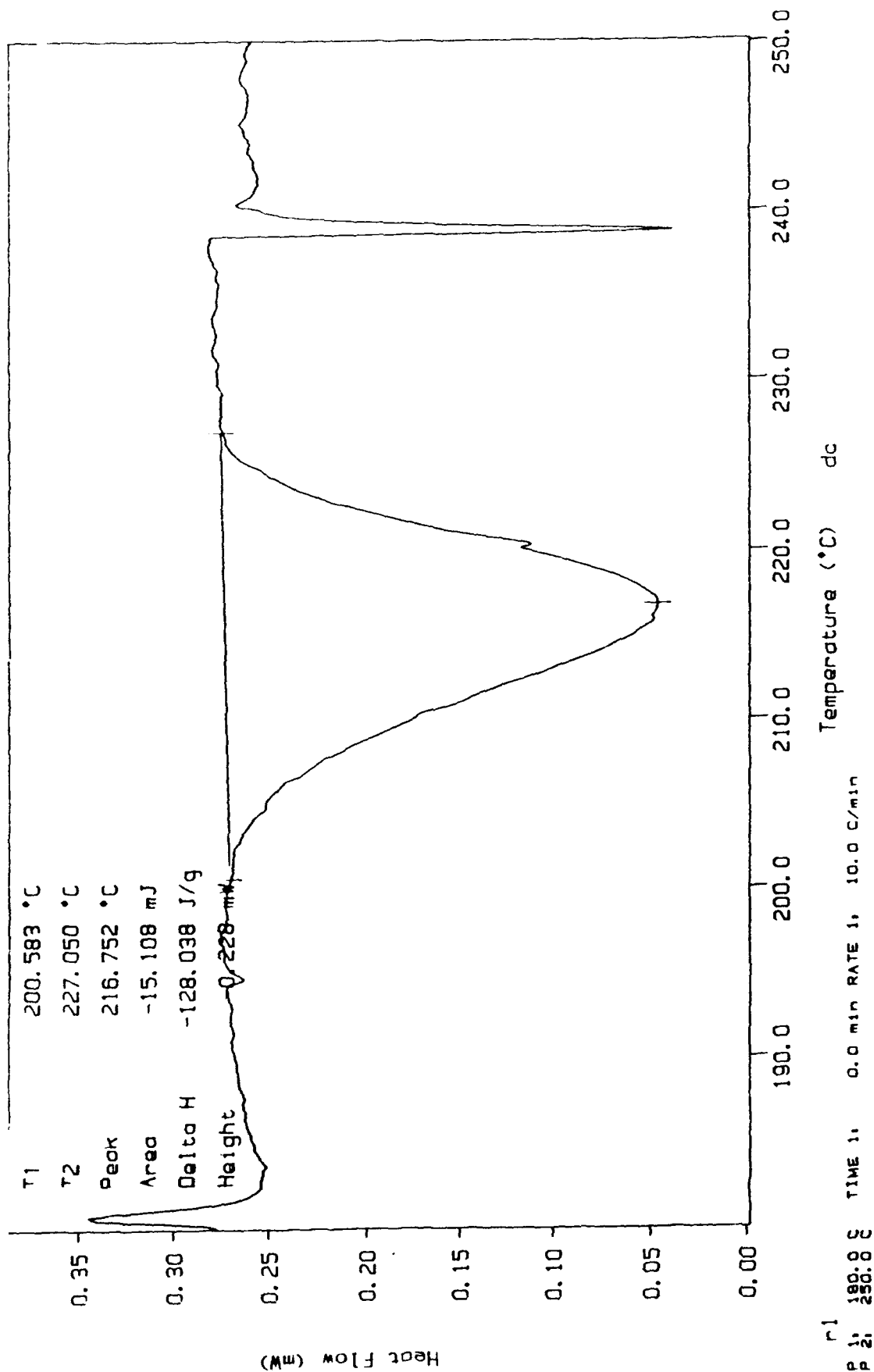
Thu Apr 09 23:25:24 1987

pl0 casevop 5/18/90

(Subtracted)

P\_L\_R\_K\_I\_N L\_M\_L\_R

7 Series Thermal Analysis System



DSC Subtraction

Sample Weight: 0.116 mg

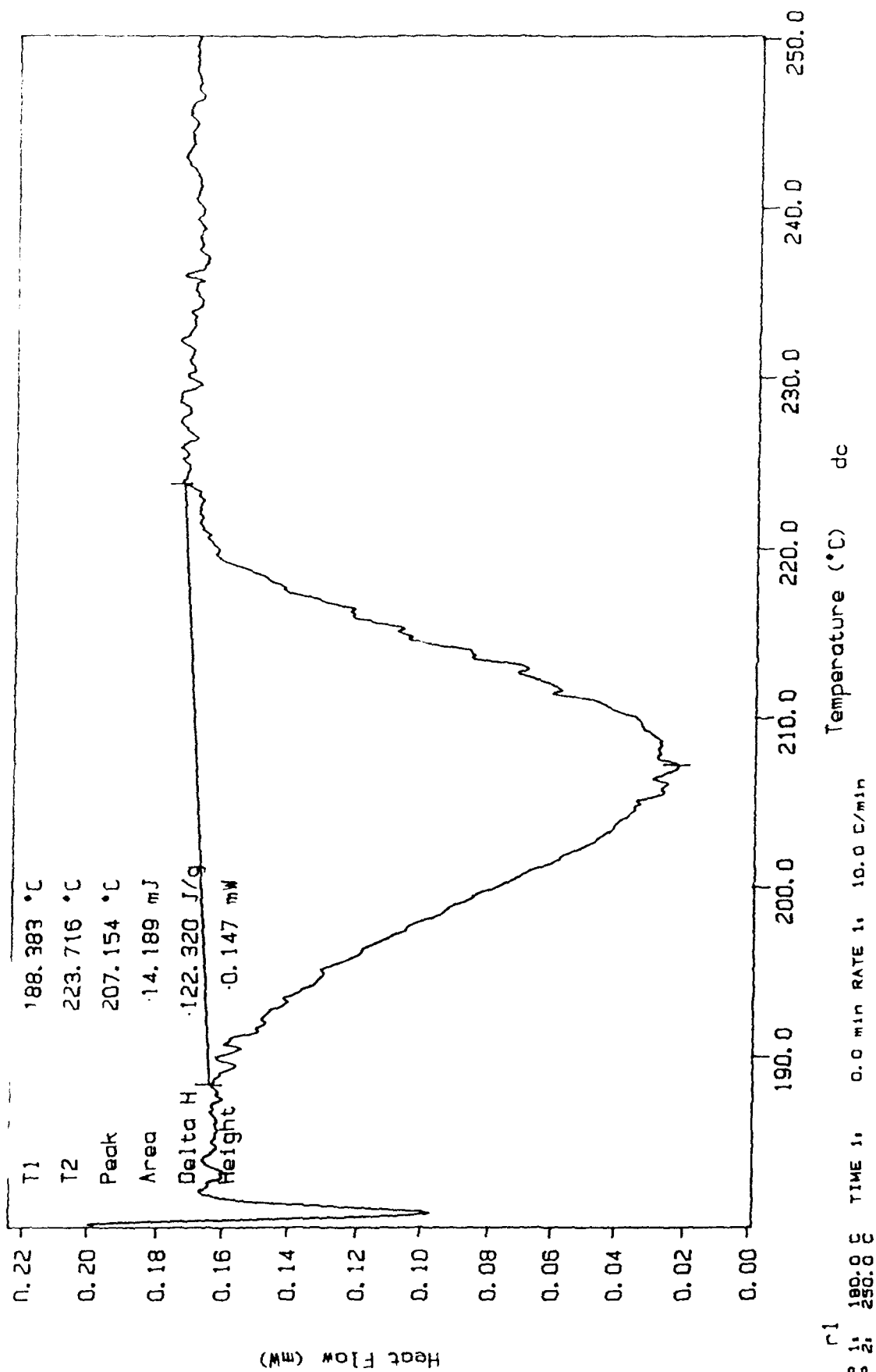
Thu Apr 09 23:50:30 1987

pl1 asevap 5/18/90

(Subtracted)

PLKIN-ELMER

7 Series Thermal Analysis System



DSC Subtraction

Sample Weight: 0.114 mg

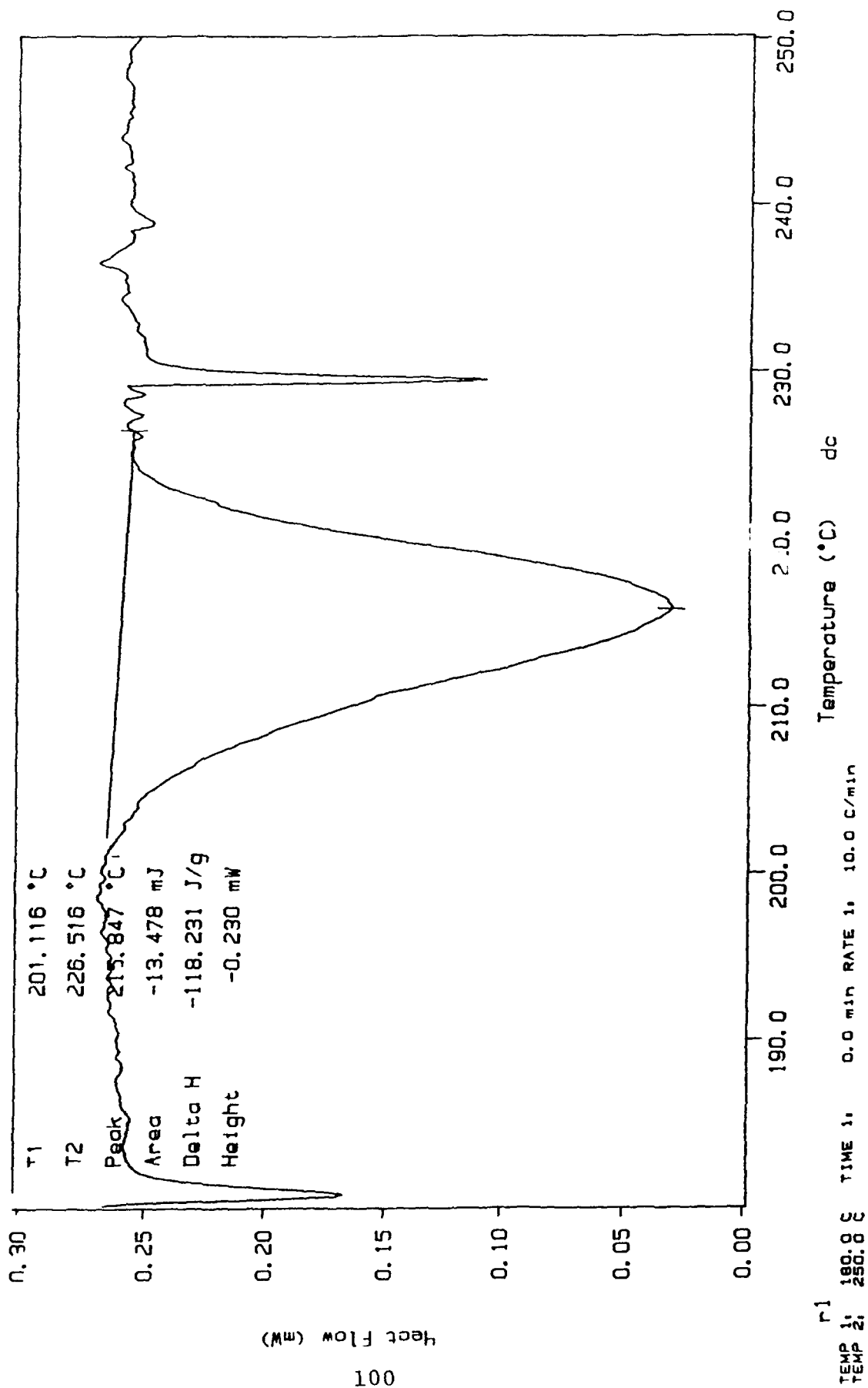
1st Apr 10 00:17:32 1987

p12 csevap 5/18/90

(Subtracted)

PARKIN LLMR

7 Series Thermal Analysis System



DSC Subtraction

Sample Weight: 0.118 mg

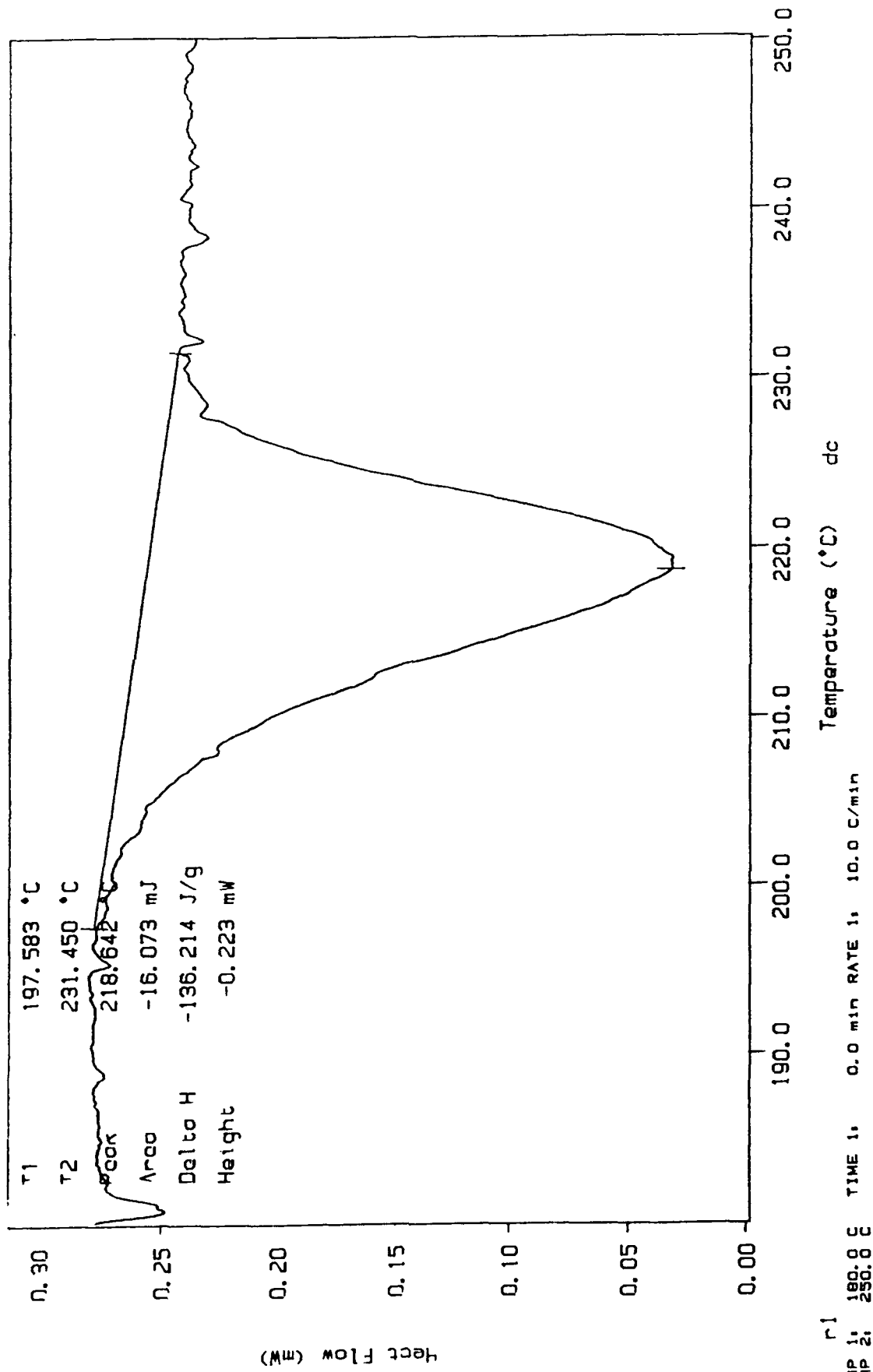
Run Apr 10 00:44:05 1987

p13 asc/op 5/18/90

(Subtracted)

PLRKTN L\_MLR

7 Series Thermal Analysis System



DSC Subsequence

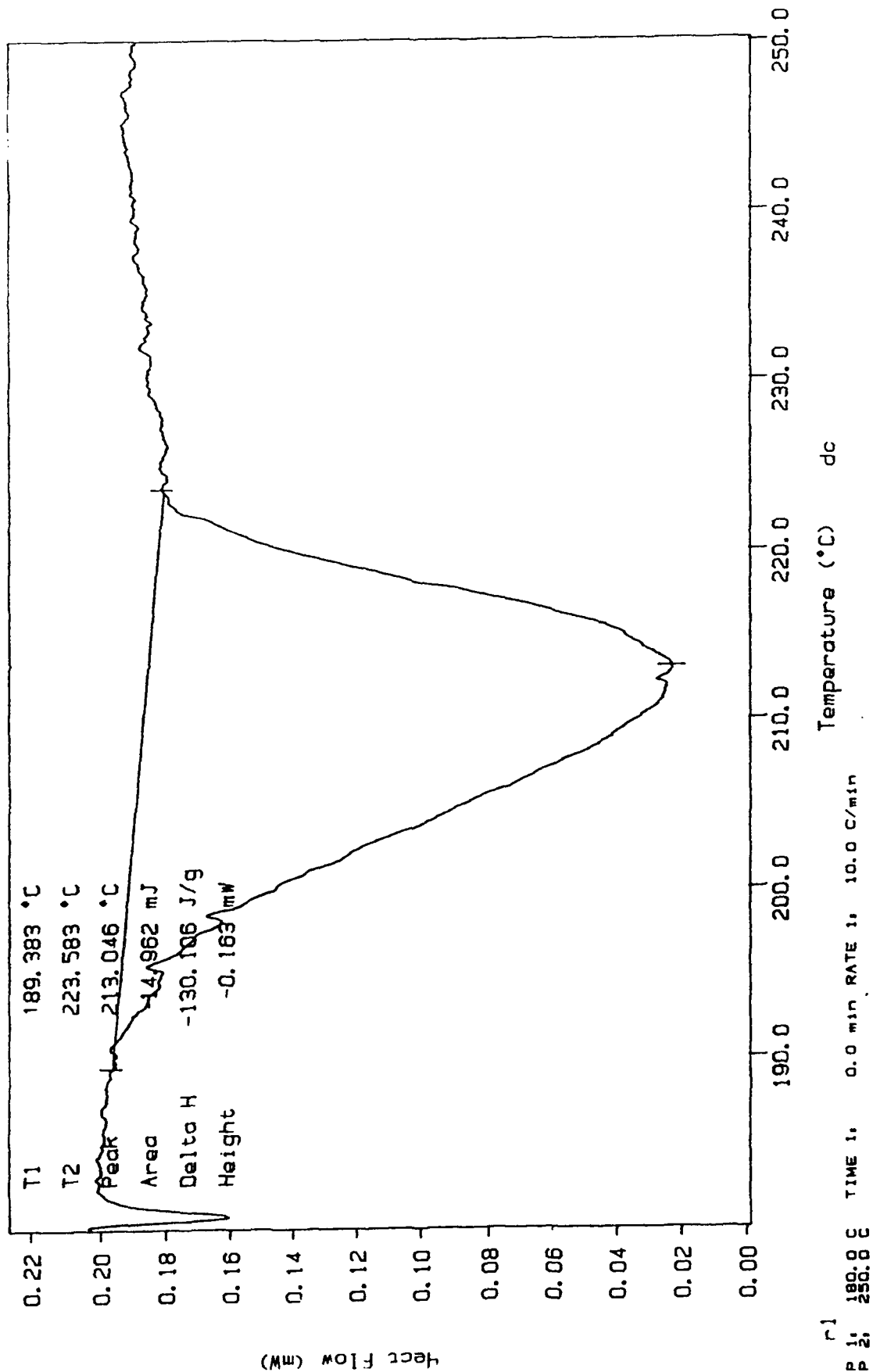
Sample Weight: 0.115 mg

Run Date: Apr 10 01:09:57 1987

File Name: p14 dscvap 5/18/90

(Subtracted)

# P\_RKIN-ELMER 7 Series Thermal Analysis System



DSC Subroutine

Sample Weight: 0.114 mg

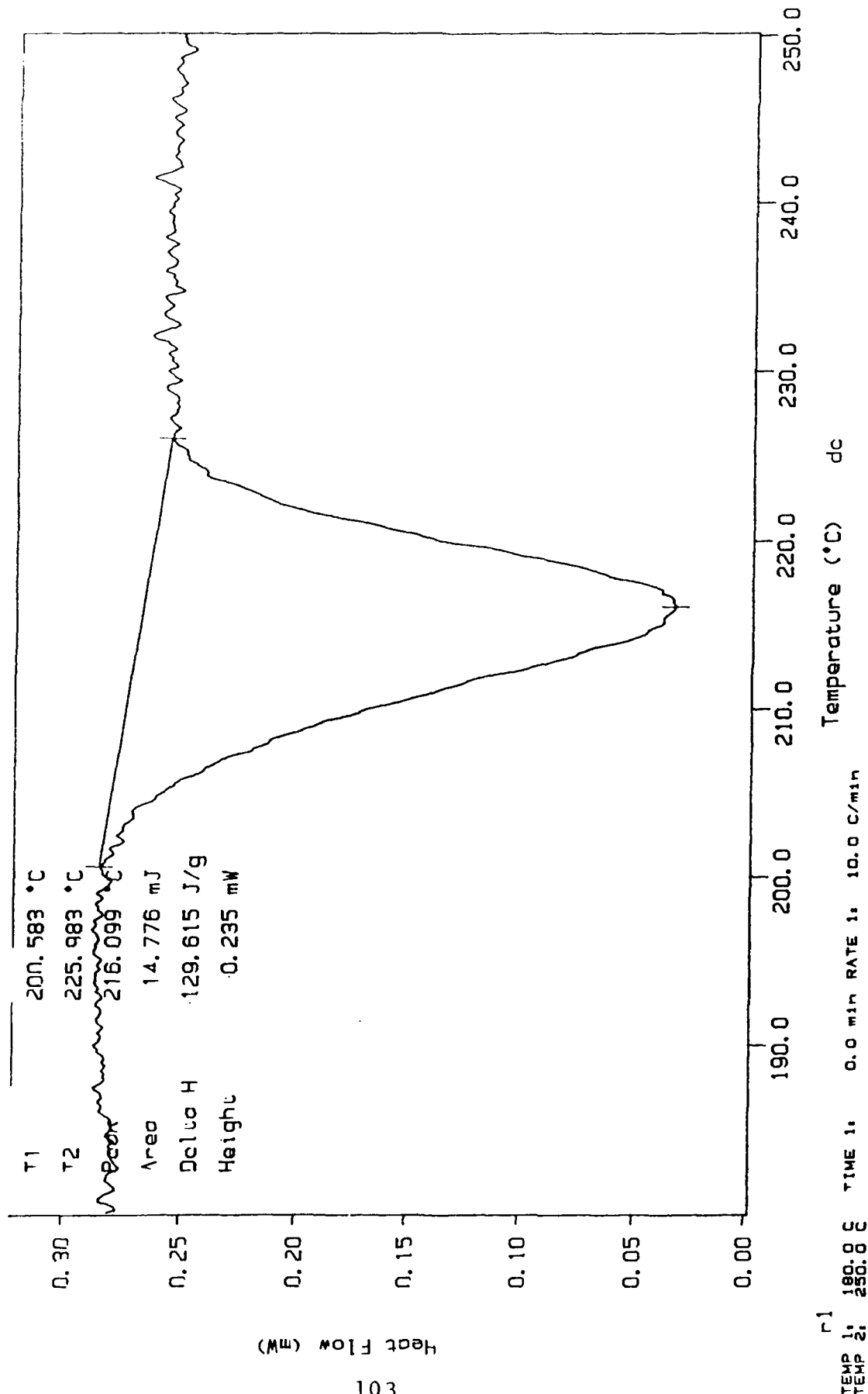
Date: 10 01:37:16 1987

File: cse/ap 5/18/90

(Subtracted)

PLRkin LMLR

7 Series Thermal Analysis System



DSC Subtraction

Sample Weight: 0.112 mg

Fri Apr 10 02:05:54 1987

P16 cse/vp 5/18/90

(Subtracted)

PLRkin-ELMLR

7 Series Thermal Analysis System

